Shallow layer modelling of dense gas clouds

Ott, Søren; Nielsen, Morten

Publication date:
1997

Document Version
Publisher's PDF, also known as Version of record

Risø-R-901(EN)

Shallow Layer Modelling of Dense Gas Clouds

Søren Ott & Morten Nielsen

Risø National Laboratory, Roskilde, Denmark
November 1996

Abstract The work presented in this report was done as part of the Fladis field experiments (Nielsen & Ott (1996)), a project under the CEC research programme ENVIRONMENT. The objective was to develop a shallow layer model for dense gas dispersion.

Shallow layer models are intermediate in complexity between box models and full 3d models. The motivation for making shallow layer models is that they can deal with complex terrain at a modest computational cost compared to 3d codes. They also model the gravity induced flow dynamically. The main disadvantage is that the air-cloud interactions have to be parameterized, where 3d models inherit the correct dynamics from the fundamental equations.

In Chapter 2 a discussion of the properties of the inviscid shallow water equations is given, focusing on existence and uniqueness of solutions and on the self-consistency of the whole concept. It is demonstrated that breaking waves and fronts pose a severe problem, that can only be overcome if the hydrostatic approximation is given up and internal friction is added.

In Chapter 3 a set of layer integrated equations is derived starting from the Navier-Stokes equations. The equations describe budgets for mass, contaminant, momentum and turbulent kinetic energy. Turbulence, energy dissipation and entrainment are discussed, and an attempt to give precise definitions is made. The various steps in the derivation are accompanied by plausibility arguments. Although some of these may be characterized as 'hand-waving', they are the scientific basis of the model.

In Chapter 4 the principle of least action is introduced as a means of generating discrete equations for numerical models. In this framework discrete models automatically obey conservation laws and the hydrostatic approximation can be improved in a natural way. A numerical model called SLAM (Shallow LAyer Model) is presented. The model uses a triangular grid (sectioning the cloud into triangular prisms). SLAM has some distinct features compared to other shallow layer models:

- Explicitly account for the turbulent kinetic energy budget.
- The entrainment rate is estimated on the basis of the local turbulent kinetic energy.
- Non-hydrostatic pressure.
- A Lagrangian, moving grid.
- Numerical methods ensure conservation laws.

Thorney Island trial 8, an instantaneous isothermal release, is used as a reference case. The entrainment constants are tuned by means of concentration data from sensors located at several heights in order to reproduce the doughnut shape of the cloud. The results are in reasonable agreement with observations, even when a small number of cells (e.g. 16) is used.

Further data comparison is needed to validate the model.

Contracts No. EV5V–CT92–0069 (CEC)

The project was funded by the Environment and Climate Programme under D.G. XII of the Commission of the European Communities.

ISBN 87–550–2188–3
ISSN 0106–2840

Grafisk Service · Risø · 1997

Contents

1 Introduction

The work presented in this report was done as part of the Fladis field experiments project (Nielsen & Ott (1996)) under the CEC research programme ENVIRONMENT. The objective was to develop a shallow layer model for dense gas dispersion.

Shallow layer models are intermediate in complexity between box models and full 3D models. The motivation for having a shallow layer model is that it contains the essential dynamics of gravity induced flows, and thus should be able to deal with complex terrain at a modest computational cost compared to a 3D code. The main disadvantage is that the air-cloud interactions still have to be added 'by hand', where 3D models inherit the correct dynamics from the fundamental equations.

The idea is to use the shallow water equations as a starting point, since these have some desired features:

- Dynamical modeling of gravitational effects.
- Treatment of complex terrain.
- Relatively low computational costs (compared to 3D)
- Simplicity of model concepts.

The bare, frictionless shallow water equations accurately describe long waves in a shallow fluid layer. Dense gas tends to spread on the ground forming shallow clouds, so the analogy is obvious. There are, however, also some differences. The upper 'surface' of a dense cloud is generally not sharp, and mixing with the surrounding air will take place. The cloud is also generally turbulent and the vertical velocities may not be small compared to the lateral components. The two dimensional gravity induced spreading of the cloud is indeed predominantly horizontal, when we restrict our attention to large scales of the flow. At smaller scales (smaller than the cloud height) the flow is turbulent and three dimensional. A cloud model developed from the shallow water concepts should therefore only reproduce large scale features, since small scale shallow water motion (e.g. short waves) are not likely to represent the small scales of real clouds. Still the model must in some way take effects of turbulence into account. The incorporation of air entrainment and the representation of turbulent kinetic energy in the equations will be discussed in Chapter 3. The edges of a dense gas cloud, at places where the cloud intrudes into the ambient flow, are observed to be elevated and sharp. At the leading edge of a starting dense gas cloud a front vortex forms, which gives the cloud head a characteristic shape. The front vortex of an intruding edge is very much a three dimensional thing, which can not be represented directly in the two dimensional shallow water picture. Shallow water and dense clouds can, however, exhibit similar discontinuities in the form of bores and hydraulic jumps. The velocity of a travelling jump is controlled by the speed of gravity waves, which is about the same as observed velocity of dense gas fronts. Receding edges (upwind front of a puff or created by a shift of the wind direction) , are generally flat, without a characteristic vortex and leave a tail of gas stuck in the grass. This is an effect of the shear, which is absent in the shallow water picture.

The bare shallow water equations therefore possess useful features for dense gas modeling, but they will have to be modified at several points.

The primary purpose here is to investigate the potentials of the shallow water concept as a model, and try to find out how it works. In this context the word 'model' should not simply be understood as 'a collection equations', but more like a 'toy universe'. Thus we require that the equations form a self consistent

representation of the behaviour of a model system. In a self consistent mechanical universe we are able to use common knowledge of physics to reason on the behaviour of the system and to make changes of the design in order to make it work as closely as possible in parallel with the real system. We can also be sure always to arrive at the same solution to a problem independent of the angle of attack used. The behaviour of non-linear dynamical systems is extremely rich, and even very simple non-linear systems can do unexpected things. Therefore it is important to maintain a model universe that, at least, is not in conflict with itself. By defining a system that obeys the laws of mechanics and in which all material parts are following well-defined trajectories we should be able to limit unexpected and spurious behaviour.

One should also be concerned with the proper use and possible mis-use of models in practical risk analysis. Models are used intensively for risk assessments and eventually conclusions must be drawn from the way things work in the model universe. But no model is the real thing (that is why we call it a model), hence all models have unrealistic features. The best guidance to the proper use of a model and interpretation of its results is probably a solid understanding of how the model universe has been put together. This is not simply a matter of which equations were written down, which terms were neglected and which numerical methods were used.

2 Properties of the Shallow Water Equations

In this section we will discuss the simple shallow water equations describing an incompressible, inviscid fluid layer bounded from below by a rigid surface (the ground) and with an upper free surface. The upper surface is assumed to be completely sharp, like a water surface, and the pressure is assumed constant at the interface. There is no mixing and no friction, so it should not be regarded as a realistic model of dense gas clouds. We discuss this simple model here because it takes gravity into account and forms the backbone of more realistic models. In Chapter 3 a dense turbulent layer embedded in, and mixing with, a lighter ambient fluid will be considered.

At the start of the project some simple implementations of the shallow water equations were made. This was done in order to gain experience in solving the equations, to make numerical experiments and to learn about numerical difficulties. Most of these programs solve 1D problems. In many cases a simple solver works well, but it soon became clear that there are problems at the edges and when hydraulic jumps or bores develop. It is well known that the shallow water equations have such problems. Nevertheless it is sometimes stated that the shallow water equations have discontinuous solutions ('weak solutions'), and there exist numerical methods that can produce hydraulic jumps from the shallow water equations. We did not find hydraulic jumps using less advanced numerical methods. Instead we found that near discontinuities the solutions perform wild oscillations. Although these oscillations are indeed spurious (depending on grid size and discretization method) they did not seem to originate from a spurious source of mechanical energy. If the shallow water equations represent a self consistent mechanical system mechanical energy is conserved, while in reality energy is dissipated in a hydraulic jump. A numerical method capable of producing a hydraulic jump that does not oscillate must therefore introduce dissipation in a way that is not transparant to the model developer (or the user of the model). The question therefore arose whether these instabilities are simply numerical artefacts or if they are inherent in the model in some way, perhaps because the description is inconsistent. Speculations of this kind provoked an analysis, reported below, of the nature of the system described by the shallow water equations. The main purpose is to be able to introduce energy dissipation in a controlled way and to make a model system with well behaved fronts.

2.1 The model fluid

We assume that we have an incompressible inviscid fluid with constant density ρ. The fluid forms a layer with a free surface above it. The pressure is assumed to be zero at the upper surface. Such a system is governed by the Euler equations

$$\frac{\partial u}{\partial x}+\frac{\partial v}{\partial y}+\frac{\partial w}{\partial z} = 0 \tag{1}$$

$$\rho\left\{\frac{\partial u}{\partial t}+u\frac{\partial u}{\partial x}+v\frac{\partial u}{\partial y}+w\frac{\partial u}{\partial z}\right\} = -\frac{\partial p}{\partial x} \tag{2}$$

$$\rho\left\{\frac{\partial v}{\partial t}+u\frac{\partial v}{\partial x}+v\frac{\partial v}{\partial y}+w\frac{\partial v}{\partial z}\right\} = -\frac{\partial p}{\partial y} \tag{3}$$

$$\rho\left\{\frac{\partial w}{\partial t}+u\frac{\partial w}{\partial x}+v\frac{\partial w}{\partial y}+w\frac{\partial w}{\partial z}\right\} = -\frac{\partial p}{\partial z}-\rho g \tag{4}$$

The ground is described by a bottom code $b(x,y)$ and the free surface is assumed to be described by a function $h(x,y)$, which defines the local thickness of the layer. The boundary conditions are

$$\begin{aligned} w(x,y,h+b) &= \frac{\mathrm{d}(h+b)}{\mathrm{d}t} \\ &= \left\{\frac{\partial}{\partial t} + u(x,y,h+b)\frac{\partial}{\partial x} + v(x,y,h+b)\frac{\partial}{\partial y}\right\}(h+b) \quad (5) \\ w(x,y,b) &= \frac{\mathrm{d}b}{\mathrm{d}t} \\ &= \left\{u(x,y,b)\frac{\partial}{\partial x} + v(x,y,b)\frac{\partial}{\partial y}\right\}b \quad (6) \end{aligned}$$

For simplicity the bottom surface (the ground) will frequently be assumed to be horizontal ($b = 0$) in the following, even if this is not strictly necessary.

2.2 Derivation of the shallow water equations

We make use of the hydrostatic pressure approximation and replace (4) by

$$p(x,y,z) = \rho g(h(x,y) - z) \quad (7)$$

From (7) we see that

$$\frac{\partial^2 p/\rho}{\partial x \partial z} = \frac{\partial^2 p/\rho}{\partial y \partial z} = 0 \quad (8)$$

Differentiating (2) and (3) with respect to z and using (1) and (8) we get

$$\frac{\mathrm{d}}{\mathrm{d}t}\frac{\partial u}{\partial z} = \frac{\partial u}{\partial z}\frac{\partial v}{\partial y} - \frac{\partial u}{\partial y}\frac{\partial v}{\partial z} \quad (9)$$

$$\frac{\mathrm{d}}{\mathrm{d}t}\frac{\partial v}{\partial z} = \frac{\partial u}{\partial x}\frac{\partial v}{\partial z} - \frac{\partial u}{\partial z}\frac{\partial v}{\partial x} \quad (10)$$

Assume now that u and v are independent of z in the initial state. Since all other terms in (10) contain either $\frac{\partial u}{\partial z}$ or $\frac{\partial v}{\partial z}$ it follows, that $\frac{\partial u}{\partial z} = \frac{\partial v}{\partial z} = 0$ is a solution [1]. The solution has the property that all fluid particles initially located in a column over the same point will continue to move together as a vertical column. Since u and v are independent of z it follows from (1) that w is linear in z and it follows from (5) and (6) that

$$\frac{\partial w}{\partial z} = \frac{w(h+b) - w(b)}{h} = \frac{1}{h}\frac{\mathrm{d}h}{\mathrm{d}t} = \frac{1}{h}\left\{\frac{\partial h}{\partial t} + u\frac{\partial h}{\partial x} + v\frac{\partial h}{\partial y}\right\} \quad (11)$$

Inserting this into (1) and rearranging terms yields

$$\frac{\partial h}{\partial t} + \frac{\partial hu}{\partial x} + \frac{\partial hv}{\partial y} = 0 \quad (12)$$

This is the shallow water equation of continuity. Inserting (7) into (2) and (3) gives

$$\frac{\partial u}{\partial t} + u\frac{\partial u}{\partial x} + v\frac{\partial u}{\partial y} = -g\frac{\partial h}{\partial x} \quad (13)$$

$$\frac{\partial v}{\partial t} + u\frac{\partial v}{\partial x} + v\frac{\partial v}{\partial y} = -g\frac{\partial h}{\partial y} \quad (14)$$

[1] Strictly speaking this solution is only unique as long as the horizontal velocity derivatives are regular. If e.g. the fluid splashes against an obstacle it seems unlikely that the perfect vertical alignment of fluid elements will not be upset.

Using (12) this can also be written in the form:

$$\frac{\partial hu}{\partial t}+\frac{\partial uhu}{\partial x}+\frac{\partial vhu}{\partial y} = -gh\frac{\partial h}{\partial x} \quad (15)$$

$$\frac{\partial hv}{\partial t}+\frac{\partial uhv}{\partial x}+\frac{\partial vhv}{\partial y} = -gh\frac{\partial h}{\partial y} \quad (16)$$

(15) and (16) are the shallow water momentum equations.

In this derivation the hydrostatic approximation was made. In effect this approximation consists in neglecting the inertia terms in the vertical (w) momentum equations, which is justified when $\mathrm{d}w/\mathrm{d}t$ is small. In the middle of a flat and relatively calm dense gas cloud the approximation can be expected to give a good description of the mean flow. It may, however, not be justified at the cloud edges, in the presence of bores, if the cloud splashes against an obstacle etc. Applying the shallow water equations to such situations is not compatible with an assumption of $\mathrm{d}w/\mathrm{d}t$ being small. Below we shall give examples of solutions to the shallow water equations for perfectly 'shallow' initial conditions, which nevertheless develop discontinuities after a finite time. So even if we make sure that $\mathrm{d}w/\mathrm{d}t$ is arbitrarily small for the initial conditions it can not be avoided that $\mathrm{d}w/\mathrm{d}t$ becomes arbitrarily large later on. Therefore there is a conflict between the shallow water equations and the assumptions underlying their derivation.

We are obviously not asking for solutions for which $\mathrm{d}w/\mathrm{d}t = 0$. If this is to be regarded as a condition imposed *on the system* the equation has be added to the set of Euler equations, and we end up with a fluid that is unable to accelerate in the vertical direction. Although we can say that this defines a model system this is clearly too restrictive. Therefore we can not throw away the term $\mathrm{d}w/\mathrm{d}t$ in equation (4) and at the same time claim that the resulting equations represent a mechanical model system.

However, we can get rid of $\rho\mathrm{d}w/\mathrm{d}t$ by claiming that $\rho = 0$. The density appears elsewhere, but with different physical meanings. The laws of mechanics allow the inertial mass to be a tensor[2] so the various ρ's in the inertial terms may be regarded as different physical quantities. The ρ on the rhs, multiplied by g, represents gravitational mass, which is distinct from inertial mass, just as electric charge is it. We may therefore choose the inertial ρ to be a diagonal tensor with $\rho_{11} = \rho_{22} \equiv \rho_h$ and $\rho_{33} \equiv \rho_v$ and still have a mechanical model system (as long as both ρ_h and ρ_v are positive). Using the hydrostatic approximation represents a limiting case, since it means that $\rho_v = 0$. We can imagine a series of solutions for decreasing vertical inertia ρ_v. For $\rho_v \to 0$ a unique solutions to the (modified) Euler equations will exist. If the vertical acceleration remains finite as , so that $\rho_v \mathrm{d}w/\mathrm{d}t \to 0$, a *unique* hydrostatic solution is approached, which will obey the shallow water equations. This solution describes the behaviour of an inviscid fluid in a model universe where vertical inertia is zero, and hence the equations represent a (hypothetical) physical system. This may seem odd, but it is the only way to postulate that there is a model system behind the shallow water equations. But if $\mathrm{d}w/\mathrm{d}t$ becomes singular existence and uniqueness of solutions is no longer guaranteed. Futhermore the term $\rho_v \mathrm{d}w/\mathrm{d}t$ may not vanish in the limit. In the limit it is therefore not at all clear if there is model system behind the equations, and if there is the system has strange properties, that makes it hard to imagine how things work.

Thus the model system underlying the hydrostatic approximation may behave reasonably in many situations, but it may also suddenly turn bizarre. The primary concern here is to make a model system that is always well behaved. In section 2.4 some simple examples in which the equations break down will be discussed.

[2] As long as it is a positively definite tensor. It all amounts to redefining the kinetic energy as $1/2u_iM_{ij}u_j$. The point is that this leads to a self consistent description for which any properly posed problem has a unique solution. This will be discussed further in Chapter 4.

2.3 Conservation laws and discontinuities

The shallow water budgets for mass, momentum and energy can be written as

$$\left(\frac{\partial}{\partial t}+\frac{\partial}{\partial x_\beta}u_\beta\right)h = 0 \tag{17}$$

$$\left(\frac{\partial}{\partial t}+\frac{\partial}{\partial x_\beta}u_\beta\right)\rho h u_\alpha = -\frac{\partial \frac{1}{2}\rho g h^2}{\partial x_\alpha} \tag{18}$$

$$\left(\frac{\partial}{\partial t}+\frac{\partial}{\partial x_\beta}u_\beta\right)\left(\rho h(\frac{1}{2}u_\alpha u_\alpha+\frac{1}{2}gh)\right) = -\frac{\partial u_\beta \rho \frac{1}{2} g h^2}{\partial x_\beta} \tag{19}$$

Here, and in the following, greek subscripts always run from 1 to 2 and denote horizontal components, so that (u,v) is written as (u_1,u_2). We will also use the summation convention for repeated subscripts, so that $u_\alpha u_\alpha = u_1^2 + u_2^2$. Roman subscripts are used occasionally to indicate that the summation is over all three components. Note that the equations only contain horizontal components.

The energy equation (19) is not an independent equation. It is obtained after multiplication by u_α on both sides of the momentum equation (18) and use of 17. This is the usual way to derive an energy equation and it is done without additional assumptions (except for assumptions of differentiability). Note, that the vertical component u_3 turns out to be missing in the definition of the kinetic energy. This is consistent with the previous discussion of the nature of the hydrostatic approximation. If the vertical component of the momentum ($\rho_v u_3$) is zero there can be no kinetic energy associated with vertical motion, hence $1/2\rho_v u_3^2 = 0$.

The rhs of (18) is the exchange of momentum due to internal (pressure) forces, and the rhs of (19) is the exchange of energy due to work done by the pressure. Integrating both sides of these equations over the whole domain we see that, apart from input at the boundaries, the total volume, the total (lateral) momentum and the total energy of the system are conserved.

For a steady flow in one dimension over a horizontal surface the fluxes of mass, momentum and energy will be constants:

$$\rho h u = Q_m \qquad \text{(mass)} \tag{20}$$

$$\rho h\left(u^2+\frac{1}{2}gh\right) = Q_p \qquad \text{(momentum)} \tag{21}$$

$$\rho h\left(\frac{1}{2}u^2+gh\right) = Q_e \qquad \text{(energy)} \tag{22}$$

It is easy to see that for given values of the fluxes these equations have at most one solution: constant values of h and u. In real shallow water flows there can be hydraulic jumps, where h and u change values in a narrow region and have constants asymptotic values far to the left and to the right. A water mill can be represented by another kind of discontinuity (involving an external force). A bore is also possibility, but this can be regarded as a hydraulic jump, if we observe it in a moving coordinate system. In the hydraulic jump turbulence is generated and energy is lost, while the momentum can be regarded as conserved because the turbulence is mainly created by internal forces in the fluid. Therefore the conservation of energy, a consequence of the shallow water equations, is not realistic and the model has to be modified in order to account for the energy dissipation in the transition region. Hydraulic jumps and bores develop naturally after the breaking of waves, but the shallow water equations cannot handle such situations[3]. The

[3]It is sometimes stated that the shallow water equations have piecewise constant solutions, socalled 'weak solutions'. Such 'solutions' are not differentiable, so in order to maintain this view a generalization of the concept of differentiability would have to be invented. Conventional distributions (δ-functions etc.) do not work since products of distributions can not be defined. Therefore such 'solutions' do not seem to fit into any existing mathematical framework.

model system may 'try' to develop a jump, but it can only get rid of the kinetic energy by exiting small scale waves. A possible way out of this problem is to install internal friction into the model, and this will be discussed in Section 2.5.

The equations are symmetric with respect to rotations and translations as well as the scaling

$$\begin{aligned} h(x,y,t) &\mapsto h(\gamma x, \gamma y, \gamma t) \\ u_\alpha(x,y,t) &\mapsto u_\alpha(\gamma x, \gamma y, \gamma t) \end{aligned} \tag{23}$$

Using this transformation we can widen or narrow any solution. This means that there is no natural horizontal length scale. For real waves the ratio of the wavelength and h must be of importance, but apparently this is not so for solutions to the shallow water equations.

The equations are also invariant under a Gallilean transformation:

$$\begin{aligned} t' &= t \\ x'_\alpha &= x_\alpha - \mu_\alpha t \\ h'(x',t') &= h(x,t) \\ u'_\alpha(x',t') &= u_\alpha(x,t) - \mu_\alpha \end{aligned} \tag{24}$$

We also mention that

$$\left(\frac{\partial}{\partial t} + \frac{\partial}{\partial x_\beta} u_\beta\right)\left(\frac{\partial v}{\partial x} - \frac{\partial u}{\partial y}\right) = 0 \tag{25}$$

The quantity $\frac{1}{h}\left(\frac{\partial v}{\partial x} - \frac{\partial u}{\partial y}\right)$ is therefore a constant of motion for each fluid particle (conservation of angular momentum per unit mass in a 'pirouette').

2.4 Some analytic results

Below we give some simple examples illustrating problems with the shallow water equations. The examples have been chosen because they can be solved analytically. The purpose is to find out in more detail what goes wrong, and search for possible cures for the problems.

Example 1: Breaking wave

Consider for the moment the one-dimensional shallow water equations:

$$\frac{\partial u}{\partial t} + u\frac{\partial u}{\partial x} = -g\frac{\partial h}{\partial x} \tag{26}$$

$$\frac{\partial h}{\partial t} + \frac{\partial hu}{\partial x} = 0 \tag{27}$$

It is instructive to rewrite these equations in the following form:

$$\left(\frac{\partial}{\partial t} + (u + \sqrt{gh})\frac{\partial}{\partial x}\right)(u + 2\sqrt{hg}) = 0 \tag{28}$$

$$\left(\frac{\partial}{\partial t} + (u - \sqrt{gh})\frac{\partial}{\partial x}\right)(u - 2\sqrt{hg}) = 0 \tag{29}$$

The equations tell us, that the quantity $u + 2\sqrt{hg}$ is unchanged for an observer moving with velocity $u + \sqrt{hg}$, and that the quantity $u - 2\sqrt{hg}$ is unchanged for an observer moving with velocity $u - \sqrt{hg}$.

Suppose that the initial conditions are the following (where V is a constant)

$$h(x, t = 0) = h_0(x)$$

$$u(x, t = 0) \quad = \quad 2\sqrt{gh_0} + V \tag{30}$$

Then $u - 2\sqrt{hg} = V$ everywhere from the start, and, due to (29) this condition will continue to be valid for all $t > 0$ - unless we run into a singularity. Inserting $u = 2\sqrt{gh} + V$ into (28) we find that

$$\left(\frac{\partial}{\partial t} + (3\sqrt{gh} + V)\frac{\partial}{\partial x}\right) h = 0 \tag{31}$$

This tells us that h is unchanged for an observer moving with the (constant!) velocity $3\sqrt{gh} + V$. We must therefore have the relation

$$h(x, t) = h_0(x - (3\sqrt{h(x, t)g} + V)t) \tag{32}$$

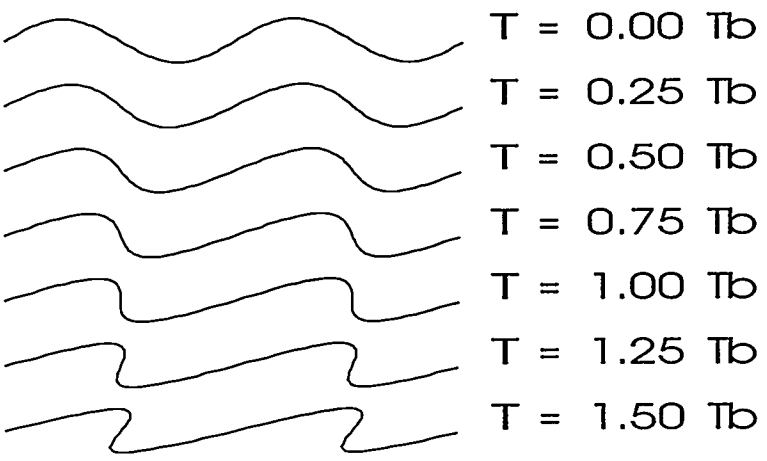

Figure 1. Analytical solution to the 1D shallow water equations.

A graphical solution is simple: First make a plot of $h_0(x)$ and then move each point (x, h_0) on the graph to $(x+(3\sqrt{gh_0}+V)t, h_0)$ in order to get the shape at time t. Figure 1 shows an example in which $h_0(x) = H + A\sin(kx)$ and $V = -2\sqrt{gH}$. For small values of A the solution approaches a fundamental mode of the linearized equations, so it will be a tiny traveling sine wave on top of an otherwise stationary fluid. This is not in any way a strange or pathological example - and we certainly would like our model to be able to handle it. The wave evidently breaks as the crests catch up on the troughs. This mechanism is likely to work in general, not just for the present example. The wave breaks at the time $t_b = \frac{2\sqrt{H}}{Ak\sqrt{g}}$. For very shallow waves t_b is long, and may not be of practical importance, but still it is not realistic that a tiny little ripple on the surface develops into a breaking wave. At $t = t_b$ the height becomes triple valued, and h is no longer a solution to the original equations, since it is no longer a function. The three branches (excluding the 'turning points') represent three individual solutions, but somehow we forgot to inform the surface in the middle, that the fluid is located above it, not underneath it. We also need to count the volume under the middle branch as negative in order to conserve mass. This clearly demonstrates that the equations do not have a solution beyond t_b. It is the end of the model universe, so to speak. The example indicates a flaw in the mathematical framework, since the layer is unable to fold.

Example 2: Breaking of a dam

The behaviour of the cloud edges should concern us, since here vertical accelerations are not small. Consider the following initial conditions:

$$\begin{aligned} h(x,t=0) &= \begin{cases} h_0 & \text{if } x<0 \\ 0 & \text{if } x>0 \end{cases} \\ u(x,t=0) &= \begin{cases} 0 & \text{if } x<0 \\ \text{irrelevant} & \text{if } x>0 \end{cases} \end{aligned} \tag{33}$$

The equations as well as the boundary conditions are invariant under the scaling given in (23). If there is a unique solution it therefore must obey

$$\begin{aligned} u(x,t) &= u(\gamma x, \gamma t) \\ h(x,t) &= h(\gamma x, \gamma t) \end{aligned} \tag{34}$$

for any $\gamma > 0$, and hence u and h must be functions of a single variable $s = x/t$. Inserting this into e.g. (28) and (29) the following solution is easily deduced:

$$\begin{aligned} h(x,t) &= \begin{cases} h_0 & \text{if } x/t < -\sqrt{gh_0} \\ h_0\left(\frac{2}{3} - \frac{x}{3t\sqrt{gh_0}}\right)^2 & \text{if } -\sqrt{gh_0} < x/t < 2\sqrt{gh_0} \\ 0 & \text{if } x/t > 2\sqrt{gh_0} \end{cases} \\ u(x,t) &= \begin{cases} 0 & \text{if } x/t < -\sqrt{gh_0} \\ \frac{2}{3}\left(\sqrt{gh_0} + \frac{x}{t}\right) & \text{if } -\sqrt{gh_0} < x/t < 2\sqrt{gh_0} \\ \text{irrelevant} & \text{if } x/t > 2\sqrt{gh_0} \end{cases} \end{aligned} \tag{35}$$

This is essentially the solution found by Benjamin (1968). It is worth noting that a solution in fact exists. Initially the discontinuity at the front gives rise to an infinite acceleration, but for all $t > 0$ the front edge is continuous, and it does not lead to a break down of the solution, since we are so lucky that the vertical alignment the fluid elements is not upset.

Example 3: Lock exchange

More generally we can consider a lock exchange flow with initial conditions

$$\begin{aligned} h(x,t=0) &= \begin{cases} h_0 & \text{if } x<0 \\ h_1 & \text{if } x>0 \end{cases} \\ u(x,t=0) &= 0 \end{aligned} \tag{36}$$

Here the argument that h and u must be functions of x/t is still valid, but there is no solution (if both $h_0 > 0$ and $h_1 > 0$). We must conclude, that the shallow water equations are unable to handle this situation. It is, however, not a break down of the inviscid hydrostatic model, because the problem actually has a solution. In order to see this we assume, without serious loss of generality, that $h_0 > h_1$. The solution is simply that the fluid below h_1 remains at rest at all times and serve as a floor for the fluid above it, so that $h - h_1$ will follow Benjamin's solution. This means that fluid columns are broken in two at $z = h_1$. The upper part of the fluid slides on top of the lower part, which remains at rest. This behaviour is not allowed by the shallow water equations, and therefore they have no solution.

The problem in the lock exchange flow is the discontinuity of the hydrostatic pressure, which gives the fluid at the front an infinite vertical acceleration. Such a discontinuity exists at the cloud edges if there is a front ($h > 0$). The laboratory experiments by Simpson & Britter (1980) show how the gravity current head is shaped by the ambient velocity profile. The cloud edges are elevated and sharp at

placed where the cloud intrudes into the ambient flow and more gradually growing up from $h = 0$ for receding edges. Therefore it seems to be a good idea that the model should be able to develop and maintain a sharp, discontinuous edge.

This is not achieved by installing friction into the model, unless the friction is a δ-function located at the front, which, from a numerical standpoint, is not tractable. Some models (e.g. DRIFT, Webber, Jones, Tickle & Wren (1992)) use a boundary condition specifying the front velocity (in still air) as

$$u_f = k_f \sqrt{\frac{\Delta \rho g h}{\rho_a}} \tag{37}$$

where $k_f \sim 1$. There is good experimental evidence for this relation, see Nielsen (1997) for a review of experiments. In the experimental results of Billeter (1996) a slight time (aspect ratio) dependence of the value of k_f can be seen, but for practical purposes (37) must be regarded as having a sound experimental basis. Choosing a boundary condition does not, however, help us with the lock exchange problem, because here the discontinuity is not located at the edge.

van Ulden (1986) uses an edge drag force of the form

$$F_D = \frac{1}{2} C_D h \rho_a u_f^2 \tag{38}$$

in his box model. This can to generalised to a bulk force (see Chapter 3) that can handle internal fronts as in the lock exchange flow. As long as the hydrostatic approximation is applied[4] the two approaches are equivalent, because material at the front will experience an infinite acceleration until F_D exactly balances the hydrostatic pressure drop, and we end up with (37). In real flows, on the other hand, discontinuities of the hydrostatic pressure are not forbidden, because it is the real pressure that counts. Therefore it seems to be a good idea to drop the hydrostatic pressure approximation. In Chapter 3 a simple, and computationally inexpensive, anhydrostatic approximation will be proposed.

2.5 Internal friction

The internal friction term represents work done by internal forces in the fluid, which convert energy of the mean flow to turbulence. It can be represented by an extra term in the momentum equation, viz.

$$h\rho \frac{\partial u_\alpha}{\partial t} + h\rho u_\beta \frac{\partial u_\alpha}{\partial x_\beta} = -g\rho \frac{\partial h}{\partial x_\alpha} + F_\alpha^{\text{int}} \tag{39}$$

The internal friction can be viewed as caused by fluid columns exchanging momentum. The absorption of momentum by a column can be regarded as an inelastic collision. Proceeding along these lines we could derive the expression for the form of the internal friction force from physical reasoning. The following mathematical argument gives the same result, and shows that we have little freedom in modeling F^{int}.

The total momentum will be conserved by internal forces, hence

$$\int F_\alpha^{\text{int}} \, dx dy = 0 \tag{40}$$

This must always hold even for initial conditions, where h can be specified. The only way is if F^{int} is a derivative, so that

$$F_\alpha^{\text{int}} = \frac{\partial \phi_{\alpha\beta}}{\partial x_\beta} \tag{41}$$

The internal friction must also be a dissipative process, so we must have

[4] Van Ulden does not use hydrostatic pressure in his model.

$$\int u_\alpha F_\alpha^{\text{int}}\,dxdy = \int u_\alpha \frac{\partial \phi_{\alpha\beta}}{\partial x_\beta}\,dxdy = -\int \frac{\partial u_\alpha}{\partial x_\beta}\phi_{\alpha\beta}\,dxdy < 0 \tag{42}$$

This is achieved if $\phi_{\alpha\beta}$ has the form

$$\phi_{\alpha\beta} = \rho h\, K_{\alpha\gamma}\frac{\partial u_\gamma}{\partial x_\beta} \tag{43}$$

and $K_{\alpha\gamma}$ is positively definite. K can be interpreted as an eddy viscosity, which can be modelled as a product of a turbulent length scale l and a turbulent velocity scale $\tilde{u}$, viz.:

$$K_{\alpha\gamma} = C_K \delta_{\alpha\gamma} l\tilde{u} \tag{44}$$

Alternatively we can choose

$$\phi_{\alpha\beta} = \rho h\, K\frac{1}{2}\left(\frac{\partial u_\alpha}{\partial x_\beta} + \frac{\partial u_\beta}{\partial x_\alpha}\right) \tag{45}$$

or linear combinations of (44) and (45) .

There is one interesting thing about the internal friction term, that should be mentioned. As noted above the bare shallow water equations do not have hydraulic jump solutions, because it would violate conservation laws. This situation changes when internal friction is added. To illustrate this we write the shallow water equations in 1D for a stationary flow as

$$\begin{aligned} u\frac{\partial u}{\partial x} &= -g\frac{\partial h}{\partial x} + \frac{1}{\rho h}\frac{\partial}{\partial x}Kh\frac{\partial u}{\partial x} \\ \frac{\partial hu}{\partial x} &= 0 \end{aligned} \tag{46}$$

For simplicity we can take K to be a constant, but weaker assumptions will also do. Due to the presence of a second order derivative these equations now have solutions[5] where u and h approach constant values in the limits $x \to \pm\infty$ with a (rounded) jump in between. The total mass and the total momentum are conserved, but the energy flux into the system is larger than the energy flux out of the system, the difference being equal to

$$\text{dissipation} = \int \rho K h\left(\frac{\partial u}{\partial x}\right)^2 dx \tag{47}$$

Now we make the scaling

$$\begin{aligned} u(x) \mapsto u'(x) &= u(\alpha x) \\ h(x) \mapsto h'(x) &= h(\alpha x) \\ K(x) \mapsto K'(x) &= \frac{1}{\alpha}K(\alpha x) \end{aligned} \tag{48}$$

The functions u' and h' are solutions to an equation similar form as (46), but with K replaced by K'. As α approaches ∞, K' approaches zero, and h' gains a progressively steeper jump, which eventually becomes a discontinuity (see figure 2). The total dissipation, however, is unchanged since

$$\int K'h'\left(\frac{\partial u'}{\partial x}\right)^2 dx = \int Kh\left(\frac{\partial u}{\partial x}\right)^2 dx \tag{49}$$

Note that the integrand vanishes at all points (except one, perhaps) as $\alpha \to \infty$, but the integral remains the same. Therefore the dissipation term formally disappears from the equations as $K' \to 0$, but the dissipation stays. We add a term, set it

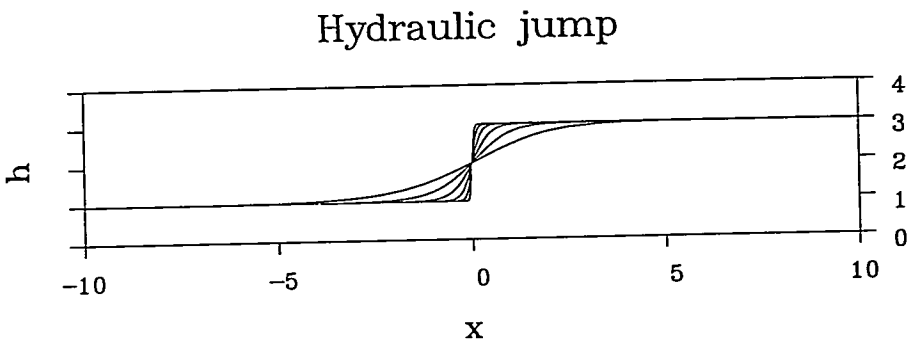

Figure 2. Static hydraulic jump solutions to the shallow water equations with internal friction added. The curves illustrate the limit $K \to 0$, where the jump approaches a sharp step.

equal to zero, and, voila, energy is no longer conserved! Such a term we will refer to as an 'invisible hand'.

The internal friction term we have constructed allows for hydraulic jump solutions that preserve mass and momentum, but not energy. This is usually taken to be appropriate for real hydraulic jumps. We could have obtained different jumps by adding a term of the form $Kh\nabla^2 u$, which is another example of an invisible hand. Letting $K \to 0$ this one leads to stationary solutions that preserve energy, but not momentum.

An invisible hand that dissipates energy seems to be a good idea, and it might be even better to include a finite (visible) internal friction term. The second example of an invisible hand is one that we should be avoided, because it implies an external force (external forces should be applied explicitly, not implicitly).

Figure 3 shows the results of a numerical solution to the breaking wave problem with a small internal friction included in the model (see Section 4.2 for more details). The improvement is obvious when figure 3 and figure 5 are compared.

Osher & Sweby (1987) pointed out that the popular flux corrected transport scheme of (Zalezak (1981)) in effect uses invisible hands to obtain discontinuous solutions. In short the flux corrected transport method is to switch to a low order numerical differentiation in regions where gradients are steep. The low order scheme will develop a stable jump, because of the presence of an invisible hand. Away from discontinuities a higher order scheme is assumed to be better, but at the jump it is unstable because it conserves energy.We shall not use flux corrected transport, because physical attributes are added to the system via the numerical solution method in a complicated way, making it difficult to write down the kinetic energy budget. It would also be rather tedious to verify that the right conservation law (energy) is broken by the invisible hand.

2.6 Summary of results

The results of the analysis of the bare shallow water equations can be summarized as follows.

[5] (46) leads to the equation
$\frac{K}{\rho\sqrt{g}}\sqrt{2h_1h_2(h_1+h_2)}\frac{\partial h}{\partial x} = -(h+h_1+h_2)(h-h_1)(h-h_2)$
where h_1 and h_2 are the two asymptotic values of h.

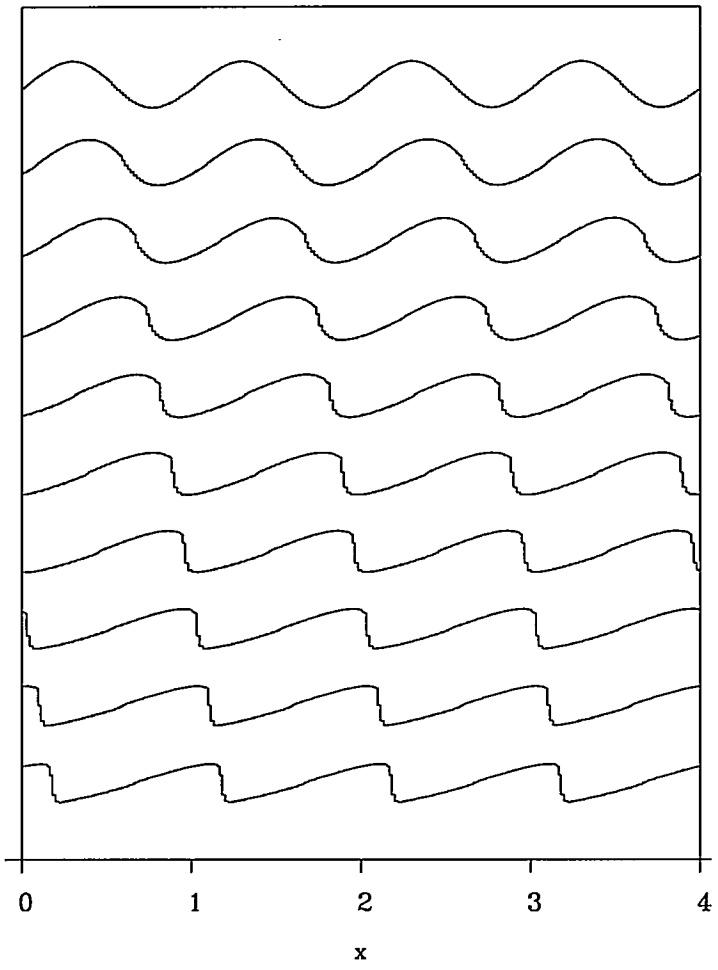

Figure 3. Numerical solution to breaking sine wave problem with internal friction (the model is discribed in Section 4.2). Upper curve: $t = 0$. Lower curve: $t = 2t_b$.

- Solutions to the shallow water equations can be characterized as a class of non-turbulent flows, which are also solutions to the Euler equations in the hydrostatic approximation.
- The hydrostatic approximation is not always justified for dense gas clouds, e.g at cloud edges.
- The class of flows has unwanted features. Thus
  - Initial conditions to the shallow water equations can be given for which there is no solution.
  - Initially 'shallow' conditions may develop singularities after a finite time.
- The shallow water equations do not have solutions with discontinuities. This rules out formation of hydraulic jumps, bores and elevated cloud fronts.
- Singularities are associated with discontinuities of the hydrostatic pressure. They should disappear if the hydrostatic approximation is given up.

- The (bare) shallow water equations conserve energy, but energy dissipation is essential for dense gas clouds. The inclusion of an (arbitrarily small) internal friction term solves this problem.

3 Layer integrated equations

In this section we will deduce a set of layer integrated equations for a dense gas cloud. The equations are budgets for

- momentum
- mass
- contaminant gas
- turbulent kinetic energy

The enthalpy budget will not be considered here, although it would not be difficult to include it. Hence the model is limited to isothermal releases.

A main objective of this work is to include turbulent kinetic energy in a layer integrated model, since is seems that this has not been done before. Considering the turbulent kinetic energy budget in dense gas models is not new. Thus the box models of van Ulden (1986) and Webber & Wheatley (1987) include turbulent kinetic energy. The idea of including it in a shallow layer model dates (at least) back to Wheatley & Webber (1984).

We will refer to equations derived by layer integration as 'layer integrated equations' and let 'shallow water equations' refer to the inviscid equations derived in Chapter 2.

3.1 Definitions

Real clouds are entangled with the air above it in a complicated way. The top 'surface' is extremely complex, and probably best described as a fractal, but we wish to avoid such complexity in the model. Therefore we choose $h(t,x,y)$ to be a smooth function defining an envelope under which the cloud material is located. In general there will be an ensemble of flows, differing only in the details of small scale structures, all compatible with the same smooth envelope defined by h. For this ensemble we define a Reynolds decomposition of variables

$$Q = \overline{Q} + Q' \tag{50}$$

where $\overline{Q}$ is the ensemble average and Q' is the fluctuating part. Note that $\overline{Q}$ is generally time dependent and that, by definition of the ensemble, $h' = 0$.

In any individual realization matter will pass through the top surface. The vertical volume flux, better known as the entrainment velocity, w_e, is defined by the equation

$$\frac{\partial h}{\partial t} + \overline{u}(h) \cdot \nabla h = \overline{w}(h) + w_e \tag{51}$$

The definition of w_e is closely linked to the definition of h. We have chosen h to be above the cloud in order to make sure that w_e is positive, so that matter passes from outside *into* the cloud in consistency with the notion of *en*trainment. However, we should not take h to be extremely large, rather it should be 'just above' the cloud. Admittedly, this description of h is somewhat imprecise. It can be a matter of interpretation precisely how h is be measured, so h is not an observable. This lack of precision reflects on the 'definitions' of w_e and the Reynolds decomposition. Messing up definitions and model assumptions is a bad habit, because the use of un-observable variables prevents unambiguous experimental tests of models. A more stringent measure of the cloud height is the height of the centroid z_c

defined as [6]

$$z_c = \frac{\int_0^\infty z\Delta\rho\, dz}{\int_0^\infty \Delta\rho\, dz} \tag{52}$$

where $\Delta\rho = \rho - \rho_a$ is the difference between the local density and the density of the ambient air. It therefore seems a better suggestion that h be defined as $\frac{z_c}{\beta}$, where β is a constant. This makes h an observable, but the problem is not fully solved, since we have to claim that this defines a cloud envelope covering all the released material (we make use of this in the following). But if we want to be absolutely certain that no material escapes from the envelope, we must use a very small value of β. This will water down the concept of a layer average and weaken the predictive power of models based on it. Therefore β should be large, but small enough to enable us to argue (in principle verify experimentally) that the role of deportment is insignificant. In the following we shall use both definitions interchangeably, and treat β as a model parameter. We merely note here that this involves a postulate.

Experimental mean density profiles tend to look like something between gaussians and exponentials - perhaps more gaussian at the bottom and more exponential at the top. In a review of mixing experiments Britter (1988) suggests that most concentration profiles obtained in the laboratory are well reproduced by the form $C(z) = C_{max}\ \exp(-Az^n)$. In laboratory experiments Britter & Snyder (1988) found $n \approx 1.5$ for passive plumes and $n \approx 1$ for dense gas plumes. The parameter n shapes the profile both at the top and at the bottom, so n probably depends on the fitting procedure. The main differences between dense gas and passive gas are found at the bottom, while the tails of the concentration profiles (at the top) are hard to distinguish. For field data the instantaneous (1-10 s average) dense gas profiles are found to be somewhat irregular, but by and large triangular. There is a strong vertical correlation of fluctuations so that the profile mostly fluctuates 'as a whole' keeping a fairly triangular shape (see Nielsen (1997)). The mean profiles are well described as exponential ($n = 1$). The kind of profile that we are interested in here is the mean profile given a certain cloud height (in fact given the history of $h(x, y, t)$ everywhere). This profile can be expected to be sharper at the top than profiles averaged unconditionally (over different heights). The mean of an ensemble of triangles (with different heights) may become close to an exponential, so a triangular profile (for a fixed value of h) is probably quite realistic. The triangular profile corresponds to $\beta = \frac{1}{3}$. The most popular choice is $\beta = \frac{1}{2}$ corresponding to a top hat (rectangular) profile. It should be noted, however, that experimental evidence contradicts the picture of a dense gas cloud as well mixed layer well separated from the surrounding flow by a sharp interface. (Britter & Snyder (1988)) compared neutral and dense gas plumes released under similar conditions and found roughly gaussian profiles in both cases. The vertical dense gas concentration profiles measured by Britter & Snyder (1988) are even less 'top hat' than corresponding neutral profiles. A top hat density profile is therefore not consistent with observations. The shallow layer equations we are about to derive will not be very sensitive to the choice of density profile (represented through β), but the interpretation of model results in terms of concentrations at specific locations is. In this respect better results are obtained for triangular or exponential profiles than for a tophat profile. I should be noted that van Ulden (1987) found $n = 0.5$ to be the best fit to the laboratory data of Havens & Spicer (1985) (instantaneous release in still air), so a very strong belief in universal values of n and

[6] Other definitions of h (and thereby of w_e) are sometimes used, when profile data are not available. Thus Stretch (1986) uses $h = \int \Delta\rho dz / \Delta\rho(z = 0)$.

β may not be justified.

Below we will make a layer integrated model. For this purpose we define the layer average (or depth averages) $[Q]$ of a quantity Q (which in general will be a function of x and y):

$$[Q] \equiv \frac{1}{h}\int_b^{h+b} Q(x,y,z)dz \tag{53}$$

The corresponding fluctuating part of Q will be denoted $\hat{Q}$ ($\equiv Q - [Q]$).

In general the layer averaging does not commute with differentiations, because extra terms are generated. For example:

$$\begin{aligned}\frac{\partial}{\partial t}[Q] &= \left[\frac{\partial Q}{\partial t}\right] + \frac{Q(x,y,h+b)-[Q]}{h}\frac{\partial h}{\partial t}\\ \frac{\partial}{\partial x}[Q] &= \left[\frac{\partial Q}{\partial x}\right] + \frac{Q(x,y,h+b)-[Q]}{h}\frac{\partial h}{\partial x}\\ &\quad + \frac{Q(x,y,h+b)-Q(x,y,b)}{h}\frac{\partial b}{\partial x}\end{aligned} \tag{54}$$

We note the following relation valid for any Q

$$h\left[\frac{\partial Q}{\partial t} + \nabla\cdot uf\right] = \frac{\partial}{\partial t}h[Q] + \nabla\cdot h[uQ] - Q(h)(w_e - w'(h) + u'(h)\cdot\nabla h) \tag{55}$$

Here most boundary terms cancel due to the boundary conditions (5) and (6).

Equation (55) holds for each individual flow in the ensemble specified by the common function h, but we will seek equations for layer averaged *and* ensemble averaged quantities. To this end we define the combined average and corresponding fluctuating part of a variable Q as

$$\begin{aligned}\{Q\} &\equiv \overline{[Q]} = [\overline{Q}] = \frac{1}{h}\int_0^h \overline{Q}\,dz\\ \tilde{Q} &\equiv Q - \{Q\} = [Q'] + \hat{\overline{Q}} + \hat{Q}'\end{aligned} \tag{56}$$

The two kinds of averages obviously commute since $h' = 0$. Note that the combined average $\{Q\}$ is time dependent, and it will contain the spatial structure of the flow imposed by the particular movements of the top surface, at least as far as these are resolved by the model equations. The fluctuating part $\tilde{Q}$ can therefore be expected to be somewhat smaller than fluctuations based on time averages. Taking the ensemble average of (55) we get

$$h\left\{\frac{\partial Q}{\partial t} + \nabla\cdot uQ\right\} =$$

$$\frac{\partial}{\partial t}h\{Q\} + \nabla\cdot h\{uQ\} - \overline{Q}(h)w_e + \overline{Q'(h)w'(h)} - \overline{Q'(h)u'(h)}\cdot\nabla h \tag{57}$$

This relation is very useful for generating layer averaged equations.

The layer average of a (perfect) logarithmic profile is equal to [7]

$$\{u\} = \frac{1}{h}\int_0^h \frac{u_*}{\kappa}\log(z/z_0)\,dz = \frac{u_*}{\kappa}\log(h/z_0) - \frac{u_*}{\kappa} \tag{58}$$

The fluctuations around the mean are independent of h:

$$\{\tilde{u}^2\} = \left(\frac{u_*}{\kappa}\right)^2 \tag{59}$$

[7] log mean natural logarithm

Surface layer profiles are only logarithmic on the average, and (59) will therefore contain an additional contribution from turbulent fluctuations. However, fluctuations at different heights are correlated, and instantaneous wind profiles often look logarithmic, and such fluctuations will be incorporated in $\{\tilde{u}^2\}$. Therefore 59 can be expected to be fairly accurate even for a real fluctuating wind profile.

3.2 Turbulence

Turbulence is an essential ingredient in dense gas dispersion modeling, since it is responsible for the mixing of the cloud with the surrounding air. The general understanding is that shear in the mean flow produces turbulence at 'large' length scales and that the turbulent kinetic energy is cascaded to fine scales, where it is dissipated into heat by viscous forces. In dense gas clouds the stable density stratification in the top leads to damping of the turbulence and hence to a reduced mixing compared to the mixing of a passive contaminant. The damping can be seen as a result of shifting the centre of gravity of the cloud upwards in the course of the mixing, which represents a sink of turbulent kinetic energy. A second effect of the stratification is the reduction of the length scale of the turbulence. For a passive contaminant the cloud height is, loosely speaking, determined by the largest eddy within the cloud. For a dense gas cloud the available amount of kinetic energy per unit mass may be too small to lift dense material from the bottom of the cloud to the top against the buoyancy forces. Therefore large eddies will be smaller than the cloud height, and the mixing of top and bottom material must take place as a series of turbulent 'events'.

Assuming a Kolmogorov spectrum with a lower cut-off, the dissipation, ϵ, and the turbulent kinetic energy, e, are related as follows (e.g. Tennekes & Lumley (1972))

$$e \sim \int_{1/l}^{\infty} \epsilon^{2/3} k^{-5/3}\, dk \sim (\epsilon l)^{2/3} \qquad \text{or} \qquad \epsilon \sim \frac{e^{3/2}}{l} \tag{60}$$

where l represents the scale of energy containing eddies. The reduced length scale therefore leads to an increase of dissipation for a given level of turbulent kinetic energy.

The mean velocity profile is also affected because the turbulent diffusion of momentum is reduced. According to standard Monin-Obukhov theory (see e.g. Panofsky & Dutton (1984)) the velocity profile for a constant flux layer [8] is given by

$$\frac{dU}{dz} = \frac{u_*}{\kappa}\left(\frac{1}{z} + \frac{C_L}{L}\right) \tag{61}$$

where $C_L \sim 5$ (J.A. Businger & Bradley (1971)) and the Monin-Obukhov length L is given by

$$L = \frac{u_*^3 \rho_a}{\kappa g \overline{w'(\rho - \rho_a)}} \tag{62}$$

Thus the shear is larger in a stable layer than in a neutral layer exposed to the same stress. In most situations the cloud velocity does not exceed the velocity of the ambient flow, so there is a limit to how large the stresses in the dense layer can be. Therefore the stress (u_*) is probably not constant through the layer and the situation becomes complicated. One of the lessons learned from the Thorney Island trials is that cloud advection speed is consistently slower than the undisturbed wind speed. Wheatley & Prince (1987) found that the the cloud speed is only about half of what could be expected from a simple momentum balance. An abnormally

[8] A dense gas cloud is not a constant flux layer, since the buoyancy flux differs from bottom to top.

high bottom friction is not a likely explanation, so the wind speed at the top of the cloud (the lateral speed of the entrained air) must be less than the undisturbed wind speed. Turbulence measurements show, as expected, a considerable reduction inside the cloud, but reduced turbulence levels at positions well above the cloud ($z \sim$ 2-3 times h) are also seen (Mercer & Davies (1987)). Similar observations were made during the Lathen trials (unpublished). This indicates that the flow in the region above the cloud is affected by its presence in a non-local way. Local Monin-Obukhov theory, based on a local value of L, would for example not work, because $\overline{w'\rho'} = 0$ high above the cloud.

For a Monin-Obukhov profile the layer averaged shear production of turbulent kinetic energy, π, is given by

$$[\pi]h = \int_0^h u_*^2 \frac{dU}{dz}\, dz = \frac{u_*^3}{\kappa} + C_L B \tag{63}$$

where, for a horizontally uniform layer, we find[9]

$$B = \frac{g}{\rho_a}\int_0^h z\frac{\partial\overline{\Delta\rho}}{\partial t}\, dz = \frac{g}{\rho_a}\frac{\partial}{\partial t}\int_0^h z\overline{\Delta\rho}\, dz = \frac{gh[\Delta\rho]}{\rho_a}\frac{dz_c}{dt} = \beta\frac{gh[\Delta\rho]}{\rho_a}w_e \tag{64}$$

where $z_c = \beta h$ is the height of the centroid. Note that B is equal to the buoyant destruction of turbulence due to the lifting of the centre of mass. Thus for a given stress (u_*), the shear production increases with stability, and the increase is about 5 times larger than the buoyant destruction. In steady state (which we may not have) we can equate dissipation and net production:

$$[\epsilon]h = [\pi]h - B = \frac{u_*^3}{\kappa}\log(h/z_0) + (C_L - 1)B \tag{65}$$

This result uses local theory (L is determined by local values), which is questionable. Nevertheless, it must be safe to conclude, that both dissipation and shear production are increased compared to the neutral case (with the same u_*). Under the more general, transient, conditions only the difference between production and dissipation counts, and the net effect may be small. Therefore we choose to neglect the effect and model the dissipation as[10]

$$[\epsilon]h = C_\epsilon \tilde{u}^3 \log(h/z_0) \tag{66}$$

Here we have used $\tilde{u}$ instead of u_*/κ. In order to get the correct passive limit $C_\epsilon = \kappa^2 = 0.16$.

The shear production is represented in the model by four terms: top friction, bottom friction, internal friction and an inelastic collision term. The bottom friction is equal to $\rho {u_*}^2$ evaluated at the bottom of the cloud, and both $\kappa\tilde{u}$ and $\kappa u/\log(h/z_0)$ are candidates as a substitutes for u_*. The simplest way to get a vector is to use a combination of both and write the bottom friction as

$$F_\alpha^{bot} = -C_f\,\{\rho\}\tilde{u}\frac{\{u_\alpha\}}{\log((h+z_0)/z_0)} \tag{67}$$

This introduces the roughness length into the model in a natural way. The value of C_f should be close to 1.

The top friction is caused by the velocity gradient at the top of the cloud, so it is natural to take it to be proportional to the velocity difference between the cloud and the ambient flow.

$$F_\alpha^{top} = C_f\,\rho_a\tilde{u}(u_{top\alpha} - \{u_\alpha\}) \tag{68}$$

[9] using $\int \overline{\Delta\rho w'}\, dz = -\int z\frac{\partial}{\partial z}\overline{\Delta\rho w'}\, dz$ and $\frac{\partial\overline{\Delta\rho}}{\partial t} + \overline{\Delta\rho w'} = 0$.

[10] We take the liberty of writing $\tilde{u}$ instead of the correct (but clumsy) notation $\sqrt{\{\tilde{u}^2\}}$.

We recall that for a logarithmic profile we have $u(h) = \{u\} + u_*/\kappa$ and $\{\hat{u}^2\} = u_*^2/\kappa^2$ so that $F^{top} = \rho_a C_f \tilde{u}^2 = -F^{bot}$. We must therefore use the same constant for both top and bottom friction in order to ensure conservation of momentum. We mentioned above that the turbulence is attenuated even well above the dense gas clouds show, and hence u_* of the undisturbed flow is not relevant as a boundary condition at the cloud top. Using the ambient u_* would also give problems when $u_a = 0$. It could be argued that (68) should include a Richardson number dependence. However, such a correction has little effect since the main contribution to the momentum comes from the momentum of the entrained air. It seems natural to assume that the velocity of the entrained air u_{top} is equal to the ambient velocity (evaluated e.g. at $z = h$), but it is generally accepted that this value is too high in an acceleration phase. The following expression

$$u_{top} = \frac{1}{2}\left(\left(C_a + \frac{1 - C_a}{1 + C_b \widetilde{Ri}}\right) u_a(h) + \{u\}\right) \tag{69}$$

where u_a is the undisturbed velocity profile, $C_a \sim 0.8$ and $C_b \sim 10$ gave good results for Thorney Island trial 8.

3.3 The entrainment rate

The mixing process takes different forms depending on the strength of the density gradient (or rather: Richardson number). For very large density differences the turbulence almost completely dies out, and takes the form of gravity waves[11]. In that case the dominant mixing process is breaking waves or formation of cusps on wave crests. This type of mixing is very inefficient since oscillatory motion does not in itself lead to dispersion. However, this extreme situation is not representative for most accidental releases, since the production of turbulent kinetic energy at the source generally causes considerable mixing before the turbulence is damped by the stratification. Visual observations of dense gas clouds confirm that the turbulence has the character of three dimensional eddies rather than waves, and that engulfment of ambient air is a dominant mixing mechanism. According to Bo Pedersen (1980) laser sheet visualizations of plane jets made in the laboratory show that the mixing is caused by the coalescing of vortex pairs, and this is more likely to be the mechanism in dense gas clouds than breaking gravity waves. The energy required to bring a parcel of air into the cloud may still be large compared to the available turbulent kinetic energy. The energy required to bring a parcel of air the distance l' into the cloud is, roughly speaking, $\Delta\rho g l'$, where $\Delta\rho$ is a typical density difference. The kinetic energy available to do the job is something like $\rho\tilde{u}^2$, and equating the two we get

$$l' = \frac{\rho\tilde{u}^2}{\Delta\rho g} \equiv \frac{h}{\widetilde{Ri}} \tag{70}$$

where we have defined the Richardson number $\widetilde{Ri} \equiv \frac{\Delta\rho g h}{\rho\tilde{u}^2}$. Typically l' will be somewhat smaller than h, but of comparable magnitude. The initial downward motion of the fluid parcel will be decorrelated by two processes: the buoyancy force (length scale l') and the presence of the ground (length scale h). When $\widetilde{Ri}$ is large (l' is small compared to h) the entrainment can be regarded as being a result of many independent processes in analogy with collisions in molecular diffusion. Making the analogy to molecular diffusion, the diffusivity can be written as $v^2\Delta t$, where v is the particle velocity and $\frac{1}{\Delta t}$ is the collision rate, i.e. the rate at which v becomes decorrelated. If several (independently random) collision/decorrelation processes take place the rates are additive. In our case we identify $v = \tilde{u}$ and we

[11] Gravity waves should perhaps not be regarded as turbulence.

have two 'collision' processes with rates $\frac{\widetilde{u}}{l'}$ and $\frac{\widetilde{u}}{h}$, respectively. This should give a diffusivity something like

$$K \approx \frac{C_e \widetilde{u}}{\frac{1}{h} + \frac{C'}{l'}} \tag{71}$$

Comparing this to (44) we get the estimate

$$l = \frac{1}{\frac{1}{h} + \frac{C'}{l'}} = \frac{h}{1 + C'\widetilde{Ri}} \tag{72}$$

Loosely speaking w_e is the effective drift velocity of air into the cloud, and, as an order of magnitude estimate, we will write it as $w_e = \frac{h}{t_e}$, where t_e is the average time required to reach from the top to the bottom of the cloud. Treating the entrainment as essentially a diffusion process we have $h^2 \sim Kt_e$, so that $w_e \approx K/h$ or

$$w_e = \frac{C_w \widetilde{u}}{1 + C_R \widetilde{Ri}} \tag{73}$$

A relation of this form was proposed by Eidsvik (1980), and is used in many dense gas models (e.g. DEGADIS, Havens & Spicer (1985)). The experimental support mainly stems from laboratory experiment (e.g. Kantha, Phillips & R.S.Azad (1977), McQuaid (1976), Stretch (1986)). Britter (1988) gives asymptotic values for the entrainment rate in the neutral and strongly stratified limits from which the empirical constants in (73) can be determined. Britters recommendations are based on $[u]$ or u_* (measured either inside or above the layer) as the characteristic velocity in the numerator and in the definition of the Richardson number. In (73) $\widetilde{u}$ enters as the characteristic velocity, but it is probably consistent with the experimental results from channel flows. In a channel flow all characteristic velocities tend to become constant along the flow and hence also to have constant ratios. Definitions of h also vary, so the constants must be adjusted accordingly. We propose to use $\widetilde{u}$ as the characteristic velocity, because $\widetilde{u}$ is a direct measure of the amount of kinetic energy available for the mixing process[12].

Many box models employ both top-entrainment and edge-entrainment, so that the growth of the cloud volume is written as

$$\frac{\mathrm{d}V}{\mathrm{d}t} = \pi R^2 w_e + 2\pi R H u_e \tag{74}$$

where the edge entrainment velocity u_e is modelled as

$$u_e = C_e \frac{\mathrm{d}R}{\mathrm{d}t} \tag{75}$$

with $C_e \sim 0.15$ (Simpson & Britter (1979)). Reviewing box model estimates of top- and edge-entrainment and data and from the instantaneous releases of Thorney Island Phase I, Brighton (1987) found that the contribution from edge-entrainment dominates that from top-entrainment in the initial phase of large scale releases. Top-entrainment first takes over when the concentration drops below some fraction of a percent. Thus box models essentially explain the Thorney Island data by means of edge-entrainment. Using only top-entrainment determined by (73) leads to vast overpredictions of concentrations. Nevertheless, we intend to model the entrainment as top-entrainment only and use (73) with $\widetilde{u}$ as the velocity scale. The reason why edge-entrainment need not be modelled explicitly is that $\widetilde{u}$ automatically grows large at the cloud edges, so that edge entrainment can be considered as an integral part of the model.

[12] It includes the energy that can be produced by inelastic collisions of fluid parcels from different places in the velocity profile.

In box models the concentration, as well as other quantities characterising the cloud, is represented by a single average value taken over the cloud volume. Therefore the redistribution of entrained air within the cloud is not considered, as it is merely counted as being either inside or outside the cloud. In real clouds air entrained at the cloud edge does not immediately affect concentrations near the cloud centre. The same is true in shallow layer models and other models that deal with a sectioned cloud. After a few hundreds of seconds the instantaneous releases of Thorney Island formed clouds some 5 or 10 meters high and several hundred meters wide, and transport of material the long distance from the edge to the centre is not likely to have had a large effect. Therefore concentrations near the centre must still be determined by top-entrainment. The main reason for the failure of box models with only top-entraiment in explaining the Thorney Island data is probably that they base the Richardson number on an *average* cloud height. In the trials clouds were observed to have a doughnut shape, so that the cloud is considerably more shallow near the centre than at the edges. Basing Ri on the local height may therefore solve the problem.

3.4 Layer integrated equations

The shallow water equations were derived as special solutions of the Euler equation describing a fluid mono-layer. We shall now derive a similar set of equations for a two-fluid system starting from the Navier-Stokes equations and conservation laws for mass and for the two fluid species. Heat transfer and chemical reactions are not considered. In addition we assume incompressibility and disregard molecular diffusion (but keep viscosity). This gives the following set of basic equations

$$\frac{\partial \rho u_i}{\partial t} + \nabla \cdot u\,\rho u_i = -\nabla P + \eta \nabla^2 u_i + \rho g_i \tag{76}$$

$$\frac{\partial \rho}{\partial t} + \nabla \cdot u\rho = 0 \tag{77}$$

$$\nabla \cdot u = 0 \tag{78}$$

Note that (77) and (78) imply that ρ is constant along a streamline. The two fluids are of course the air and a heavy contaminant gas. The molar (volume) concentration of the contaminant is equal to $C = \frac{\rho - \rho_a}{\rho_0 - \rho_a}$, where ρ_a is the density of the ambient air and ρ_0 is the density of the concentrated dense gas. We will prefer to work with ρ rather than C[13].

The idea is to write down equations relating the layer averaged quantities $\{\rho\}$, $\{u\}$, $\{\tilde{u}^2\}$ and h. Layer averages are taken over the cloud volume, so no attempt is made to determine the flow outside the cloud. The boundary terms left over from the layer averaging are the only links between the cloud and the surrounding air, and they will have to be estimated in some way. The determination of the entrainment rate is also taken as a separate problem although in principle w_e is hidden in the basic equations. In addition closure assumptions are used to estimate higher order moments such as $\{\rho u\}$ etc. Making these estimates is the crucial part of the process, and there is some room for creativity in making them. For this reason the derivation is given in some detail. Some of the terms were discussed in the preceding paragraph.

[13] We are taking advantage of the assumption that the cloud is isothermal. Generally there will be density effects when the cloud and the air has different temperatures, and buoyancy will not be conserved. Thus a cold natural gas cloud may change from positive to negative buoyancy when it is mixed with hotter air. This is because natural gas, like many other substances, has a larger molecular specific heat than air.

Volume

It is convenient to use the general conservation equation (57) to generate the equations. Inserting $Q = 1$ in (57) and using (78) yields

$$\frac{\partial}{\partial t}h + \frac{\partial}{\partial x_\beta}h\{u_\beta\} = w_e \tag{79}$$

This equation is exact, so it is a matter of taste whether to use (79) or (51) to define w_e.

Mass

Inserting $Q = \rho$ and using (77) yields

$$\frac{\partial}{\partial t}h\{\rho\} + \frac{\partial}{\partial x_\beta}h\{\rho u_\beta\} = \rho_a w_e \tag{80}$$

In this equation we replace $\{\rho u\}$ by $\{\rho\}\{u\}$ and write it as

$$\frac{\partial}{\partial t}h\{\rho\} + \frac{\partial}{\partial x_\beta}h\{\rho\}\{u_\beta\} = \rho_a w_e \tag{81}$$

In (81) turbulent diffusion in the horizontal directions has been neglected, and so has the fact that the density is higher at the bottom of the layer, where the velocity is low. In reality the average advection speed of mass must therefore be smaller than $\{u\}$. The replacement of $\{\rho u\}$ by $\{\rho\}\{u\}$ may not be as innocent as it seems, because it prevents lateral redistribution of matter due to velocity shear, which is probably important in the front region. Simpson & Britter (1979) made a detailed study of the flow in a the gravity current head, showing that material is fed into the head by a dense bottom current, while less dense material is receding from the edge at the top of the cloud. The approximation prevents such a circulation.

Combining (79) and (81) we find that

$$\frac{\partial h\{\Delta\rho\}}{\partial t} + \frac{\partial h\{\Delta\rho\}\{u_\beta\}}{\partial x_\beta} = 0 \tag{82}$$

where $\Delta\rho = \rho - \rho_a$

Horizontal momentum and pressure

Setting $Q = \rho u_\alpha$ (the two horizontal components of the momentum) and using (76) we get the equation

$$\begin{aligned}&\frac{\partial}{\partial t}h\{\rho u_\alpha\} + \frac{\partial}{\partial x_\beta}h\{u_\beta \rho u_\alpha\} \\ &= -h\left\{\frac{\partial \overline{P}}{\partial x_\alpha}\right\} + h\left\{\eta\nabla^2\overline{u_\alpha}\right\} + \rho_a\overline{u_\alpha}(h)w_e\rho_a\overline{u'_\alpha w'} - \rho_a\overline{u'_\alpha(h)u'}\cdot\nabla h\end{aligned} \tag{83}$$

We will replace ρ by $\{\rho\}$ in all the inertial terms. This is similar to the Boussinesq approximation where ρ is replaced by ρ_a, but perhaps slightly better since $\{\rho\}$ is still a 'local' value. In this way we get rid of a large number of terms involving $\tilde{\rho}$. The left hand side can then be written as

$$\begin{aligned}&\frac{\partial}{\partial t}h\{\rho u_\alpha\} + \frac{\partial}{\partial x_\beta}h\{u_\beta \rho u_\alpha\} \\ &\approx \frac{\partial}{\partial t}h\{\rho\}\{u_\alpha\} + \frac{\partial}{\partial x_\beta}h\{\rho\}\{u_\beta u_\alpha\} \\ &= \frac{\partial}{\partial t}h\{\rho\}\{u_\alpha\} + \frac{\partial}{\partial x_\beta}h\{\rho\}\{u_\beta\}\{u_\alpha\} + \frac{\partial}{\partial x_\beta}h\{\rho\}\{\tilde{u}_\beta\tilde{u}_\alpha\}\end{aligned} \tag{84}$$

We shall now estimate the terms on the right hand side of (83). First we note that we only take horizontal gradients of P, so it does not matter if we replace $\overline{P}$ by the deviation from the ambient hydrostatic pressure $\overline{p} = \overline{P} + \rho_a g z$. Furthermore we will use the hydrostatic approximation inside the cloud and write $\overline{p}$ as

$$\overline{p}(z) = \overline{p}_a + \int_z^h \overline{\Delta\rho} g \, dz = \overline{p}_a + \overline{p}_H \tag{85}$$

where the last equality defines $\overline{p}_H$. The pressure at the top of the cloud, $\overline{p}_a$, is kept as a boundary condition. Since it does not depend on z we have

$$h\left\{\frac{\partial \overline{p}_a}{\partial x_\alpha}\right\} = h\frac{\partial \overline{p}_a}{\partial x_\alpha} \tag{86}$$

The best way to estimate p_a would come from modeling of the flow around the cloud, but that would complicate things considerably. Besides it is probably a small term compared to the advection term, at least away from fronts and jumps. Therefore we will choose to neglect it here, but keep in mind that the presence of the term allows us to add external forces where ∇h is large. For the remaining hydrostatic pressure we get

$$h\left\{\frac{\partial \overline{p}_H}{\partial x_\alpha}\right\} = \int_0^h \frac{\partial}{\partial x_\alpha} \int_z^h \overline{\Delta\rho}(z') g \, dz' \, dz = \frac{\partial}{\partial x_\alpha} \int_0^h z\overline{\Delta\rho}(z) g \, dz \sim \frac{1}{3}\frac{\partial}{\partial x_\alpha}\{\Delta\rho\} g h^2 \tag{87}$$

In the last equality a triangular profile has been inserted for $\overline{\Delta\rho}(z)$. The use of the hydrostatic approximation inside the cloud is questionable. We shall make a better approximation in the next chapter.

The viscous term is small except near the ground, where it is responsible for the bottom friction. The lateral component can be absorbed into the internal friction term leaving

$$h\left\{\eta\frac{\partial^2 u_\alpha}{\partial z^2}\right\} = \eta\frac{\partial u_\alpha(h)}{\partial z} - \eta\frac{\partial u_\alpha(0)}{\partial z} \sim -\eta\frac{\partial u_\alpha(z=0)}{\partial z} = F_\alpha^{bot} \tag{88}$$

The last two terms in (83) are boundary terms describing entrainment and turbulent diffusion of momentum through the cloud top. We choose to neglect horizontal turbulent diffusion and drop the last term $-\rho_a \overline{u'(h)u'} \cdot \nabla h$. The term $\rho_a \overline{u'w'}$ is identified with top friction F^{top} discussed in section 3.2.

To sum up we have deduced the following momentum equation

$$\begin{aligned}
&\frac{\partial h\{\rho\}\{u_\alpha\}}{\partial t} + \frac{\partial \{u_\beta\} h\{\rho\}\{u_\alpha\}}{\partial x_\beta} = \\
&-\frac{\partial}{\partial x_\alpha}\frac{1}{3}\{\Delta\rho\} g h^2 - h\frac{\partial p_a}{\partial x_\alpha} + F_\alpha^{bot} + F_\alpha^{top} \\
&-\frac{\partial}{\partial x_\beta} h\{\rho\}\{\tilde{u}_\beta \tilde{u}_\alpha\} + w_e \rho_a \overline{u}_{a\alpha}
\end{aligned} \tag{89}$$

The term $\{\tilde{u}_\beta \tilde{u}_\alpha\}$ can be split into two, viz.:

$$\{\tilde{u}_\beta \tilde{u}_\alpha\} = [\overline{u'_\beta u'_\alpha}] + [\hat{\overline{u}}_\beta \hat{\overline{u}}_\alpha] \tag{90}$$

The first term represents turbulent diffusion of momentum in horizontal directions, and is analogous to the horizontal components of the usual Reynolds stress tensor. It is, however, based on a more restricted flow ensemble, so that $\overline{u}$ contains some of the fluctuations conventionally assigned to u', and the term is expected to be small. Representing internal friction, it can be modeled by means of an eddy viscosity as

$$[\overline{u'_\beta u'_\alpha}] \sim \frac{1}{2} K(\nabla_\alpha\{u_\beta\} + \nabla_\beta\{u_\alpha\}) \tag{91}$$

with $K = C_K h\tilde{u}$. This is the 'invisible hand' discussed in section 2.5. It was argued that such a term is more than welcome, even if K is arbitrarily small.

The second term on the right hand side of (90) represents a correction for the shear of the mean wind profile. For a logarithmic profile it is equal to $(u_*/\kappa)^2$. Below we will write an equation for $\{\tilde{u}^2\}$, the trace of the stress tensor, so only the off-diagonal elements have to be modelled. If there is right-left symmetry with respect to the direction given by $\{u\}$ the off-diagonal elements are zero. This would, by and large, be the situation if gradients are generally pointing in the streamwise direction, so we make the estimate

$$\frac{\partial}{\partial x_\beta} h\{\rho\}[\hat{\tilde{u}}_\beta \hat{\tilde{u}}_\alpha] \sim \frac{\partial}{\partial x_\alpha} h\{\rho\}\{\tilde{u}^2\} \tag{92}$$

This is also a small term, which can be neglected.

Mechanical energy of the mean flow

We shall now derive kinetic energy equations. The plan is first to derive two equations: one for the total mechanical energy (including turbulent kinetic energy) and one for the mechanical energy of the mean flow (excluding turbulent kinetic energy). Subtraction of the two will then yield an equation for the turbulent kinetic energy.

The kinetic energy of the mean flow is equal to

$$T_m = \frac{1}{2}\{\rho h\}(\{u\}^2 + \{v\}^2) \tag{93}$$

Assuming a triangular profile for $\overline{\Delta\rho}$ the potential energy of the layer is

$$V_m = h\{\Delta\rho g z\} = \frac{1}{3}\{\Delta\rho\} g h^2 \tag{94}$$

and the mean flow mechanical energy becomes

$$E_m = \frac{1}{2}\rho h(\{u\}^2 + \{v\}^2) + \frac{1}{3}\{\Delta\rho\} g h^2 \tag{95}$$

Combining the momentum equation (89), the volume conservation equation (79) and the continuity equation (81) it follows that E_m satisfies the equation

$$\frac{\partial h E_m}{\partial t} + \nabla\cdot\{u\} h E_m = \frac{1}{2}\rho_a w_e \overline{u}_a^2 + \{u\}\cdot(F^{top} + F^{bot}) - \{u_\alpha\}\nabla_\beta h\{\rho\}\{\tilde{u}_\alpha\tilde{u}_\beta\}$$
$$-\frac{1}{2}\rho_a w_e(\{u\} - \overline{u}_a)^2 + \frac{1}{3}\{\Delta\rho\} g h^2 w_e - \nabla\cdot\{u\}\frac{1}{3}\{\Delta\rho\} g h^2 \tag{96}$$

The first term on the right hand side of (96) represents the kinetic energy of the entrained air. The second term is the friction loss. The third term is the redistribution of energy caused by the stresses. The fourth term can be regarded as an energy loss resulting from the inelastic collision between the entrained air and the cloud. This is the input to the energy cascade. We note that there is no viscous dissipation term. The fifth term is work done against the cloud overpressure in order to 'inflate' it (alternatively: the potential energy gained in the mixing process by lifting the cloud centre of mass). The last term is the work done by (mean) horizontal pressure forces.

With sinks and sources appearing on the right hand side of (96) the the mean flow mechanical energy E_m is not conserved. It need not be, since E_m applies a cloud moving with the velocity $\{u\}$ as a rigid body, whereas in reality the velocity is fluctuating around a z-depending profile. The inelastic term and the inflation term describe energy exchange due to the mixing process, which is maintained by the turbulence. These two terms should therefore appear with opposite signs in the turbulent kinetic energy budget.

Total mechanical energy

In order to set up the total mechanical energy budget we first make a depth average of the equation for the total kinetic energy E defined as

$$E = \frac{1}{2}\rho u_\alpha u_\alpha + \Delta\rho g z \tag{97}$$

We recall the convention used here that repeated greek subscripts (α) are summed from 1 to 2, so $\frac{1}{2}\rho w^2$ is missing in the kinetic energy. As has been previously noted this is consistent with the use of the hydrostatic approximation. Taking the liberty of replacing ρ by $\{\rho\}$ in the kinetic energy, we have

$$\{E\} \approx E_m + \frac{1}{2}\{\rho\}\{\tilde{u}^2\} \tag{98}$$

E satisfies the equation

$$\frac{\partial}{\partial t}E + \nabla_j u_j E = -u_\alpha \nabla_\alpha p + \Delta\rho g w + u_\alpha \eta \nabla^2 u_\alpha \tag{99}$$

Using (57) with $Q = E$ leads to the following depth integrated equation

$$\begin{aligned}
&\frac{\partial}{\partial t}h\{E\} + \nabla \cdot h\{uE\} = \\
&-h\{u_\alpha \nabla_\alpha p - \Delta\rho g w\} + h\{u_\alpha \eta \nabla^2 u_\alpha\} \\
&-\overline{E'(h)w'(h)} + \overline{E'(h)u'(h)} \cdot \nabla h + \overline{E}(h) w_e
\end{aligned} \tag{100}$$

Next step is to estimate the terms on the right hand side of this equation.

In the hydrostatic approximation we have $\overline{\Delta\rho} g = -\frac{\partial \overline{p}}{\partial z}$, and since $\overline{p}(h) = 0$ it follows that the first term can be written as

$$\begin{aligned}
&-h\{u_\alpha \nabla_\alpha p - \Delta\rho g w\} = -h\{\nabla_i u_i P\} = -\nabla_\alpha h\{u_\alpha p\} \approx -\nabla_\alpha \{u_\alpha (h-z)^2\}\{\Delta\rho\} \\
&= -\nabla_\alpha \frac{1}{3}\{u_\alpha\}\{\Delta\rho\} g h^2 - \nabla_\alpha \{\tilde{u}_\alpha (h-z)^2\}\{\Delta\rho\}
\end{aligned} \tag{101}$$

Here ($\approx$) means that $\overline{u\Delta\rho} \approx \overline{u}\,\overline{\Delta\rho}$ and that a triangular profile is used for $\overline{\Delta\rho}$.

The viscous term (second term on the right hand side of (100)) is split into energy dissipation and molecular transport of kinetic energy and only the first part is retained.

$$\begin{aligned}
&\{u_\alpha \eta \nabla^2 u_\alpha\} = \\
&-\{\eta(\nabla_\beta u_\alpha)(\nabla_\beta u_\alpha)\} + \{\eta \nabla^2 \frac{1}{2}u^2\} \\
&\sim -h\rho\epsilon
\end{aligned} \tag{102}$$

The next two terms on the right hand side of (100) are written as

$$\begin{aligned}
&-\overline{E'(h)w'(h)} + \overline{E'(h)u'(h)} \cdot \nabla h \\
&= \frac{1}{2}\rho_a \overline{u'^2 u'} \cdot \nabla h - \frac{1}{2}\rho_a \overline{u'^2 w'} + \rho_a \overline{u}_\alpha \left(\overline{u'_\alpha u'_\beta} \nabla_\beta h - \overline{u'_\alpha w'}\right) \\
&\sim \overline{u}(h) \cdot F^{top}
\end{aligned} \tag{103}$$

All velocities are evaluated at the cloud top. The term $\frac{1}{2}\rho_a \overline{u'^2 u'} \cdot \nabla h - \frac{1}{2}\rho_a \overline{u'^2 w'}$, describing turbulent diffusion of turbulent kinetic energy through the cloud top, involves triple correlations, which are expected to be small, and hence this term is neglected. In the same fashion we approximate the last term on the right hand side of (100) by

$$\overline{E}(h) w_e = \frac{1}{2}\rho_a \overline{u^2(h)}\, w_e \sim \frac{1}{2}\rho_a \overline{u}^2(h)\, w_e \tag{104}$$

On the left hand side of (100) ρ is replaced by $\{\rho\}$ in the kinetic energy terms and it is rewritten as

$$\begin{aligned}
&\frac{\partial}{\partial t}h\{E\} + \nabla \cdot h\{uE\} \\
= \;& \frac{\partial}{\partial t}h\{E\} + \nabla \cdot h\{u\}\{E\} + \\
&\nabla_\alpha h\{\tilde{u}_\alpha \Delta\rho g z\} + \nabla_\alpha h\{\rho\}\{u_\beta\}\{\tilde{u}_\beta \tilde{u}_\alpha\} + \nabla_\alpha h\frac{1}{2}\{\rho\}\{\tilde{u}_\alpha \tilde{u}^2\}
\end{aligned} \tag{105}$$

Making again use of the triangular form of $\overline{\Delta\rho}$ we write

$$\nabla_\alpha h\{\tilde{u}_\alpha \Delta\rho g z\} \approx \nabla_\alpha\{\Delta\rho\} g\{\tilde{u}_\alpha 2z(h-z)\} \tag{106}$$

The last term of third order in $\tilde{u}$ can be written as

$$\{\tilde{u}_\alpha \tilde{u}^2\} = \left[\overline{u'_\alpha u'_\beta u'_\beta}\right] + 2\left[\hat{\overline{u}}_\beta \widehat{\overline{u'_\beta u'_\alpha}}\right] + \left[\widehat{\overline{u}_\alpha \overline{u'_\beta u'_\beta}}\right] + \left[\hat{\overline{u}}_\alpha \hat{\overline{u}}_\beta \hat{\overline{u}}_\beta\right] \tag{107}$$

The first term on the right hand side describes turbulent diffusion of turbulent kinetic energy in horizontal directions, which will be disregarded. The two following terms should be small, since Reynolds stresses in a boundary layer do not dependent much on z, so that $\widehat{\overline{u'_\beta u'_\alpha}} \approx 0$. The last term can be estimated by means of a logarithmic profile for $\overline{u}$ for which

$$\{\tilde{u}^3\} \sim \left[\hat{\overline{u}}^3\right] \sim \frac{1}{h}\left(\frac{u_*}{\kappa}\right)^3 \int_0^h (\log(z/h)+1)^3 \, dz = -2\left(\frac{u_*}{\kappa}\right)^3 \sim -2\{\tilde{u}^2\}^{3/2} \tag{108}$$

Using this the last term on the right hand side of (105) is approximated by

$$\nabla_\alpha h\frac{1}{2}\{\rho\}\{\tilde{u}_\alpha \tilde{u}^2\} \sim -\nabla_\alpha h\{\rho\}\{\tilde{u}^2\}^{3/2}\frac{\{u_\alpha\}}{|\{u\}|} \tag{109}$$

Putting everything together we have derived the following equation for the mechanical energy

$$\begin{aligned}
&\frac{\partial h\{E\}}{\partial t} + \nabla \cdot \{u\} h\{E\} + \nabla_\alpha\{\Delta\rho\} g\{\tilde{u}_\alpha 2z(h-z)\} \\
&+\nabla_\alpha h\{\rho\}\{u_\beta\}\{\tilde{u}_\beta \tilde{u}_\alpha\} - \nabla \cdot \{u\}/|\{u\}|\{\rho\} h\{\tilde{u}^2\}^{3/2} = \\
&-\nabla_\alpha \frac{1}{3}\{u_\alpha\}\{\Delta\rho\} g h^2 - \nabla_\alpha\{\tilde{u}_\alpha (h-z)^2\}\{\Delta\rho\} g \\
&-h\{\rho\}\epsilon + \overline{u_a} \cdot F^{top} + \frac{1}{2}\rho_a \overline{u_a}^2 w_e
\end{aligned} \tag{110}$$

Comparing (110) with (96) we note that the inelastic collision term is now absent, but viscous dissipation is there. The bottom friction term is also missing, as it should, since the velocity is zero at the ground (no work is performed), and the top friction is $\overline{u_a} \cdot F^{top}$ rather than $\{u\} \cdot F^{top}$.

Turbulent kinetic energy

Subtracting (96) from (110) we finally get the following turbulent kinetic energy equation

$$\begin{aligned}
&\frac{\partial}{\partial t}\frac{1}{2}h\{\rho\}\{\tilde{u}^2\} + \nabla \cdot \{u\}\frac{1}{2}h\{\rho\}\{\tilde{u}^2\} = \\
&+F^{top} \cdot (\overline{u}_a - \{u\}) + F^{bot} \cdot \{u\} + \frac{1}{2}\rho_a (\overline{u}_a - \{u\})^2 w_e
\end{aligned}$$

$$-\frac{1}{3}\{\Delta\rho\}ghw_e - h\{\epsilon\} - C_\epsilon\{\rho\}\{\tilde{u}^2\}\left(|u| + \sqrt{\{\tilde{u}^2\}}\right)$$
$$+\nabla_\alpha \cdot \{\Delta\rho\}g\{\tilde{u}_\alpha z^2\} + \frac{K}{4}\left(\nabla_\alpha u_\beta + \nabla_\beta u_\alpha\right)\left(\nabla_\alpha u_\beta + \nabla_\beta u_\alpha\right)$$
$$-h\{\rho\}\{\tilde{u}_\alpha\tilde{\overline{u}}_\beta\}\nabla_\alpha pha\{\overline{u}_\beta\} + \nabla_\alpha\frac{\{u_\alpha\}}{|\{u\}|}\{\rho\}h\{\tilde{u}^2\}^{3/2} \qquad (111)$$

We have used (90) and the closure (91) on $\{\tilde{u}_\alpha\tilde{u}_\beta\}$. The last two terms of (111) are small and we wish to neglect them. Note that for a 2d (line source) neutral plume we have

$$\begin{aligned}\nabla_\alpha h\{\rho\}\{u_\beta\}\{\tilde{\overline{u}}_\beta\tilde{\overline{u}}_\alpha\} &= +\rho_a\frac{u_*^3}{\kappa^3}\frac{\partial h}{\partial x}\\ -\nabla_\alpha h\{\rho\}\{\tilde{u}^2\}^{3/2}\frac{\{u_\alpha\}}{|\{u\}|} &= -\rho_a\frac{u_*^3}{\kappa^3}\frac{\partial h}{\partial x}\end{aligned} \qquad (112)$$

The two terms therefore cancel, which we will take as a good excuse for disregarding them altogether.

The term in (111) involving $\{\tilde{u}_\alpha z^2\}$ prevents a closure of the set of equations. Without the assumption of a triangular density profile it would contain the factor $\{\tilde{u}(P - z\partial P/\partial z)\}$, which is equal to zero for a rectangular $\Delta\rho$ profile. We are more in favour of a triangular profile, but since the term does not seem to add any essential physics to the model, we will simply neglect it.

Equation (111) differs from the usual turbulent kinetic energy equations, since the turbulence is defined relative to the layer average velocity rather than the local mean velocity. Apparently this has the effect of introducing an extra term: the production of turbulence by inelastic collision (second term on the right hand side). Such a term is present in the model of Webber & Wheatley (1987), but not in the one proposed by van Ulden (1986).

In the limit $\Delta\rho \to 0$ a lot of other terms, which has been estimated by the use of a triangular density profile, vanish. Some of the other terms were retained mainly to be sure to get a correct passive limit. Therefore we will discuss the passive limit now.

3.5 The passive limit

In the passive limit ($\Delta\rho = 0$) there are two simple cases: a flat cloud with the same height everywhere, and a steady plume from a line source. In the first case all spatial derivatives are zero, and in the latter case time derivatives are zero.

For the passive flat (horizontally homogeneous) cloud the volume conservation equation (79), the momentum equation (89) and the turbulent kinetic energy equations (111) simplefy to [14]

$$\begin{aligned}\frac{\partial h}{\partial t} &= w_e\\ \frac{\partial hu}{\partial t} &= C_f\tilde{u}(u_a - u - \tilde{u}) + w_e u_a\\ \frac{\partial \frac{1}{2}h\tilde{u}^2}{\partial t} &= C_f(\tilde{u}(u_a - u)^2 + \tilde{u}^2|\{u\}|) + \frac{1}{2}(u - u_a)^2 w_e - C_\epsilon\tilde{u}^3\log(h/z_0)\\ w_e &= C_w\tilde{u}\end{aligned} \qquad (113)$$

Inserting

$$u_a = \frac{u_*}{\kappa}\log(h/z_0)$$

[14] from now on we will drop { } and also write $\tilde{u}$ instead of $\sqrt{\{\tilde{u}^2\}}$ etc.

$$
\begin{aligned}
u &= \frac{u_*}{\kappa}(\log(h/z_0) - 1) \\
\tilde{u} &= \frac{u_*}{\kappa}
\end{aligned}
\tag{114}
$$

we find that the equations are satisfied provided that

$$C_\epsilon = C_f \tag{115}$$

In this limit the friction is equal to $\rho u_*^2 = \rho\kappa^2\tilde{u}^2$, so we can estimate

$$C_f = C_\epsilon = \kappa^2 \approx 0.16 \tag{116}$$

The first three equations in (113) are in fact satisfied for any choice of w_e. In the absence of density differences nothing in the derivation of the equations tells us what h should be, and consequently we must be allowed to define h in whatever way we want. However, if we want to estimate the entrainment rate from the formula given above we must choose h to be *just above* the cloud (i.e. always enveloping the initial material of the layer). Using this h and $w_e = C_w\tilde{u}$ we get

$$h(t) = C_w\tilde{u}t \tag{117}$$

For the plume we get

$$
\begin{aligned}
\frac{\partial hu}{\partial x} &= w_e \\
\frac{\partial hu^2}{\partial x} &= C_f\tilde{u}(u_a - u - \tilde{u}) + w_e u_a - \frac{\partial}{\partial x}h\tilde{u}^2 \\
\frac{\partial u\frac{1}{2}h\tilde{u}^2}{\partial x} &= C_f(\tilde{u}(u_a - u)^2 + \tilde{u}^3) + \frac{1}{2}(u - u_a)^2 w_e \\
w_e &= C_w\tilde{u}
\end{aligned}
\tag{118}
$$

Again the equations are satisfied for a logarithmic profile and any choice of w_e. It should be noted that this would not have been the case if we had dropped the Reynolds stress term $\frac{\partial}{\partial x}h\tilde{u}^2$ in the momentum equation, so it is seems best to keep it.

For $w_e = C_w\tilde{u} = C_w u_*/\kappa$ we get

$$h(\log(h/z_0) - 1) = C_w\, x \tag{119}$$

Dutton and Panofsky (1988) give the following correlation for the growth of the height δ of an internal boundary layer at a surface roughness shift

$$\delta(\log(\delta/z_0) - 1) = 0.5x - z_0 \tag{120}$$

suggesting that

$$C_w \sim 0.5 \tag{121}$$

Stretch (1986) found $w_e = 0.41u_*$ in the passive limit and this result is used in the DEGADIS model. Assuming that the definition of the cloud height corresponds to $0.5h$ this gives

$$C_w \sim 0.33 \tag{122}$$

Hunt & Webber (1979) deduced the following formula for z_c, the centroid of the concentration distribution

$$z_c U(cz_c) = \kappa u_* x \tag{123}$$

where $c = \mathrm{e}^{-\gamma}$ and γ is the Euler constant ($c \sim 0.56$). Assuming $z_c = 1/3h$ and a logarithmic profile this can be written as

$$h(\log(h/z_0) - 1.66) = 3\kappa^2 x \tag{124}$$

suggesting

$$C_w = 3\kappa^2 \sim 0.48 \tag{125}$$

In the SLAM model we use $C_w = 0.5$.

3.6 Interactions with the ambient flow field

The pressure term $h\nabla\overline{p}_a$ represents a drag force at the cloud/air interface (in addition to the momentum transfer by entrainment). It can be expected to be small in flat and shallow regions of the cloud, but where the cloud seriously disturbs the flow of the surrounding air it may become important. This will happen at places where ∇h is large, in particular at the cloud edges, where the characteristic sharp front develops. Here the term should cancel the discontinuity of the hydrostatic pressure term $\frac{1}{3}\Delta\rho g h^2$. An argument something like the following is needed.

Consider a frame of reference moving with a constant velocity V, in such a way that the cloud stands still (does not change shape in the neigbourhood of a point in time and space). In this frame the air moves around the cloud with the velocity $u_a - V$, so following Bernoulli we may assume a dynamic pressure $p_a = \frac{1}{2}\rho_a(u_a - V)^2$ so that

$$-h\nabla\overline{p_a} \sim h\nabla\frac{1}{2}\rho_a(u_a - V)^2 \tag{126}$$

Although there may be an element of truth in such an argument, it is not satisfactory. Vertical velocities have been neglected, even if these will be important for e.g. a vertical front, and it would have looked nicer with h to the right of ∇, because the term should play a role where ∇h is large. The ambient velocity u_a should also be the disturbed velocity, which is unknown, so (126) does not really solve the problem. Apart from that the gradient is ill-defined at the cloud edge, since h is not defined at a discontinuity (another reason for wanting h to the right of ∇).

The motivation for considering the term is that we need something to compensate the hydrostatic pressure gradient at the cloud edges, thereby maintaining a sharp front that does not accelerate freely and collapse. An alternative is therefore to model the term as a gradient in the following way

$$-h\nabla\overline{p_a} \sim \nabla h C_d\frac{1}{2}\rho_a(\{u_a\} - V)^2 \tag{127}$$

where $\{u_a\}$ is the depth average of the *undisturbed* wind profile (this makes sure that the term vanishes for a cloud that follows the wind). A motivation could be that the stagnation pressure for a streamline terminating of the front is equal to $\frac{1}{2}\rho_a(u_a - V)^2$, where u_a is measured in the air away from the cloud. This works best in 2d. In 3d there may not be a stagnation point since streamlines may run parallel to the front. On the other hand the requirement that the cloud does not change shape in the moving coordinate system only determines the component of V parallel to ∇h, so that the component of V perpendicular to ∇h can be determined so that we get a stagnation point. The best guess seems to be to choose V so that the $\{u_a\} - V$ is parallel to ∇h, leading to the following suggestion

$$-h\nabla\overline{p_a} \sim \nabla h C_d\frac{1}{2}\rho_a((\{u\} - \{u_a\})\cdot n)^2 \tag{128}$$

where $n = \nabla h/|\nabla h|$ is a unit vector pointing 'uphill'. This is a bulk force, which can be convenient in case the solution technique does not determine the location of cloud edges and internal jumps. For a front in steady motion (not accelerating) we have

$$hC_d\frac{1}{2}\rho_a((\{u\} - \{u_a\})\cdot n)^2 = \frac{1}{3}\{\Delta\rho\}h^2 \tag{129}$$

or

$$|(\{u\} - \{u_a\})\cdot n| = \sqrt{\frac{2}{3C_d}}\sqrt{\frac{\{\Delta\rho\}gh}{\rho_a}} \tag{130}$$

This is the standard relation for the front velocity, usually written as

$$U_f = k_f \sqrt{\frac{H\Delta\rho g}{\rho_a}} \tag{131}$$

The experimental value of k_f is 1.1 to 1.2 (e.g Billeter 1995), from which we get $C_d = 0.5$. It should be noted, that even if the definition of H and h may differ, $H\Delta\rho$ always has the same meaning, so k_f is not affected.

In case the solutions technique allows discontinuities of h to be determined it might be best to apply the drag force only at the discontinuities. The force per unit length along an edge will be equal to

$$nC_d\frac{1}{2}\rho_a(n\cdot(\{u_a\}-u))^2|\Delta h| \tag{132}$$

where n is a unit vector perpendicular to the edge.

Another problem is the velocity of the ambient air at the top of the cloud, u_a. Again the best way to estimate it would be to run a flow model. Above u_a was set equal to the undisturbed ambient windspeed, but this can only be correct for passive plumes. As has already been mentioned better results are obtained if u_a is replaced by u_{top} given by (69).

3.7 Summary of results

The discussion above lead to the following set of depth averaged equations

$$\frac{\partial}{\partial t}h + \nabla hu = w_e \tag{133}$$

$$w_e = \frac{C_w\tilde{u}}{1+C_R\widetilde{Ri}} \qquad \widetilde{Ri} = \frac{g(\rho-\rho_a)h}{\rho_a\tilde{u}^2} \tag{134}$$

$$\frac{\partial}{\partial t}h\rho + \nabla\cdot h\rho u = \rho_a w_e \tag{135}$$

$$\begin{aligned}\frac{\partial h\rho u}{\partial t} + \nabla\cdot u\,h\rho u &= -\nabla\frac{1}{3}\Delta\rho g h^2 + \nabla_\beta\frac{1}{2}C_k\tilde{u}h^2(\nabla_\alpha u_\beta + \nabla_\beta u_\alpha)\\ &+C_f\left(\rho_a\tilde{u}(u_a-u) - \rho\frac{\tilde{u}u}{\log(h/z_0)-1}\right) - \nabla\cdot uh\rho\frac{\tilde{u}^2u}{u^2} + w_e\rho_a u_a\end{aligned} \tag{136}$$

where

$$\begin{aligned}&\frac{\partial}{\partial t}\frac{1}{2}h\rho\tilde{u}^2 + \nabla\cdot u\frac{1}{2}h\rho\tilde{u}^2 =\\ &+C_f\tilde{u}\left(\rho_a(u_a-u)^2 + \rho\frac{u^2}{\log(h/z_0)-1} - \tilde{u}\log(h/z_0)\right) + \frac{1}{2}\rho_a(u_a-u)^2 w_e\\ &+\nabla_\beta\frac{1}{4}C_k\tilde{u}h^2(\nabla_\alpha u_\beta + \nabla_\beta u_\alpha)(\nabla_\alpha u_\beta + \nabla_\beta u_\alpha) - \beta\Delta\rho g h w_e\end{aligned} \tag{137}$$

This set of shallow layer equations was derived from the Navier-Stokes equations. The derivation is not straight forward if all approximations are to be justified. The intention has been to give arguments for the various manipulations, even if, admittedly, some are of a hand waying nature. Validations of dense gas models often treat them as black boxes and focused on their ability to reproduce concentration measurements. This is fine for the models that reproduce data well, but less informative for models that fail to do so, because we also want to know what went wrong. For that purpose experiments are needed that focus on the individual model assumptions rather than the overall input-output relation. A full

validation of a model would therefore require experimental justification of all the steps in the derivation of the model.

The most critical points in the present argumentation, which could be subject to further investigations, are:

- It is difficult to make a definition of the cloud height in terms of observables, which allows us to rely on the assumption that $\rho = \rho_a$ at the cloud top (no deportment). Consequently h and w_e are difficult to measure unambiguously.
- The approximation $\{\rho u\} \sim \{\rho\}\{u\}$ prevents the model from describing e.g. dense bottom currents within the layer.
- A better understanding of why the velocity of the entrained air seems to be so low is required.
- In the layer integrated model the modeling of the entrainment rate is a separate matter. In a stratified layer turbulent diffusion may be well described by gradient transfer (K-theory), although perhaps best with non-locally determined eddy diffusivities. Within such a framework it would be possible to calculate w_e and to find the effective velocity of the entrained air etc. However, we only have solid eddy diffusivity theory for a constant flux layer.
- The interactions at the cloud top are not trivial. They are not accounted for in the framework of layer averaged equations, where they appear as boundary terms, and they have to be put in by hand. This could be subject to experimental investigation.

4 Numerical modelling

Below a numerical method for solving the model is described. The method is based on a Lagrangian grid, i.e. a grid made from material points following the flow. The advantage of a Lagrangian over an Eulerian, fixed, grid is that fewer points are needed (no grid points outside the cloud) and that the grid automatically adjusts itself to the the growing dimensions of the cloud. We demand that the numerical solution converges as the grid gets finer, so that we can be reasonably confident that a numerical solution represents the continuous solution. It should be remembered, however, that the model itself is not a very accurate representation of the cloud - it is meant to reproduce only coarse features of the flow - so a very fine resolution is not needed for practical purposes. A good numerical scheme should therefore not only converge, it should also make sense when relatively few, large grid cells are used. For the present model it is also important to avoid spurious sinks and sources of energy, since that may spoil the turbulent kinetic energy budget. What we are looking for is a discrete version of the model rather than a discretization of space (and time). These goals can be achieved by applying the principle of least action. The mathematical framework to be set out is convenient for making model improvements. This will also be discussed.

4.1 The principle of least action

The formulation of the principle of least action, also known as Hamilton's principle, is one of the milestones of nineteenth century physics. From this all the major classical theories of physics (Newtonian mechanics, electrodynamics and the relativity theories) can be derived, and the action integral even plays a central role in the path integral formulation of quantum mechanics. Apart from being fundamental it also very useful as a concise and rational means of generating models for mechanical systems, and it is in this sense we shall use it. Readers unfamiliar with the principle of least action are referred to Goldstein (1966). An enthusiastic and very readable introduction to the subject is given by Feynman & Sands (1964). The idea of using the principle of least action in connection with shallow fluid layer systems is not new (see e.g. Salmon (1982)), and the use of variational principles are common in numerical analysis in general, see Mitchell & Wait (1977) for an introduction. In the following a brief and self-contained explanation of the subject will be given.

The principle of least action (hereafter referred to as PLA) is very simple, saying

> *A mechanical system evolves from a specific initial state to specific final state in such a way that the action integral $\mathcal{S}$ is minimal.*

This calls for some additional explanations. The 'state', or configuration, is a list of parameters specifying the positions of every material part of the system. The list of parameters $x = (x_1, x_2, \ldots)$, is referred to as the generalised coordinates. A list of cartesian or polar coordinates for all particles in the system is one way of specifying the state. For a pendulum a single parameter (e.g. an angle) may be enough. A train may also be described by a single parameter - it has many parts, but they are constrained to move with only one degree of freedom. It is often an advantage to use a minimal set of generalized coordinates, equal in number to the degrees of freedom, because then the x's can be chosen independently. The time derivative of x_n is called a generalized velocity and denoted by $\dot{x}_n$ or u_n.

The action integral $\mathcal{S}$, or simply 'the action', is defined as (t_1 and t_2 refer to the initial and final states)

$$\mathcal{S} \equiv \int_{t_1}^{t_2} \mathcal{L}(x, u)\, dt \tag{138}$$

where $\mathcal{L}$ is the Lagrangian of the system. $\mathcal{L}(x,u)$, in turn, is equal to $\mathcal{T}(x,u) - \mathcal{V}(x,u)$, where $\mathcal{T}(x,u)$ is the kinetic energy of the system and $\mathcal{V}(x,u)$ is the potential energy. Thus $\mathcal{L}(x,u)$ is a definite mathematical expression involving x's and u's.

It is understood that the initial and final states are predetermined, so that the values $x(t_1)$ and $x(t_2)$ are fixed. Otherwise $x(t)$ is determined so as to minimize $\mathcal{S}$.

The governing equations are derived by means of calculus of variations. The point is that $\mathcal{S}$ is stationary with respect to any infinitesimal variation. If generalized coordinates form a minimal set the problem has the following standard solution, known as the Euler-Lagrange equations[15]

$$\frac{\mathrm{d}}{\mathrm{d}t}\frac{\delta \mathcal{L}}{\delta u_n} - \frac{\delta \mathcal{L}}{\delta x_n} = 0 \tag{139}$$

PLA is a powerful and rational tool. Existence and uniqueness of solutions, for example, follow from the fact that it is a minimum principle. It is rational since all that is needed in order to specify a mechanical systems is to define generalized coordinates and write down the Lagrangian. The derivation of the governing equations then follows in a systematic and fail-safe manner.

The main objection against using PLA is that it only applies to frictionless systems. This seems to rule out friction and dissipation of energy, which are both important in turbulent flow. We will return to this in a later section.

Below (in Section 4.3) we will show that the Euler equations can be derived from the principle of least action. [16]

We first define generalized coordinates of the system. They must uniquely specify the position of every mass element of the system at any time. This can be done by means of a map of the fluid from some reference state which could be chosen as the initial state, onto the current state of the system at time t. The space coordinates of a fluid element in the reference state will be named $\xi = (\xi_1, \xi_2, \xi_3)$, while $x = (x_1, x_2, x_3)$ will denote the coordinates of the same fluid particle in the current state at time t. The idea is that ξ always refers to the same fluid particle, so that $x(\xi, t)$ specifies the path of a particle, when ξ is kept fixed and t is varied. Note that it is immaterial how we choose the reference state, since ξ only serves as a particle name.

The Lagrangian is given by

$$\mathcal{L} \equiv \int d^3\xi \left(\frac{1}{2}\rho u^2(\xi, s) - \rho g x_3(\xi, s) \right) \tag{140}$$

Furthermore it is convenient to work with two time variables: s together with ξ and t together with x, and to regard the map as being of the form $(\xi, s) \mapsto (x, t)$, where $s = t$. The reason for using two symbols for time is that we can define $\frac{\partial}{\partial s}$ as the partial derivative with respect to s keeping ξ fixed, and $\frac{\partial}{\partial \xi_i}$ as the partial derivative with respect to ξ keeping s fixed. In the same way x is kept fixed in $\frac{\partial}{\partial t}$ and t is kept fixed in $\frac{\partial}{\partial x}$. This allows us to write the velocity as

$$u_i = \frac{\partial x_i}{\partial s} \tag{141}$$

(but $\frac{\partial x}{\partial t} = 0$), and in general

[15] For a derivation see e.g. Goldstein (1966). We use the notation $\frac{\delta \mathcal{L}}{\delta u_n}$ and $\frac{\delta \mathcal{L}}{\delta x_n}$ to denote partial derivatives of $\mathcal{L}$ as a function of x and u evaluated as if they were independent variables. Like $\mathcal{L}$ they are definite mathematical expressions in x and u. After the derivatives have been taken the actual $x(t)$ and $u(t)$ are inserted and finally $\frac{\mathrm{d}}{\mathrm{d}t}$ is evaluated using the chain rule.

[16] A proof can probably be found in some textbook, but I have not been able to find one.

$$\frac{\partial}{\partial s} = \frac{\partial}{\partial t} + \frac{\partial x_i}{\partial s}\frac{\partial}{\partial x_i} \equiv \frac{\partial}{\partial t} + u_i\frac{\partial}{\partial x_i} \tag{142}$$

$$\frac{\partial}{\partial \xi_j} = \frac{\partial x_i}{\partial \xi_j}\frac{\partial}{\partial x_i} \equiv \mathsf{J}_{ji}\frac{\partial}{\partial x_i} \tag{143}$$

The behaviour of the system is specified by any map $(\xi, s) \mapsto (x, t)$ with $t(\xi, s) = s$, which respects rigid boundaries, and which is volume preserving (so as to maintain incompressibility). The last condition can be written as a condition of the Jacobian:

$$\det \mathsf{J} = 1 \tag{144}$$

Due to the assumption of incompressibility only volume preserving maps are allowed, and the set of generalized coordinates is not minimal. Therefore we must treat (144) as a set of constraints on the minimization problem and deal with them by means Lagrangian multipliers. In this way we get one Lagrangian multiplier for each space-time point, which we name $p(\xi, s)$, and express the stationarity of $\mathcal{S}$ in the following way

$$\delta\mathcal{S} + \int_{t_1}^{t_2} ds \int d^3\xi \, p \, \delta \det \mathsf{J} = 0 \tag{145}$$

In working out the variation of the Jacobian we can use the following identity valid for any matrix A

$$d \det \mathsf{A} = \det \mathsf{A} \ \operatorname{trace}\left(\mathsf{A}^{-1} d\mathsf{A}\right) \tag{146}$$

This gives

$$\delta \det \mathsf{J} = \det \mathsf{J} \ \frac{\partial \xi_j}{\partial x_i}\frac{\partial \delta x_i}{\partial \xi_j} = \frac{\partial \delta x_i}{\partial x_i} \tag{147}$$

We also have

$$\delta u_i = \delta\frac{\partial x_i}{\partial s} = \frac{\partial \delta x_i}{\partial s} \tag{148}$$

Inserting into (145) and rearranging we get

$$\begin{aligned} 0 &= \int_{t_1}^{t_2} ds \int d^3\xi \left(\rho u_i \frac{\partial \delta x_i}{\partial s} - \rho g \delta x_3 + p\frac{\partial \delta x_i}{\partial x_i}\right) \\ &= \int_{t_1}^{t_2} ds \int d^3\xi \left(-\rho \delta x_i \frac{\partial u_i}{\partial s} - \rho g \delta x_3 + p\frac{\partial \delta x_i}{\partial x_i}\right) \\ &= \int_{t_1}^{t_2} dt \int d^3x \left(-\rho\frac{\partial u_i}{\partial s} - \rho g \delta_{i,3} - \frac{\partial p}{\partial x_i}\right)\delta x_i \end{aligned} \tag{149}$$

Since this is valid for any δx we conclude that

$$\rho\frac{\partial u_i}{\partial s} = \rho\frac{\partial u_i}{\partial t} + \rho u_j\frac{\partial u_i}{\partial x_j} = -\frac{\partial p}{\partial x_i} - \delta_{i,3}\rho g \tag{150}$$

This is the momentum equation as promised. Note that the pressure is just a Lagrangian multiplier.

Using (146) once more we also get the equation of continuity

$$0 = \frac{\partial \det \mathsf{J}}{\partial s} = \frac{\partial \xi_j}{\partial x_i}\frac{\partial^2 x_i}{\partial \xi_j \partial s} = \frac{\partial u_i}{\partial x_i} \tag{151}$$

We note that the hydrostatic approximation is compatible with PLA. It simply means defining the kinetic energy as $\frac{1}{2}\rho(u^2 + v^2))$ instead of $\frac{1}{2}\rho(u^2 + v^2 + w^2)$.

In the next section we shall use PLA to set up governing equations for discrete systems. The equations can readily be solved on a computer.

4.2 Some discrete systems

The main reason for introducing the principle of least action here is not to derive the Euler equations. The derivation given above serves to introduce the tricks needed to apply it to a continuous fluid. Ultimately we can only solve finite systems of equations on the computer, so we are forced to convert our problem into one that involves discrete variables. This can be done in the usual way substituting differentials by differences in the governing equations, but an alternative to this procedure is to construct a mechanical system (write down a Lagrangian), which is based on similar physical principles as the original continuous system, but contains only a finite number of degrees of freedom. Using PLA we can then write down the governing equations for the discrete system. The advantage of such an approach is that the finite system automatically obeys conservation laws, and that we can interpret the behaviour of the system in terms of conventional concepts of mechanical physics. This should reduce numerical problems to rounding errors and time integration errors, so that we do not have to worry about numerical diffusion, instabilities or violations of conservation laws. This is avoided since we solve a set of governing equations for a mechanical system, which in principle could exist in real life. We can also hope that a rather coarse spatial resolution is sufficient to account for the basic behaviour of the system.

One way of making simplified systems is to use the principle of least action as discussed in the previous section, but restrict the class of maps used to minimize the action[17]. In fact, the inviscid shallow water equations can be derived in this way. It requires that the term $\frac{1}{2}\rho w^2$ is neglected in the kinetic energy part of the Lagrangian and that we restrict the maps to those that map vertical liquid columns onto vertical liquid columns. These maps are simple, because we only need to specify the base of each fluid column. These maps are volume conserving which is why we do not have a pressure term in the shallow water equations. Details of the derivation for a finite analogous system are given below.

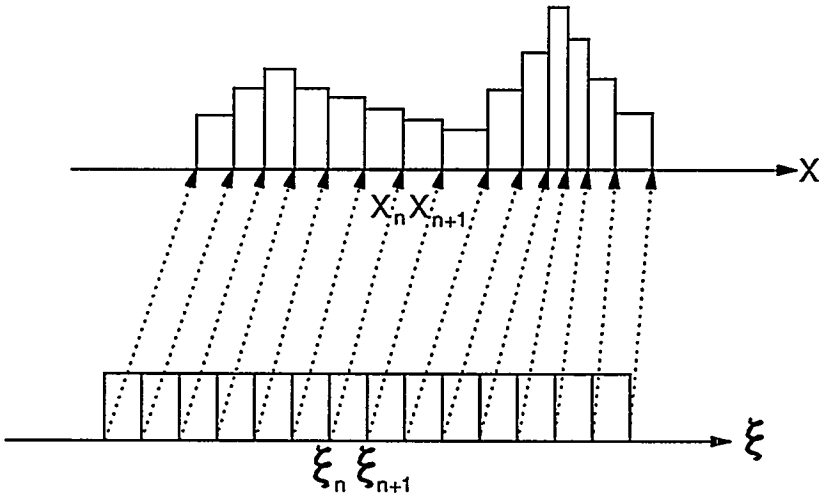

Figure 4. Map $\xi_n \mapsto x_n$ used to define a finite shallow water system

[17] This is known as the Kantorovich (1933) method.

1D box chain

A natural way to make a finite system is therefore to restrict ourselves to maps, that map rectangular cells onto rectangular cells. In one dimension (2D fluid) we can choose the reference state such that the free surface is horizontal with constant height h_0 and define a finite number of cell boundaries $\ldots\xi_n < \xi_{n+1}\ldots$. The cell bounded by ξ_n, ξ_{n+1} and h_0 is then mapped onto a rectangle bounded by x_n, x_{n+1} and h_n. Since $h_n = h_0\frac{\xi_{n+1}-\xi_n}{x_{n+1}-x_n}$ we only need to specify the set of boundaries $\{x_n(s)\}$. For simplicity we assume that all cells have the same volume (area) ΔV. The velocity varies linearly inside the cells, so the kinetic energy of a cell is given by

$$\int_0^1 d\alpha \frac{1}{2}\rho h_n \left(u_{n+1}\alpha + u_n(1-\alpha)\right)^2 = \frac{1}{6}\rho\Delta V\left(u_{n+1}^2 + u_{n+1}u_n + u_n^2\right) \tag{152}$$

The potential energy of the cell is

$$\frac{1}{2}\Delta V\rho g h_n = \frac{1}{2}\rho g\frac{\Delta V^2}{x_{n+1}-x_n} \tag{153}$$

Inserting this the Lagrangian becomes

$$\begin{aligned}\mathcal{L} &= \sum_n \rho\Delta V\left(\frac{1}{6}(u_{n+1}^2 + u_{n+1}u_n + u_n^2) - \frac{1}{2}g\frac{\Delta V}{x_{n+1}-x_n}\right)\\ &= \sum_n \rho\Delta V\left(\frac{1}{6}(2u_n^2 + u_{n+1}u_n) - \frac{1}{2}g\frac{\Delta V}{x_{n+1}-x_n}\right)\end{aligned} \tag{154}$$

Incidentally, the potential energy term in this Lagrangian consists of $\frac{1}{r}$ potentials for adjacent cell boundaries, so the system must behave much like a string of charges particles.

Since we have a discrete minimal set of variables, the usual Euler-Lagrange equations apply. Inserting (154) into (139) and making a few rearrangments we get

$$\frac{\mathrm{d}^2}{\mathrm{d}t^2}(x_{n+1} + 4x_n + x_{n-1}) = 3g\left(\frac{\Delta V}{(x_{n+1}-x_n)^2} - \frac{\Delta V}{(x_n - x_{n-1})^2}\right) \tag{155}$$

A numerical solution to these equations (with periodic boundary conditions) is shown on figure 5. The initial conditions have been chosen to be the same as for the analytic solution on figure 1. A so called symplectic integrator of order four was used, see Forest & Ruth (1990) and Yoshida (1990). This is a special type of Runge-Kutta scheme, which has been developed for separable Hamiltonian systems, mainly for the purpose of solving problems in astronomy. It has the property that the numerical solution is always a solution to a Hamiltonian system[18], even for finite timesteps. It only solves for the right Hamiltonian as the timestep approaches zero, but the fact that solutions are exact for *some* Hamiltonian guarantees the complete absence of friction even for finite timesteps. The solutions are therefore neither damped down nor will they blow up because of negative friction. From figure 5 it is seen that the numerical solution follows the analytic solution very closely right up to the point, where the wave breaks, and a strange behaviour sets in. In a way it would have been more satisfactory if an error (e.g. division by zero or a negative height) had occurred, since this would be analogous to the continuous system. Instead of breaking down the solution starts oscillating wildly generating waves of wavelength comparable to the cell size. After

[18]This mean that it is governed by Hamilton's equations involving the Hamiltonian function, which can be derived from $\mathcal{L}$. Hamilton's equations follow from 139.

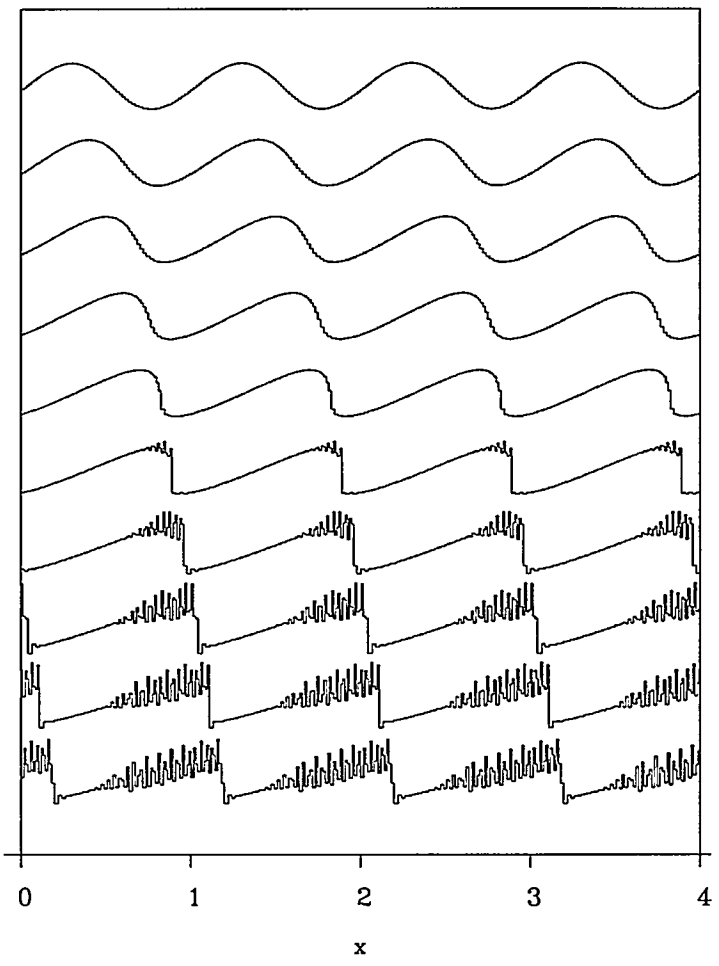

Figure 5. Numerical solution to breaking sine wave problem Upper curve: $t = 0$. Lower curve: $t = 2t_b$

a while it all becomes white noise, as can be seen on figure 6. The reason why the discrete system survives is that it is impossible for the fluid columns to change places or spill over, because it requires an infinite amount of energy to squeeze a column of finite volume to zero width (the height would become infinite). Such a potential barrier is not present in the continuous system.

The numerical accuracy of the solution is very good[19], so we can rule out numerical problems. Decreasing the cell size does not change the solution appreciably for times before the wave breaks ($t < t_b$), but the wild oscillations afterwards depend on the cell size, so that there is no continuous limit of the 'strange' part (which, of course, there should not be). Therefore the only way to prevent this strange behaviour is to be to redefine the system. The problem is that energy is conserved, so that the system cannot get rid of the kinetic energy generated

[19] The energy of the system is conserved to within 5 decimal places, and it is possible to make a time reversal and return the solution to the initial conditions - even if after it has been continued to the state shown on figure 4.

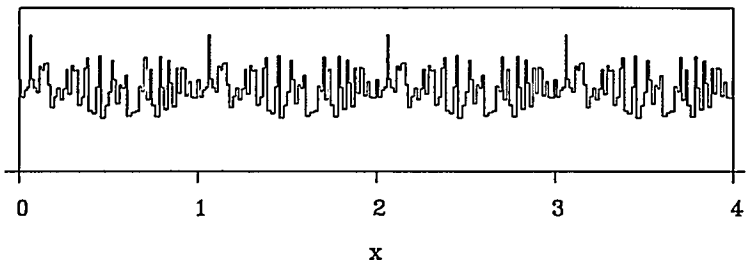

Figure 6. A totally broken sine wave ($t = 8t_b$)

by the breaking wave. Thinking in terms of statistical mechanics we expect the principle of equipartitioning of the energy to apply. According to this all modes should eventually be excited with the same energy (in the mean), and, as the energy spectrum becomes flat, spatial correlations disappear. The solutions therefore must either stop after a finite time, which it does not, or degenerate into uncorrelated white noise. The energy spectrum (in terms of amplitudes of solutions to the linearized equations) does in fact become flat. Thus we are forced to conclude, that the strange behaviour is inevitable, and the only cure for it is to introduce energy dissipation as discussed in Section 2.5. Figure 3 shows the results of a calculation with internal friction added to the model. The effect of adding friction is obviously to damp the wild oscillations and a regular (grid size independent) solution is obtained.

Blobs

The derivation of the shallow water equations by PLA works essentially in the same way a the deriviation of the 1D chain equations. However, for the continuous system there is a weak point: It has to be assumed that x is a monotonous function of ξ. In other words, we rule out the possibility of the layer being folded. It is always possible to make infinitesimal variations of the map $\xi \rightarrow x(\xi)$ so that $x(\xi)$ is no longer monotonous. This restriction is therefore not natural, and it seems that a 'folded' map is sometimes needed to minimize the action integral (cfr. the breaking wave problem of Chapter 2). Therefore the natural development of the finite system could be that the fluid columns jump on top of each other. For the finite system the columns are constrained to stand 'shoulder by shoulder' since we only used one variable x_n to mark the interface between two neighbour columns. 'Folding' the finite system is therefore prevented by a potential barrier, which the continuous system does not have. This explains why the finite system does not break down. We could have chosen to allocate two individual variables for each cell, so that the cells are no longer necessarily 'glued together'. In such a system the cells are allowed to slide on top of each other, which takes only a finite amount of energy. This is done in the following one dimensional blob model.

We choose to define the motion of the n-th liquid parcel ('blob') by a linear map

$$\xi \mapsto x = \xi\sigma + x_n \tag{156}$$

It is understood that the map takes columns (vertical slices of the blob) onto

columns. In the reference position (on the ξ axes) the blob is described by a shape function

$$h_0(\xi) = \phi(\xi) \tag{157}$$

In the current position (on the x-axis) it will therefore have the shape

$$h_n(x) = \frac{\Delta V}{\sigma_n}\phi\left(\frac{x - x_n}{\sigma_n}\right) \tag{158}$$

The standard shape could be a rectangle as above, but all we will demand is that

$$\begin{aligned} \int \phi(\xi)\, d\xi &= 1 \\ \int \phi(\xi)\xi\, d\xi &= 0 \\ \int \phi(\xi)\xi^2\, d\xi &= 1 \end{aligned} \tag{159}$$

This means that x_n is the center of mass of the blob and that σ_n is a measure of its width. These parameters are the generalized coordinates. The fluid height is given by

$$h(x) = \sum_n h_n(x) = \sum_n \frac{\Delta V}{\sigma_n}\phi\left(\frac{x - x_n}{\sigma_n}\right) \tag{160}$$

and the potential energy of the system is (for simplicity we take $b = 0$)

$$\begin{aligned} \mathcal{V} = \int \frac{1}{2}\rho g h^2 dx &= \frac{1}{2}\rho g \sum_{p\,q} \int \frac{\Delta V}{\sigma_p}\phi\left(\frac{x - x_p}{\sigma_p}\right)\frac{\Delta V}{\sigma_q}\phi\left(\frac{x - x_q}{\sigma_q}\right) dx \\ &\equiv \frac{1}{2}\rho g \Delta V \sum_{p\,q} \Phi(x_p - x_q, \sigma_p, \sigma_q) \end{aligned} \tag{161}$$

where Φ acts as a potential. The velocity at a position x in the n-th blob is given by

$$\dot{x} = \dot{\sigma}_n \xi + \dot{x}_n \tag{162}$$

Neglecting again the vertical velocity the kinetic energy of the system becomes

$$\begin{aligned} \mathcal{T} &= \sum_n \int \frac{1}{2}\rho \dot{x}^2 h_n(x) dx \\ &= \frac{1}{2}\rho \Delta V \sum_n \int \{\dot{\sigma}_n \xi + \dot{x}_n\}^2 \phi(\xi)\, d\xi = \frac{1}{2}\rho \Delta V \sum_n \left(\dot{\sigma}_n^2 + \dot{x}_n^2\right) \end{aligned} \tag{163}$$

Putting things together we finally get the Lagrangian

$$\mathcal{L} = \frac{1}{2}\rho \Delta V \sum_n \left(\dot{\sigma}_n^2 + \dot{x}_n^2\right) - \frac{1}{2}\rho g \Delta V \sum_{p\,q} \Phi(x_p - x_q, \sigma_p, \sigma_q) \tag{164}$$

and the equations of motion follow from the Euler-Lagrange equation. [20]

This model bears some resemblance to the blob model of Salmon (1982). The main difference is that in Salmons model the blobs all have the same fixed shape,

[20] It is worth noting that we did not have to specify which blob is on top of which in order to compute the energy. This is because all blobs have the same density. If they have different densities (e.g. as a result of entrainment) the situation becomes slightly more complicated, since we have to decide which blob is on top and it becomes necessary to kept track of how the blobs are ordered vertically.

whereas the blobs are able to adjust themselves to the flow in the present model. Salmons blob model therefore requires that the blobs form a multi-layer, with many blobs on top of each other, in order to reproduce e.g a slumping cloud. In the present model the blobs are able to deform, and the cloud would be able to slump even if it is a mono-layer.

It is straight forward to generalize this to a two (or three) dimensional blob model. Such a model describes a gas of blobs that repel each other, so it can be expected to behave much like a gas. In a way we have therefore re-invented a classical compressible gas, and we can expect the blob system to behave in an analogous fashion. The blob model has some appealing features: it is easily generalized to complex terrain, and the blobs should be able to adjust themselves to complicated geometries. A cloud of blobs can for example split up and recombine if it runs into an insurmountable obstacle - this is a rather tricky maneuvre to perform with the cells that are glued together. Unfortunately numerical experiments with a two dimensional blob model gave discouraging results. The blobs are able to change shape, and they appear to take advantage of this freedom in unexpected ways. A mono-layer of blobs in a box may, for example, soon becomes a multi-layer, if that configuration has the lowest potential energy. The blobs become very flat, all lying on top of each other like a stack of pancakes. This can be avoided by choosing a 'shouldered' shape function ϕ, but then another problem arises: the monolayer crystallizes into a hexagonal structure and acts like one big solid body. This is very annoying, because the crystalline cloud is too easily blocked by obstructions in the terrain - it does not flow like a liquid in the landscape as expected. It might be possible to invent a blob fluid that does not freeze, but it was felt that this was out of the scope of this work, and the matter was not pursued further.

Non-hydrostatic approach

Hydrostatic pressure is not natural in this framework, where it is equivalent to neglecting the 'vertical' kinetic energy term in the Lagrangian. For a finite system model we actually do not have hydrostatic pressure, because this would violate the law of action and reaction at the cell interfaces. This is because we implicitly postulate that internal forces keep the columns rectangular; these forces will be superimposed on the hydrostatic pressure. In the continuous shallow layer model the internal forces happen to be zero, and one can expect that they are small for finite systems too, or at least that they do not have spurious influences on the flow (except keeping the columns rectangular). However, the (questionable) idea of neglecting the contribution to the kinetic energy from w is the same for both systems, and we could have chosen to keep it. For a column in a finite system the map specifies the location of all fluid points, and hence w is known[21]:

$$w(z) = \frac{z}{h_n}\frac{dh_n}{dt} = -\frac{z(u_{n+1}-u_n)}{x_{n+1}-x_n} \tag{165}$$

Using this the missing energy term can be written as

$$\sum \frac{1}{2}\rho(x_{n+1}-x_n)\int_0^h w^2 dz = \sum \frac{1}{6}\rho\Delta V^3 \frac{(u_{n+1}-u_n)^2}{(x_{n+1}-x_n)^4} \tag{166}$$

Inserting into (139) leads to an equation similar in structure to (155), which does not take much more effort to solve. Instead of writing it down we will derive the corresponding equations for the continuous system, since these look more transparent.

[21] Flat terrain is assumed

The continuous system Lagrangian for non-hydrostatic shallow water on flat ground ($b = 0$) is equal to

$$\mathcal{L} = \int \rho \left(\frac{1}{2} u^2 + \frac{1}{6} \left(\frac{\partial h}{\partial s} \right)^2 + \frac{1}{2} g h \right) h_0 \, d\xi \tag{167}$$

The layer height is equal to

$$h = h_0 \left| \frac{\partial x}{\partial \xi} \right|^{-1} \tag{168}$$

Assuming that x is an increasing function of ξ the variation of h is equal to

$$\delta h = -h_0 \left| \frac{\partial x}{\partial \xi} \right|^{-2} \frac{\partial \delta x}{\partial \xi} = -h \frac{\partial \delta x}{\partial x} \tag{169}$$

As before we also have

$$\delta u = \frac{\partial \delta x}{\partial s} \tag{170}$$

Since our map automatically preserves volume the principle of least action gives

$$\delta \mathcal{S} = 0 \tag{171}$$

or

$$\begin{aligned} 0 &= \int_{t_0}^{t_1} ds \int d\xi \rho h_0 \left(u \frac{\partial \delta x}{\partial s} - \frac{1}{3} \frac{\partial h}{\partial s} \frac{\partial}{\partial s} \left(h \frac{\partial \delta x}{\partial x} \right) + \frac{1}{2} g h \frac{\partial \delta x}{\partial x} \right) \\ &= \int_{t_0}^{t_1} ds \int d\xi \rho h_0 \left(-\delta x \frac{\partial \delta u}{\partial s} + \frac{1}{3} \frac{\partial^2 h}{\partial s^2} h \frac{\partial \delta x}{\partial x} + \frac{1}{2} g h \frac{\partial \delta x}{\partial x} \right) \\ &= \int_{t_0}^{t_1} dt \int dx \rho \delta x \left(-h \frac{\partial u}{\partial s} - \frac{\partial}{\partial x} \frac{1}{3} h^2 \frac{\partial^2 h}{\partial s^2} - g h \frac{\partial h}{\partial x} \right) \end{aligned} \tag{172}$$

Since this is valid for 'any' δx we get

$$h \frac{\partial u}{\partial s} + \frac{\partial}{\partial x} \frac{1}{3} h^2 \frac{\partial^2 h}{\partial s^2} = -g h \frac{\partial h}{\partial x} \tag{173}$$

Using the relation

$$\frac{\partial h}{\partial s} = -h \frac{\partial u}{\partial x} = -\frac{h^2}{h_0} \frac{\partial u}{\partial \xi} \tag{174}$$

(173) can be written in then form

$$\left(h - \frac{\partial}{\partial x} \frac{1}{3} h^2 \frac{\partial}{\partial x} \right) \frac{\partial u}{\partial s} = -\frac{\partial}{\partial x} \frac{2}{3} h^3 \left(\frac{\partial u}{\partial x} \right)^2 - g h \frac{\partial h}{\partial x} \tag{175}$$

Numerically the main complication is the fact that the equation is implicit in $\frac{\partial u}{\partial s}$, so we must first solve the equation of the form

$$\left(1 - \frac{1}{h} \frac{\partial}{\partial x} \frac{1}{3} h^2 \frac{\partial}{\partial x} \right) \frac{\partial u}{\partial s} = S \tag{176}$$

If we regard h as a constant this equation has the analytical solution

$$\frac{\partial u}{\partial s} = \int \frac{\sqrt{3}}{2h} \exp \left(-\frac{|x - x'| \sqrt{3}}{h} \right) S(x') \, dx' \tag{177}$$

Although h is generally not constant this indicates that $\frac{\partial u}{\partial s}$ is determined by an average over an area of approximate width equal to h. A discontinuity of

the hydrostatic pressure (contained in S) will therefore be smeared out, thus preventing infinite accelerations of front cells. Thus h acts as a horizontal length scale that prevents generation of waves of arbitrarily small wave length. Numerical (lock exchange) experiments have confirmed this. The model considerably delays the steepening of gradients which is common to solutions to the shallow water equations. Solutions may eventually get noisy, but this has not been observed even for very long calculations. However, the problem of energy conservation in hydraulic jumps must still be there. In computer animations the nonhydrostatic waves appear to be much more realistic than hydrostatic waves. One actually can get seasick by looking at the screen too long. There can be little doubt that this correction is an improvement.

Terrain

The derivation above was for flat ground. The Lagrangian for $\nabla b \neq 0$ is

$$\mathcal{L} = \int \left\{ \frac{1}{2}u^2 + \frac{1}{6}\left\{ \left(\frac{\partial h}{\partial s}\right)^2 + 3\frac{\partial h}{\partial s}\frac{\partial b}{\partial s} + 3\left(\frac{\partial b}{\partial s}\right)^2 \right\} + g\left(\frac{1}{2}h + b\right) \right\} \rho h_0 \, d\xi \tag{178}$$

Although the derivation of the governing equations is again straight forward, it will generate many extra terms compared to the simple shallow water equations. A simplification can be made by dropping terms involving $\frac{\partial h}{\partial s}$. In effect this means that we set $w = \frac{\partial b}{\partial s}$ for the whole layer, so the approximation is hydrostatic, but takes accellerations down slopes into account. The resulting Lagrangian is

$$\mathcal{L} = \int \left\{ \frac{1}{2}u^2 + \frac{1}{2}\left(\frac{\partial b}{\partial s}\right)^2 + g\left(\frac{1}{2}h + b\right) \right\} \rho h_0 \, d\xi \tag{179}$$

The variation af $\mathcal{L}$ is done in the same way as in equation (172) except for the extra term, where we use

$$\delta \frac{\partial b}{\partial s} = \frac{\partial}{\partial s}\frac{\partial b}{\partial x}\frac{\partial \delta x}{\partial x}, \tag{180}$$

After a few partial integrations (as in (172)) that isolates δx we get the following equation

$$\left\{ 1 + \left(\frac{\partial b}{\partial x}\right)^2 \right\} \frac{\partial u}{\partial s} + u^2 \frac{\partial b}{\partial x}\frac{\partial^2 b}{\partial x^2} = -g\frac{\partial (h+b)}{\partial x} \tag{181}$$

This equation takes the same form as the simple momentum equation if we write it as

$$\frac{\partial}{\partial s}\sqrt{1+b'^2}u = -g\frac{1}{\sqrt{1+b'^2}}\frac{\partial (h+b)}{\partial x} \tag{182}$$

where b' is short for $\frac{\partial b}{\partial x}$. If we introduce a curved x-axis that follows the terrain, and measure the velocity along this axis, in other words make the substitutions

$$\begin{aligned} \frac{1}{\sqrt{1+b'^2}}\frac{\partial}{\partial x} &\mapsto \frac{\partial}{\partial x} \\ \sqrt{1+b'^2}\,u &\mapsto u \end{aligned} \tag{183}$$

the form of the momentum equation is the same as for flat ground. However, making this substitution the form of the equation of continuity is altered unless we also redefine h ($h/\sqrt{1+b'^2} \mapsto h$). In that case the equation of continuity is the same, but $h\sqrt{1+b'^2}$ will appear instead of h on the rhs of the momentum equation. It is not possible to have both equations unchanged at the same time. For

gently sloping terrain, however, we may set $h\sqrt{1+b'^2} \approx 1$, and get the simplified momentum equation

$$\frac{\partial u}{\partial t} + \frac{\partial u}{\partial x} = -g\frac{\partial(b+h)}{\partial x} \tag{184}$$

4.3 Least action with friction and mixing

Hamiltonian dynamics is frictionless. The layer integrated model developed in Chapter 3 is not, so it cannot be derived from PLA directly. In this section the principle of least action will be extended to cover shallow layer systems with mixing and friction.

Imagine a two-fluid system consisting of two layers: an upper ambient layer with constant density ρ_a and a constant velocity field u_a, and a lower mixed layer with variable density $\rho(x,t)$ and variable velocity field $u(x,t)$. The mixed layer consists of a mixture of the ambient fluid and a denser fluid with density ρ_0, and the density profile is such that the potential energy density (per unit area, or length in 1D) can be written as

$$\mathcal{V} = \beta\Delta\rho g h^2 - xfh \tag{185}$$

where $\Delta\rho = \rho - \rho_a$ and β is a constant corresponding to a chosen profile (e.g. $\beta = \frac{1}{3}$ for a triangular profile). The term $-xf$ is an additional potential associated with external forces (other than gravity) acting on the dense fluid, and it can be regarded as 'technical' at this point.

The kinetic energy density is evaluated in the rest frame of the ambient fluid is equal to

$$\mathcal{T} = \frac{1}{2}\rho h(u-u_a)^2 \tag{186}$$

We use this quantity to define the Lagrangian (density)

$$\mathcal{L} = \mathcal{T} - \mathcal{V} \tag{187}$$

The generalized coordinates are defined by the map $(\xi, s) \to (x,t)$, which maps a column of the dense fluid from an arbitrary unmixed reference state (height $h_0(\xi)$ and density ρ_0) to the position in the present state. Since the dense fluid will be mixed with ambient fluid (air) the map is not assumed to be volume preserving. The map traces the dense fluid while the ambient lighter fluid is just 'filling in'. The ambient fluid is therefore not regarded as a part of the mechanical system as we do not specify the exact locations of each light fluid elements. Assuming incompressibility we have (in 1D for simplicity)

$$\Delta\rho h\, dx = \Delta\rho_0 h_0\, d\xi \tag{188}$$

where $\Delta\rho_0 = \rho_0 - \rho_a$. This can also be written as

$$h = \frac{\Delta\rho_0 h_0}{\Delta\rho}\frac{1}{\frac{\partial x}{\partial \xi}} \tag{189}$$

The layer height h is indirectly determined by the rate of mixing, which we imagine to be caused by a mechanism that controls the density of the lower layer in such a way that $\rho(\xi, s)$ is a fixed and predetermined function. In reality this function is determined by the motion of the fluid, but we must regard it as a fixed function in the variations of the action integral. For the variation of h it therefore follows from (189) that

$$\delta h = -h\frac{\partial \delta x}{\partial x} \tag{190}$$

In the same way the potential xf will be regarded as a potential specific to each dense fluid element, so that $f(\xi, s)$ is a fixed, predetermined function. The physical picture is that only the fluid element corresponding to ξ responds to the potential $-xf(\xi, s)$, while all other elements are unaffected. In this way we can specify any f, even a friction force. In other words the trick is to remove friction forces and replace them by conservative, time depending, force fields, which have exactly the same effect.

The variational principle determining the governing equations can be stated as

$$\delta \int_{t_0}^{t_1} dt \int dx\, \mathcal{L} = \delta \int_{t_0}^{t_1} ds \int d\xi\, \frac{\Delta\rho_0 h_0}{\Delta\rho h}\mathcal{L} = 0 \tag{191}$$

This holds for any variation with fixed states at $t = t_0$ and $t = t_1$. Integrating by part we get

$$\begin{aligned}
0 &= \int_{t_0}^{t_1} ds \int \Delta\rho_0 h_0\, d\xi \left(\frac{(u-u_a)\rho}{\Delta\rho}\frac{\partial \delta x}{\partial s} + g\beta h\frac{\partial \delta x}{\partial x} + \frac{f}{\Delta\rho}\delta x\right) \\
&= \int_{t_0}^{t_1} ds \int \Delta\rho_0 h_0\, d\xi \left(-\delta x\frac{\partial}{\partial s}\frac{(u-u_a)\rho}{\Delta\rho} + g\beta h\frac{\partial \delta x}{\partial x} + \frac{f}{\Delta\rho}\delta x\right) \\
&= \int_{t_0}^{t_1} dt \int \Delta\rho h\, dx \left(-\delta x\frac{\partial}{\partial s}\frac{(u-u_a)\rho}{\Delta\rho} + g\beta h\frac{\partial \delta x}{\partial x} + \frac{f}{\Delta\rho}\delta x\right) \\
&= \int_{t_0}^{t_1} dt \int \delta x\, dx \left(-\Delta\rho h\frac{\partial}{\partial s}\frac{(u-u_a)\rho}{\Delta\rho} - \frac{\partial}{\partial x}g\beta\Delta\rho h^2 + hf\right)
\end{aligned} \tag{192}$$

Since this holds for any δx we finally get

$$\Delta\rho h\frac{\partial}{\partial s}\frac{(u-u_a)\rho}{\Delta\rho} = -\frac{\partial}{\partial x}g\beta\Delta\rho h^2 + hf \tag{193}$$

It also follows from (189) that

$$\frac{\partial \Delta\rho h}{\partial s} = -h\Delta\rho\frac{\partial u}{\partial x} \tag{194}$$

or

$$\frac{\partial \Delta\rho h}{\partial t} + \frac{\partial u\Delta\rho h}{\partial x} = 0 \tag{195}$$

As a measure of the entrainment we define the entrainment velocity w_e by the equation

$$\frac{\partial h}{\partial t} + \frac{\partial uh}{\partial x} = w_e \tag{196}$$

It follows that

$$\frac{\partial \rho h}{\partial t} + \frac{\partial u\rho h}{\partial x} = \rho_a w_e \tag{197}$$

and that

$$\frac{\partial \Delta\rho}{\partial t} + u\frac{\partial \Delta\rho}{\partial x} = -\frac{\Delta\rho w_e}{h} \tag{198}$$

Using these relations (193) can be rewritten as

$$\frac{\partial h\rho u}{\partial t} + \frac{\partial uh\rho u}{\partial x} = -\frac{\partial}{\partial x} g\beta\Delta\rho h^2 + \rho_a u_a w_e + hf \tag{199}$$

This equation is of the same form as the (one-dimensional version of the) momentum equation (136) derived earlier by means of debth integration of the Navier-Stokes equations [22]. The fact that (136) follows from a variational principle allow us to generate discrete versions of the system, which can serve as ideal numerical schemes, since they automatically obey conservation laws. This will be done in the following.

4.4 The SLAM model

In this section the equations for a numerical 2d shallow layer model will be derived. The model is called SLAM, an acronym for Shallow LAyer Model.

In order to proceed we must construct a discrete Lagrangian from a finite set of parameters specifying the flow. We shall use a triangular grid, since this seems to be the simplest choice. The triangles are connected side-to-side and corner-to-corner, and the corners (grid points) serve as generalized coordinates, see figure 7. We will denote the coordinates of a grid point P by $X_P = (X_{P1}, X_{P2})$, a two-component vector. Each triangle contains a fixed amount of dense gas and a varying amount of entrained air, and the density is to be regarded as a predetermined function of time as far as the variational principle is concerned.

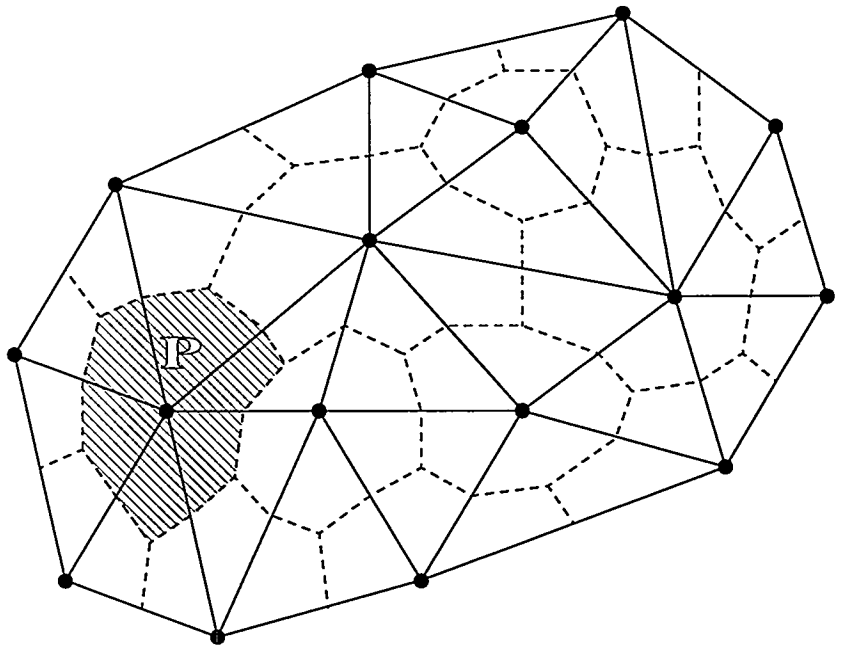

Figure 7. Triangular grid used for the SLAM model. The dashed lines indicate the contours of the point domains (Ω_P shown as hatched area).

[22] The derivation was made here for the one-dimensional case, but the conclusion also holds in the two-dimensional case.

We need to express the kinetic and the potential energies of the system in terms of the grid point coordinates $\{X_P\}$ and the velocities of the grid points $\{U_P\}$. To this end we need to specify the location of all dense fluid element of the system, not just the location of grid points themselves. In order to do this we make a map from a 'standard' triangle $A'B'C'$ onto one of the triangles, say ABC. This can be done in many ways, but the simplest choice is probably a linear transformation, where the point $\overrightarrow{O'A'} + s_1 \overrightarrow{A'B'} + s_2 \overrightarrow{A'C'}$ is mapped to the point $\overrightarrow{OA} + s_1 \overrightarrow{AB} + s_2 \overrightarrow{AC}$. The two parameters s_1 and s_2 specify a dense fluid element and they remain the same at all times (for that element). In this way the dense fluid is distributed evenly in ABC at all times, so that the height is constant inside each triangular (actually prismatic) cell in the grid. We could have used additional parameters to specify a varying height inside cells, but we will prefer to make the simplest possible approach. The velocity of a fluid element inside the triangle becomes

$$U(s_1, s_2) = U_A + s_1(U_B - U_A) + s_2(U_C - U_A) \tag{200}$$

and integrating over the triangle we get the kinetic energy

$$\begin{aligned} \mathcal{T}_{ABC} &= \frac{1}{12}\rho_{ABC} H_{ABC} \Omega_{ABC} (U_A{}^2 + U_B{}^2 + U_C{}^2 + U_A U_B + U_B U_C + U_C U_A) \\ &= \frac{1}{6}\rho_{ABC} H_{ABC} \Omega_{ABC} (U_A{}^2 + U_B{}^2 + U_C{}^2) \\ &- \frac{1}{24}\rho_{ABC} H_{ABC} \Omega_{ABC} ((U_A - U_B)^2 + (U_B - U_C)^2 + (U_C - U_A)^2 \end{aligned}$$

where H_{ABC} is the cell height and Ω_{ABC} is the area of the triangle. If h,ρ and u are smooth functions the total kinetic energy of the discrete system can be made to approach the continuum expression for fine grids, viz.

$$\sum_{\Delta} \mathcal{T}_{\Delta} \mapsto \int \frac{1}{2}\rho u^2 h dA \tag{201}$$

where the sum is taken over all triangles in the grid. The potential energy of a triangle can be defined as

$$\mathcal{V}_{\Delta} = \Omega_{\Delta} H_{\Delta} \left[\frac{1}{3} g H_{\Delta} (\rho_{\Delta} - \rho_a) - \sum_{P \in \Delta} F_{P\Delta} \cdot X_P \right] \tag{202}$$

Here $\sum_{P \in \Delta}$ means the sum over all three corner points P of the triangle Δ, and $F_{P\Delta}$ represents non-conservative forces. The form of $F_{P\Delta}$ will be determined later. This gives us the model Lagrangian $\mathcal{L} = \mathcal{T} - \mathcal{V}$ where

$$\mathcal{T} = \sum_{\Delta} \mathcal{T}_{\Delta} = \sum_{\Delta} \frac{1}{6}\rho_{\Delta} H_{\Delta} \Omega_{\Delta} \sum_{P \in \Delta} U_P{}^2 - \frac{1}{48}\rho_{\Delta} H_{\Delta} \Omega_{\Delta} \sum_{P,Q \in \Delta} (U_P - U_Q)^2 \tag{203}$$

is the kinetic energy and

$$\mathcal{V} = \sum_{\Delta} \mathcal{V}_{\Delta} = \sum_{\Delta} H_{\Delta} \Omega_{\Delta} \left[\frac{1}{3} g H_{\Delta} (\rho_{\Delta} - \rho_a) - \sum_{P \in \Delta} F_{P\Delta} \cdot X_P \right] \tag{204}$$

is the potential energy.

Since we have a discrete system the principle of least action leads to the Euler-Lagrange equation

$$\frac{d}{dt}\frac{\delta \mathcal{L}}{\delta U_P} = \frac{\delta \mathcal{L}}{\delta X_P} \tag{205}$$

Before we can write out these equations we must express H_Δ and Ω_Δ in terms of the grid point coordinates. Using conservation of buoyancy the quantity $\Delta M_\Delta = H_\Delta \Omega_\Delta (\rho_\Delta - \rho_a)$ is a constant of motion for each triangle, so we have

$$\begin{aligned} \frac{\delta \Delta M_\Delta}{\delta X_P} &= 0 \\ \frac{\delta H_\Delta \Omega_\Delta}{\delta X_P} &= 0 \\ \frac{\delta H_\Delta}{\delta X_P} = \frac{\delta}{\delta X_P} \frac{\Delta M_\Delta}{(\rho_\Delta - \rho_a)\Omega_\Delta} &= -\frac{H_\Delta}{\Omega_\Delta} \frac{\delta \Omega_\Delta}{\delta X_P} \end{aligned} \tag{206}$$

The variation of Ω_{ABC} with respect to moving one of the corners, say A, follows from simple geometry. If A, B and C label the corners counter clockwise we have

$$\frac{\delta \Omega_{ABC}}{\delta X_A} = \frac{1}{2} \widehat{BC} \equiv S_{P\Delta} \tag{207}$$

where $\widehat{BC}$ is $\overrightarrow{BC}$ rotated 90° counter clockwise. In order to streamline the notation we will write $S_{P\Delta}$ instead of $\frac{\delta \Omega_\Delta}{\delta X_P}$. Using this notation we get

$$\frac{\delta \mathcal{L}}{\delta X_P} = \sum_{\Delta \ni P} \left[\frac{1}{3} g H_\Delta^2 (\rho_\Delta - \rho_a) S_{P\Delta} + H_\Delta \Omega_\Delta F_{P\Delta} \right] \tag{208}$$

As before we define the entrainment velocity $W_{e\Delta}$, one for each triangle, and write the equation of continuity as

$$\frac{d \Omega_\Delta H_\Delta}{dt} = \Omega_\Delta W_{e\Delta} \tag{209}$$

or

$$\frac{d M_\Delta}{dt} = \rho_a \Omega_\Delta W_{e\Delta} \tag{210}$$

where $M_\Delta \equiv \rho_\Delta \Omega_\Delta H_\Delta$.

We can now write (205) more explicitly. Using (201) we find that

$$\begin{aligned} \frac{\delta \mathcal{T}_{ABC}}{\delta U_A} &= \frac{1}{12} M_{ABC} (2U_A + U_B + U_C) \\ &= \frac{1}{3} M_{ABC} U_A + \frac{1}{12} M_{ABC} \left((U_A - U_A) + (U_B - U_A) + (U_C - U_A) \right) \end{aligned} \tag{211}$$

so that in general

$$\frac{\delta \mathcal{L}}{\delta U_P} = \frac{\delta \mathcal{T}}{\delta U_P} = \sum_{\Delta \ni P} \frac{1}{3} M_\Delta U_P + \sum_{\Delta \ni P} \sum_{Q \in \Delta} \frac{1}{12} M_\Delta (U_Q - U_P) \tag{212}$$

where the first sum is taken over all triangles containing P, and the last sum is taken over all corners of such triangles (possibly double counting). Using (210) this leads to

$$\begin{aligned} \frac{d}{dt} \frac{\delta \mathcal{L}}{\delta U_P} &= \sum_{\Delta \ni P} \frac{dU_P}{dt} \frac{1}{3} M_\Delta + \sum_{\Delta \ni P} \sum_{Q \in \Delta} \frac{1}{12} M_\Delta \left(\frac{dU_Q}{dt} - \frac{dU_P}{dt} \right) \\ &\quad + U_P \frac{1}{3} \sum_{\Delta \ni P} \rho_a W_{e\Delta} + \sum_{\Delta \ni P} \sum_{Q \in \Delta} \frac{1}{12} \rho_a W_{e\Delta} (U_Q - U_P) \end{aligned} \tag{213}$$

This accounts for the left hand side of (205). The evaluation of the right hand side of (205) is easy because of (206). The following discrete momentum equation results

$$\sum_{\Delta \ni P} \frac{dU_P}{dt} \frac{1}{3} M_\Delta + \sum_{\Delta \ni P} \sum_{Q \in \Delta} \frac{1}{12} M_\Delta \left(\frac{dU_Q}{dt} - \frac{dU_P}{dt} \right)$$

$$+U_P \frac{1}{3} \sum_{\Delta \ni P} \rho_a W_{e\Delta} + \sum_{\Delta \ni P} \sum_{Q \in \Delta} \frac{1}{12} \rho_a W_{e\Delta} (U_Q - U_P)$$

$$= \sum_{\Delta \ni P} \left[\frac{1}{3} g H_\Delta^2 (\rho_\Delta - \rho_a) S_{P\Delta} + H_\Delta \Omega_\Delta F_{P\Delta} \right] \tag{214}$$

Although complicated by many terms this equation has a simple form. The main complication is that the accelerations are given implicitly, so that a set of linear equations have to be solved in each time step (using e.g. the conjugate gradient method). It should be noted that a simpler equation, giving the accelerations explicitly, can be obtained if the kinetic energy of a triangle is defined as $\frac{1}{6} \rho_\Delta H_\Delta \Omega_\Delta (U_A^2 + U_B^2 + U_C^2)$. This corresponds to a situation where the mass of the triangle is concentrated on the corners (one third on each). In the hydrostatic approximation the two approaches give almost identical results. However, when the hydrostatic approximation is dropped the equations become implicit anyway, and the alternative form of the kinetic energy is no longer a major simplification.

The next question is how to evaluate the non-conservative forces $F_{P\Delta}$. First we note that they enter the equations as

$$\sum_P F_P \equiv \sum_{\Delta \ni P} H_\Delta \Omega_\Delta f_{P\Delta} \sim \int_{\Omega_P} f h \, dA \tag{215}$$

In order to relate F_P to the continuous case we interpret F_P as the integral over a domain Ω_P surrounding P[23]. Ω_P can be defined by cutting each triangle along three line segments each connecting the centre[24] and the midpoint of one of the sides. This divides each triangle into three pieces all having the same area, and Ω_P consists of all such pieces containing P, see figure 7. (136) gives three terms of the integrand f: external friction, internal friction and a stress term. To this comes drag forces.

The stress term does not seem to add any essential physics, so we choose to drop it.

In order to evaluate F_P we express f by means of the flow field as specified by the linear map, where the velocity depends linearly on the space coordinates inside a triangle. This means that

$$\frac{\partial u_\alpha}{\partial x_\beta} = \frac{1}{\Omega_\Delta} \sum_{P \in \Delta} U_{P\alpha} S_{P\Delta\beta} \tag{216}$$

everywhere inside Δ. $S_{P\Delta}$ was defined in equation (207).

The internal friction term is evaluated as follows

$$\int_{\Omega_P} \frac{\partial}{\partial x_\beta} \frac{1}{2} \rho K h \left(\frac{\partial u_\alpha}{\partial x_\beta} + \frac{\partial u_\beta}{\partial x_\alpha} \right) dA = \int_{\partial \Omega_P} \frac{1}{2} \rho K h \left(\frac{\partial u_\alpha}{\partial x_\beta} + \frac{\partial u_\beta}{\partial x_\alpha} \right) n_\beta \, dl$$

$$= -\sum_{\Delta \ni P} \frac{\rho_\Delta K_\Delta H_\Delta S_{P\Delta\beta}}{2\Omega_\Delta} \sum_{Q \in \Delta} (U_{Q\alpha} S_{Q\Delta\beta} + U_{Q\beta} S_{Q\Delta\alpha}) \tag{217}$$

where $K_\Delta = C_K H_\Delta \tilde{u}_\Delta$. The second integral is performed along the contour of Ω_P with dl denoting a line element and n a unit vector pointing out of Ω_P.

[23] Note the abuse of notation: Ω_P and Ω_Δ have differen meanings, cfr. figure 7.

[24] The centre of the triangle is defined here as the centre of mass, i.e. the point of intersection of the medians.

The external friction term could be evaluated using the linear map, but that would produce rather voluminous expressions. Instead we simply put $u = U_P$ inside Ω_P. This gives

$$\int_{\Omega_P} C_f \tilde{u} \left(\rho_a (u_{a\alpha} - u_\alpha) - \rho \frac{u_\alpha}{\log(1 + h/z_0) - 1} \right) dA$$

$$\sim \sum_{\Delta \ni P} \frac{1}{3} \Omega_\Delta \, C_f \tilde{u}_\Delta \left(\rho_a (u_{a\alpha} - U_{P\alpha}) - \rho_\Delta \frac{U_{P\alpha}}{\log(1 + H_\Delta/z_0) - 1} \right) \quad (218)$$

In section 3.6 drag forces were discussed. In the present framework the cloud is made from triangular prisms, and it is natural to apply drag forces on the free part of the vertical sides (e.g the part in contact with the air). A drag force of the form (132) is applied where the relative motion of the air and the side of a prism is so that the air blows into the prism.

Finally the equation for the turbulent kinetic energy is derived by inspection of (137) and adding a additional term due the production of turbulent kinetic energy by internal friction. This gives

$$\frac{d}{dt} \frac{1}{2} M_\Delta \tilde{u}_\Delta^2 =$$

$$\sum_{P \in \Delta} \frac{1}{3} \Omega_\Delta \, C_f \tilde{u}_\Delta \left(\rho_a (u_a - U_P)^2 + \rho \frac{U_P^2}{\log(1 + H_\Delta/z_0) - 1} - \tilde{u}_\Delta^2 \log(1 + H_\Delta/z_0) \right)$$

$$+ \sum_{P \in \Delta} \frac{1}{6} \Omega_\Delta \rho_a (u_a - U_p)^2 \, W_{e\Delta} - \frac{1}{3} (\rho_\Delta - \rho_a) g H_\Delta \Omega_\Delta W_{e\Delta}$$

$$+ \frac{\rho_\Delta K_\Delta H_\Delta}{2\Omega_\Delta} \sum_{P,Q \in \Delta} (S_{P\Delta} \cdot U_Q \, S_{Q\Delta} \cdot U_P + S_{P\Delta} \cdot S_{Q\Delta} \, U_P \cdot U_Q) \quad (219)$$

We recall that the entrainment rate is given by

$$W_{e\Delta} = \frac{C_w \tilde{u}_\Delta}{1 + C_R Ri_\Delta} \quad (220)$$

where

$$Ri_\Delta = \frac{g H_\Delta (\rho_\Delta - \rho_a)}{\rho_a \tilde{u}_\Delta^2} \quad (221)$$

This closes the set of equations.

Non-hydrostatic corrections

From the discussions in Chapter 2 it was concluded that the hydrostatic approximation is a severe limitation of the model. It is simple, but for this simplicity we have to pay a price. As long as the cloud is 'shallow' the hydrostatic works, but dense gas clouds are not always shallow and there usually is an edge where the approximation breaks down. The problem is that the forces between cells are determined from geometry, so that the response to an external force is delayed because the cloud has to deform itself in order to react. With the inclusion of entrainment in the model numerical calculations show that the cloud edge becomes sharp and the cells at the boundaries tend to grow very large (both the height and the width become much larger than neighbour cells in the bulk). After a while the boundary cells become so large (and massive) that they squeeze the bulk cells together. Reducing the cell size does not seem to cure the problem. What seems to happen is that the boundary cells grow until the hydrostatic pressure from the

bulk is balanced by friction. In other words the boundary cells grow until they cover a large area, no matter how small they were from the beginning. In this way friction on the boundary cells prevent the cells behind them from slumping and suppress their development. Using a compensating drag force at the boundary helps a little, but it does not solve the problem.

Real clouds do not consist of columns or prisms, so denser gas behind the front will intrude under the leaner gas to form the characteristic counter rotating front vortex. There is no way to represent this front vortex in a shallow layer model, so we have to invent something that mimics the front in some way. Here the use of a front force is problematic, because it acts locally, so that the boundary cells feel a finite force no matter how small they are, with spurious large accelerations as a consequence. A reduced pressure at the edge should be transmitted immediately into the bulk (at the speed of sound, which is infinite in incompressible fluids), without waiting for the cloud to slump. This would turn the effect of a discontinuity of the hydrostatic pressure into a volume effect rather than a 'line' effect as discussed in section 4.2, and prevent a finite force from being concentrated on infinitesimal mass. The discontinuity of hydrostatic pressure across a narrow boundary cell will make it slump, but, if it is very narrow, the slumping produces large *vertical* accelerations. If vertical inertia is *not* neglected the situation is different. Then the pressure will drop inside the cell in order to create the vertical accelerations, and this pressure drop, being associated with an acceleration rather than a change of geometry, is transmitted instantly to the bulk. The actual pressure therefore becomes continuous across the boundary, and the spurious infinite accelerations of thin boundary cells is prevented. As we saw earlier it is relatively easy to make a non-hydrostatic correction within the present formalism, and we shall do this below. The derivation can be made for the continuous system or for the discrete system; we will only do it for the discrete system.

We account for the vertical inertia by adding a term to the Lagrangian corresponding to the contribution to the kinetic energy from the vertical velocity component. Neglecting entrainment[25] w is given by

$$w(z) = \frac{z}{H}\frac{dH}{dt} \tag{222}$$

and the extra kinetic energy for a cell becomes

$$\mathcal{L}'_\Delta = \frac{1}{6}M_\Delta\left(\frac{dH_\Delta}{dt}\right)^2 = \frac{M_\Delta^3}{6\rho_\Delta^2}\frac{1}{\Omega_\Delta^4}\left(\frac{d\Omega_\Delta}{dt}\right)^2 \tag{223}$$

This should first be written in terms of the generalised coordinates, the U's and the X's, and then the term

$$\sum_{\Delta \ni P}\left(\frac{d}{dt}\frac{\delta \mathcal{L}'_\Delta}{\delta U_P} - \frac{\delta \mathcal{L}'_\Delta}{\delta X_P}\right) \tag{224}$$

should be added to the left hand side of (214). Naming the corners A, B, and C we have for a single cell

$$\begin{aligned}\Omega_\Delta &= \frac{1}{2}(\hat{X}_A \cdot X_B + \hat{X}_B \cdot X_C + \hat{X}_C \cdot X_A)\\ \frac{d\Omega_\Delta}{dt} &\equiv \dot{\Omega}_\Delta = U_A \cdot S_A + U_B \cdot S_B + U_C \cdot S_C\end{aligned} \tag{225}$$

Using these relations we find after some manipulations that

[25] The final results are not affected by this assumption.

$$\frac{d}{dt}\frac{\delta \mathcal{L}'_\Delta}{\delta U_A} - \frac{\delta \mathcal{L}'_\Delta}{\delta X_A} = \frac{1}{3} M_\Delta H_\Delta^2 \left(\frac{\ddot{\Omega}_\Delta}{\Omega_\Delta^2} - \frac{2\dot{\Omega}_\Delta^2}{\Omega_\Delta^3} \right) S_A = -\frac{1}{3} \rho_\Delta H_\Delta^2 \ddot{H}_\Delta S_A \quad (226)$$

where

$$\ddot{\Omega}_\Delta = \frac{dU_A}{dt} \cdot S_A + \frac{dU_B}{dt} \cdot S_B + \frac{dU_C}{dt} \cdot S_C + U_A \cdot \hat{U}_C + U_B \cdot \hat{U}_A + U_C \cdot \hat{U}_B \quad (227)$$

The last equality in (226) shows that the extra term represents a correction to the pressure on the cell wall opposite to A. The resulting equations are implicit, since $\ddot{\Omega}_\Delta$ mixes accelerations of neighbouring points.

4.5 Comparison with experiments

The SLAM model presented above applies to instantaneous, isothermal releases. Unfortunately the amount of experimental data available to us for such releases is limited. Ideally different data sets should be used to tune model parameters and to validate the model, but the lack of data prevents this. The situation should improve much when the model is generalised to continuous releases and non-isothermal clouds.

A qualitative test

The shape of a dense gas cloud depends on the initial shape. Thus an initially cubic dense cloud released in still air does not become circular, as one might expect. Instead it develops a square footprint, which is rotated 45° with respect to the base of the initial cube. This can be demonstrated by the following kitchen table experiment.

- Make a cubic box without bottom and lid. The volume should be about 8 liters.
- Place the box on the floor and close all doors and windows to prevent draught.
- Fill half a liter of hot water (from the hot water tap) into a suitable container.
- Throw a handful of dry ice pellets (available from any chemistry lab) into the water.
- As the dry ice sublimates a thick fog develops consisting of CO_2 and water aerosols. The fog has about the same temperature as the hot water.
- Pour the fog into the box.
- Wait until the fog has come to rest.
- Lift the box.

We actually made this experiments and observed very clearly that an initially square clouds become diamond shaped. Figure 8 shows the result of a SLAM calculation. It can be seen that the model basically does the right thing and develops into a rotated square. Perhaps the real cloud had even less rounded corners.

We note that the blob model, with a mono-layer, does not work well for this example. The problem is capitalization. Soon after the square cloud has been set free the corners move outwards leaving four concave sides forming a four-legged star. In this way the four corner blobs block all the other blobs in much the same way as two stones hold the round arch of a Romanesque window.

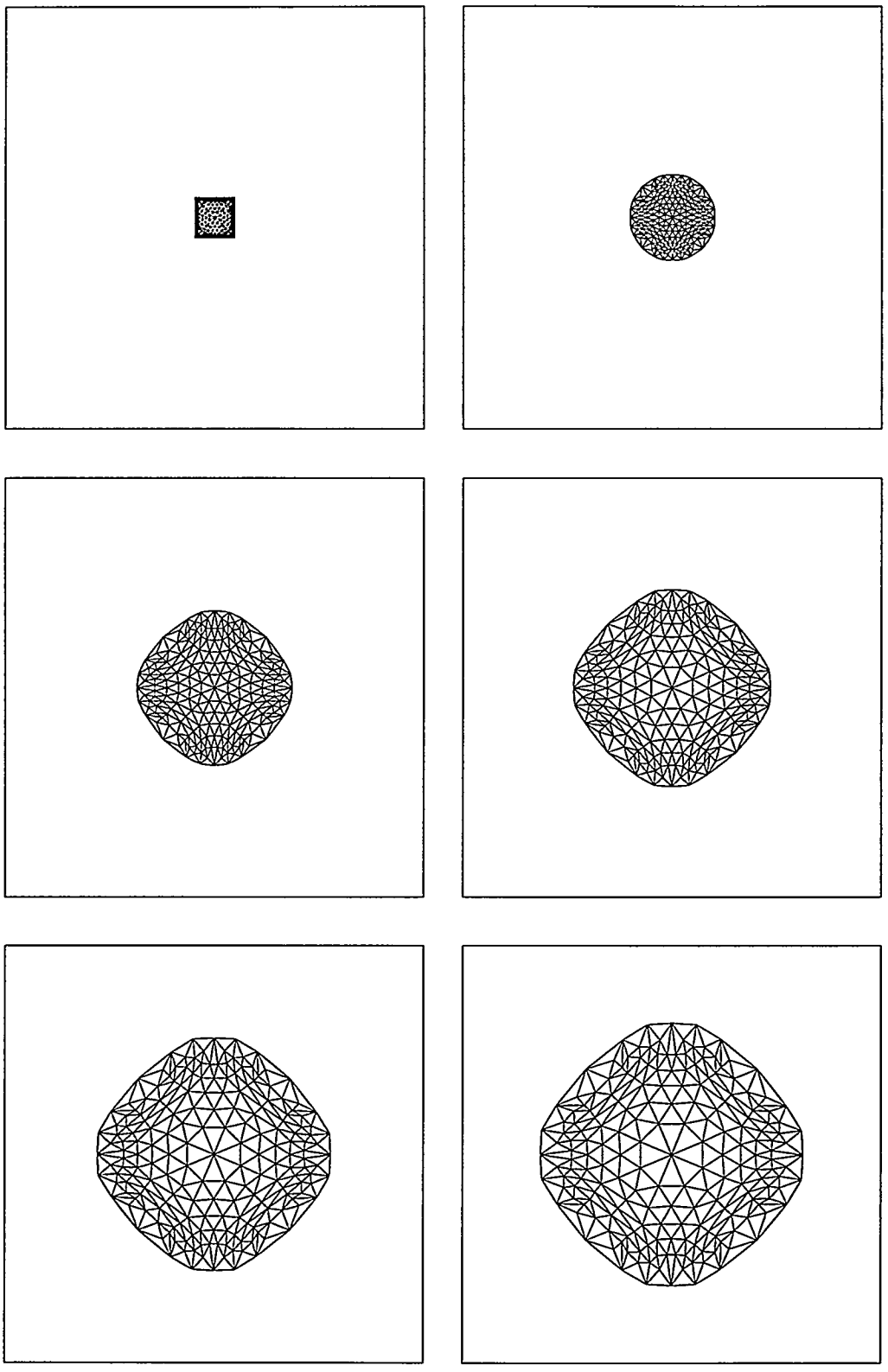

Figure 8. Footprint of a initially cubic CO_2 cloud (20 cm sides). The plots show the grid at 0.25 second intervals.

Thorney Island trial 8

Trial 8 of the Thorney Island test series is an instantaneous, isothermal release of 2000 m^3 of a Freon-Nitrogen mixture with a density 1.63 times that of the ambient air (McQuaid & Roebuck (1983)). The release was made by collapsing a cylindric tent (14 meter diameter).

This is a challenging case to model because initially the cloud was not shallow, and a large front vortex builded. Trial 8 is considered one of the most perfect of the instantaneous Thorney Island releases, and it was used as a test case through the development of the SLAM code. This means that constants have been chosen so as to reproduce this experiment, and hence the results presented below can not be used to validate the model. The purpose of presenting the results is to verify that the model at least can work and give reasonable results for this case. The model can probably be tuned to fit this particular data set much better, but that would not quarantee good results in other cases.

Meteorological data can be found in Puttock (1987). The average windspeed at 10 meter was 2.4 m/s, and the surface roughness was judged to about 12 mm. The stability was estimated as neutral (Pasquill stability class D) from visual observation, and unstable (class B) from heat flux measurements. Temperature profiles show an inversion between 9 and 16 meters, which Puttock suggests might be caused by a land-see temperature difference (the wind was coming from the see).

The results of two calculations will be presented - one using a relatively detailed grid and one using a relatively coarse grid. Figures 9 and 10 show how the grid translates in the two cases. In both cases the grid develops a self similar shape covering almost identical areas for the two resolutions. There is a fair degree of agreement between the area predicted to be visited by the cloud and the sensor positions where gas was detected.

The initial growth of the cloud area is shown on figure 12 together with experimental data by McQuaid & Roebuck (1985) determined from photographs. There is a rough agreement, but the model does not reproduce the period of about 5 seconds of hesitation before the slumping sets in. This could mean that the real flow is more complicated and produces more turbulent kinetic energy than assumed in the model, hence transferring less energy to the radial flow. After the initial slumping the measured area grows approximately linear with time, whereas the model cloud slows down. The further growth of the cloud must be judged by times of arrival and departure for concentration sensors.

In the initial slumping phase the cloud formed a huge doughnut with elevated fronts which later became a very flat pancake several hundred meter in diameter and less than 10 meters high. Figure 11 shows the shape of the slumping cloud for the finer resolution. The observed doughnut shape is well reproduced.

Figure 13 shows predicted and measured maximum concentrations. The maximum is taken over all sensor positions for a given time. Before taking the maximum all time series were averaged in blocks of 10 seconds in order to smooth out fast (and random) fluctuations. The two calculations are in fair agreement with each other and with the measurements.

Figure 14 and 15 show maximum (10 second average) concentrations for each sensor position. Here the maximum is taken over all times for a fixed sensor position. It is evident that the model generally overpredicts the maximum concentrations .

Figures 16 and 17 show measured and calculated concentration time series (for the fine grid). The calculated concentration time series have characteristic discontinuities at the interfaces between cells. Between the discontinuities the concentration will decrease because of the dilution taking place in the passing cell. The

times of arrival and departure are well reproduced for most sensor positions. This is a result of tuning the parameter C_a determining the velocity of entrained air (cfr. equation (69)). It does not work to set the velocity at the top of the cloud equal to the undisturbed velocity at the cloud top (or at the centroid βh, say), because it leads to too large translation velocities.

The predicted peak concentrations are generally too high. It seems that the central cells are developing too slowly, because they are squeezed by the larger cells surrounding them. The squeezing reduces the cell area and thereby limits the entrainment for cells near the centre of the cloud. The effect may be somewhat artificial, since in a real cloud velocity shear and turbulence will even out the concentrations and lower the Richardson numbers for central cells. Therefore the model could probably be improved by allowing diffusion of mass and turbulent kinetic energy to take place between cells. In the present model there is no horizontal diffusion except for 'diffusion' of momentum - not even numerical diffusion. The entrainment rate is estimated by a commonly used top-entrainment relation of the form $w_e = C_w\tilde{u}/(1 + C_R Ri)$, with the two constants set to $C_w = 0.5$ and $C_R = 0.2$. A better fit to the experiment can be obtained by choosing a larger value for C_w, but a larger value would not be appropriate in the passive limit. The value of C_R is also an order of magnitude smaller than e.g. proposed by Britter (1988), and therefore not entirely consistent with entrainment experiments. Using a larger value does, however, yield much too large concentrations. Similar problems were found by Würtz (1993) for his shallow layer model (like SLAM without edge entrainment). Würtz found that the Thorney Island trial 8 data from sensors at $z = 0.4$ m were best reproduced by an entrainment relation of the form

$$w_e = 0.03\sqrt{u^2 + (u - u_a)^2} \tag{228}$$

and rejected entrainment relations depending on the Richardson. With SLAM we too find that choosing $C_R = 0$ the rest of the parameters can be adjusted to yield a good fit to the data from these sensors. However, data from sensors placed higher (z=2.4m and 6.5m) is not well reproduced, because the cloud height is overestimated. We have therefore adjusted parameters so that the model reproduces the observed doughnut shape of the cloud, and then $C_R = 0$ is no longer optimal. With $C_w = 0.5$ and $C_R = 0.2$ we find reasonable predictions also for concentrations at elevated positions. It seems to be a problem with shallow layer models to get a large enough entrainment rate.

It should be noted that a positive heat flux was measured in the atmosphere before the passage of the cloud, and there may therefore have been a heat flux also in the cloud itself. That would have generated turbulence, which the model does not take into account, but it is probably not a large effect. The situation is different at the edges. Here the generation of turbulence is larger and the calculated concentrations are generally a bit too low. The enhancement of turbulent kinetic energy near the edge, and consequent enhancement of the entrainment rate, is the way the present model represents edge-entrainment. This mimics the entrainment caused by the front vortex, and it seems to work. As already mentioned in section 3.3 edge-entrainment is the dominant dilution mechanism in this experiment.

The main problem with the model is the suppression of mixing for the central cells. There is a positive feed-back in the mixing process, because mixing lowers the Richardson number thereby increasing the entrainment rate. To this comes the squeezing effect, which can reduce the top area of small cells, and further decrease the top area of large cells with high concentrations. For too large values of C_R this can lead to spurious behaviour where some cells 'loose the mixing competition' and stay at high concentrations. The incorporation of diffusion between cells (in reality caused by shear) could be a cure to this problem and should be considered in future developments of the model.

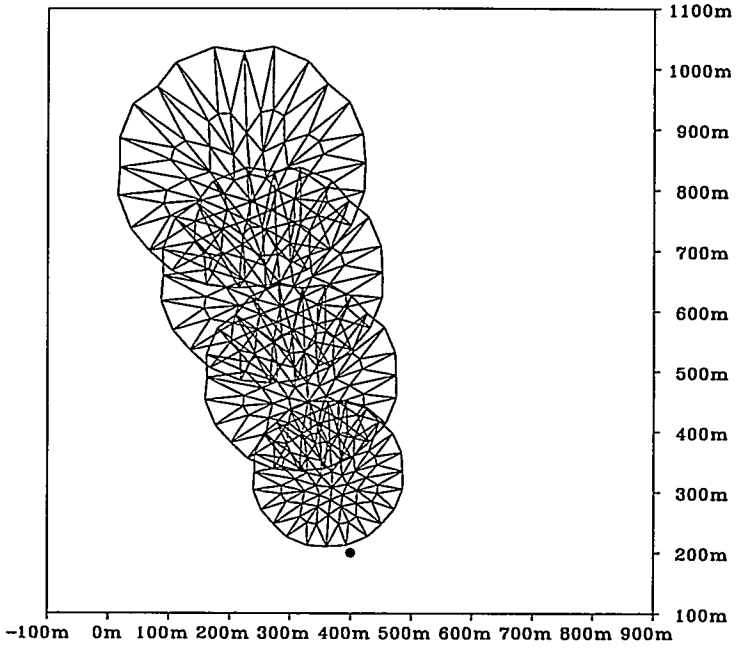

Figure 9. SLAM simulation of Thorney Island Trial 8 using a rather detailed grid. The figure shows the grid at 50 second intervals.

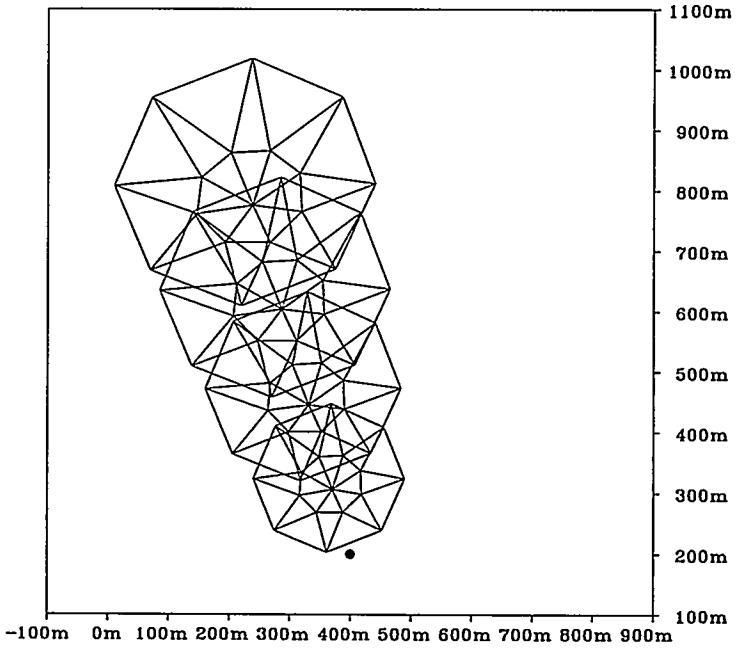

Figure 10. SLAM simulation of Thorney Island Trial 8 using a coarse grid. The figure shows the grid at 50 second intervals.

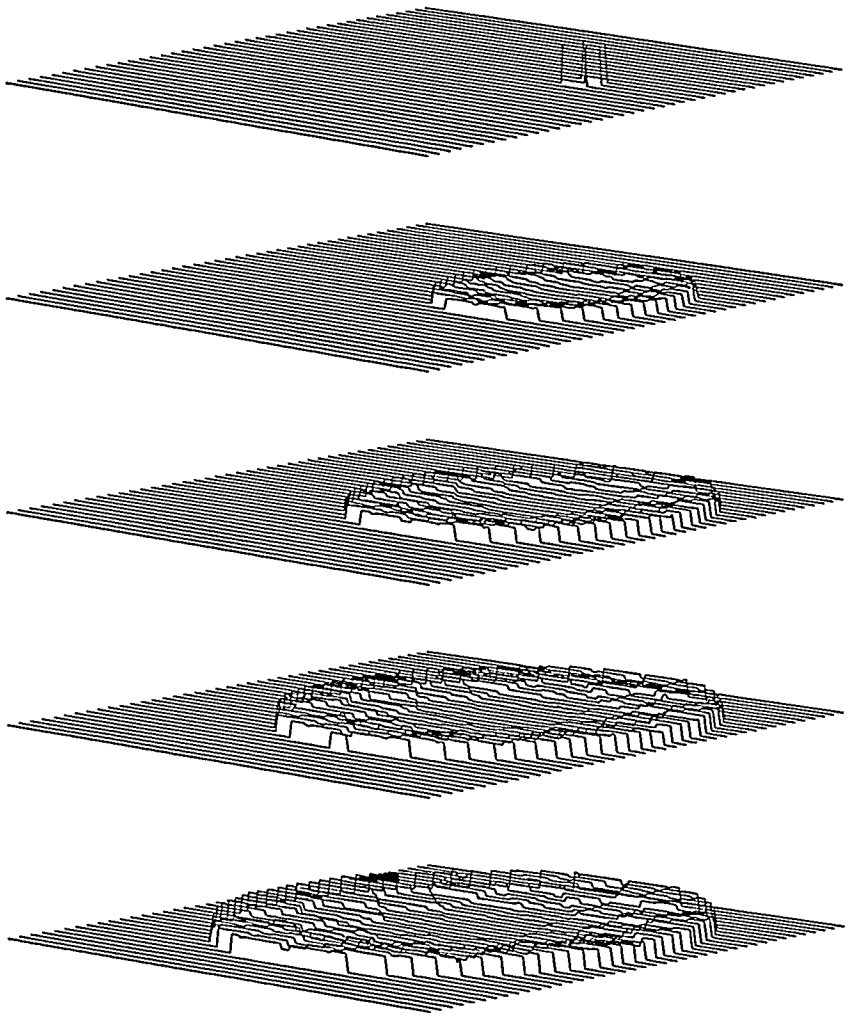

Figure 11. Simulation of Thorney Island Trial 8. Cloud shape for the first 50 seconds. The plots show a square area 200m × 200m.

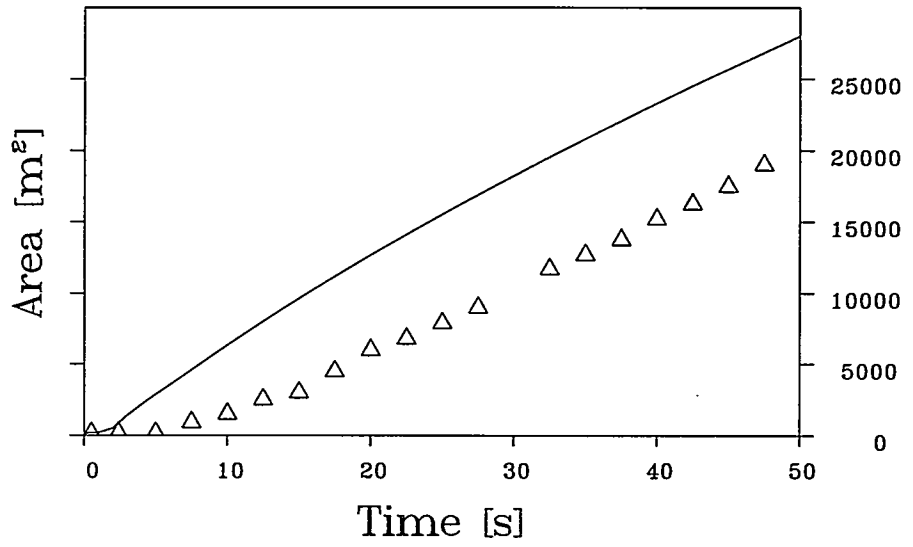

Figure 12. The initial growth of the cloud area in Thorney Island Trial 8. Solid line: SLAM simulation. Triangles: Areas data are deduced from photographs, McQuaid&Roebuck (1985).

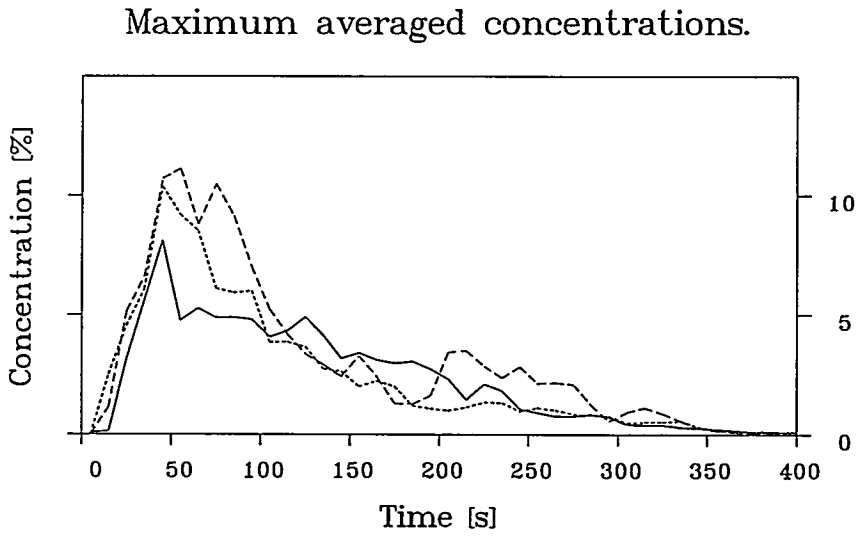

Figure 13. The graphs show the largest 10 seconds average concentration at any sensor position as a function of time for Thorney Island Trial 8. Solid line: Experiment. Dashed line: SLAM simulation with fine resolution. Dashed-dotted curve: SLAM simulation with coarse resolution.

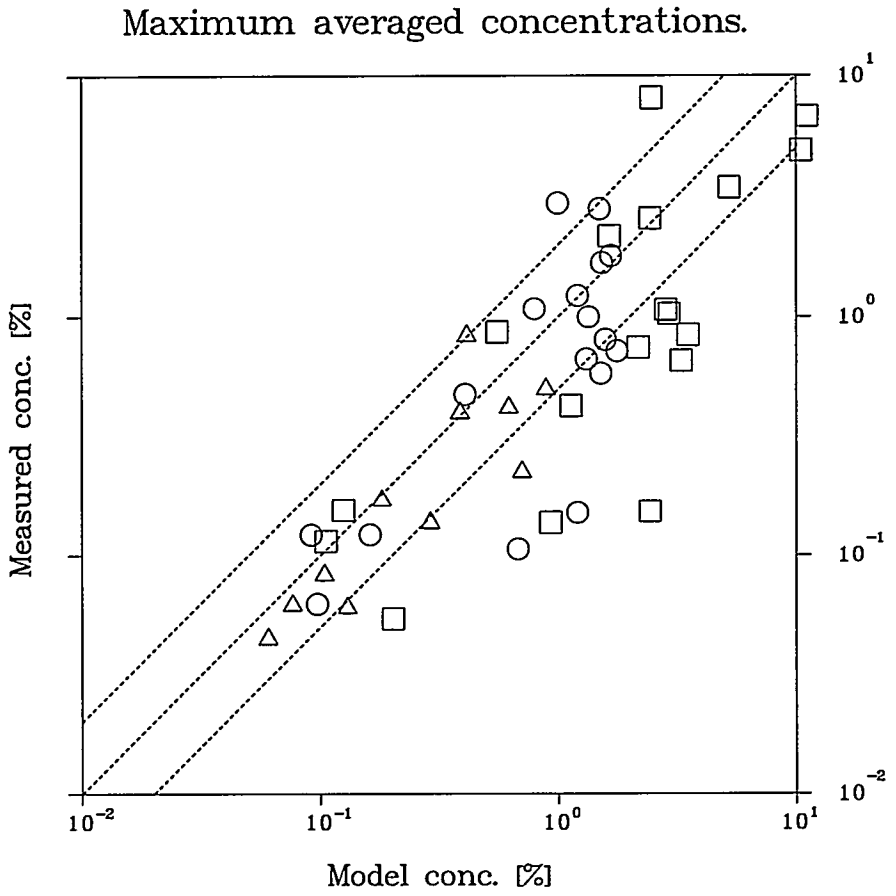

Figure 14. Scatter plot of maximum 10 seconds average concentrations for all sensor positions. SLAM simulation using fine resolution. Squares: Sensors at $z =$ 0.4 m. Circles: Sensors at $z = 2.4$ m. Triangles: sensors at $z = 4.4$ m or $z = 6.4$ m.

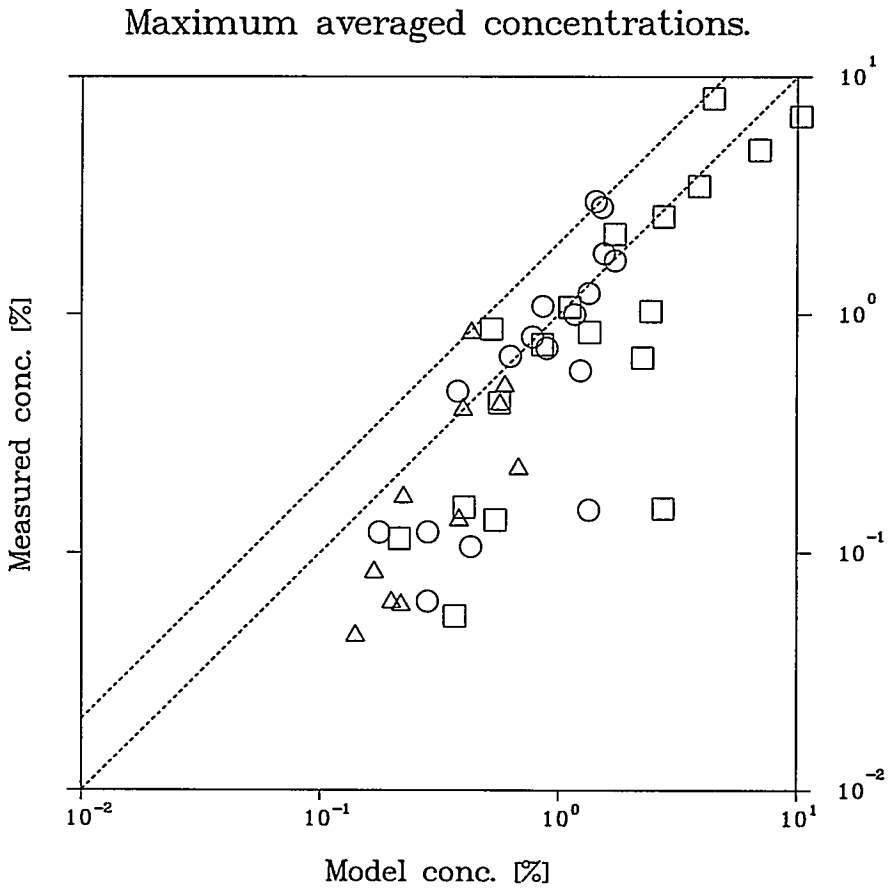

Figure 15. Scatter plot of maximum 10 seconds average concentrations for all sensor positions. SLAM simulation using coarse resolution. Squares: Sensors at $z = 0.4$ m. Circles: Sensors at $z = 2.4$ m. Triangles: sensors at $z = 4.4$ m or $z = 6.4$ m.

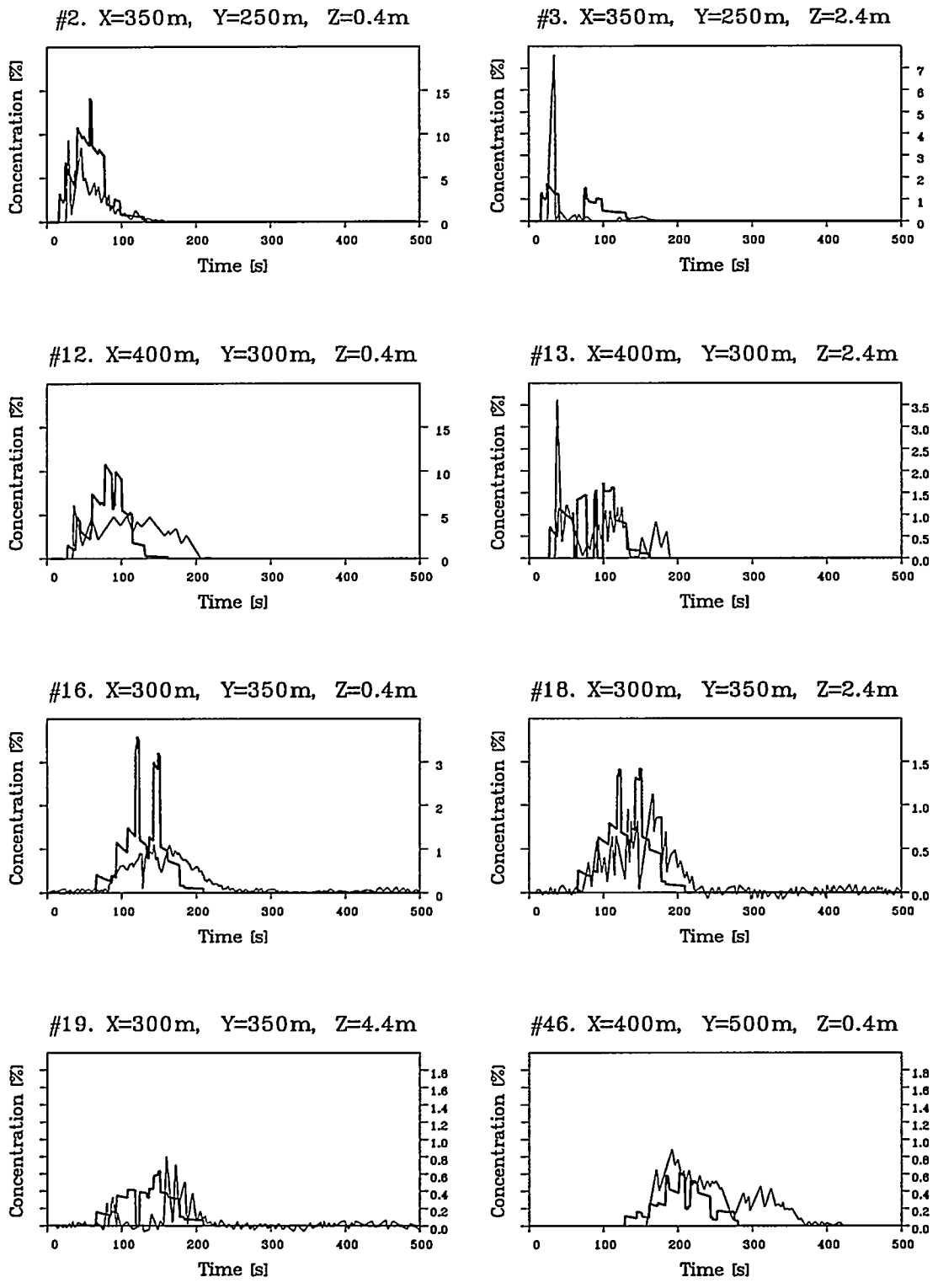

Figure 16. Thin lines: measured concentrations. Thick lines: SLAM results using fine grid.

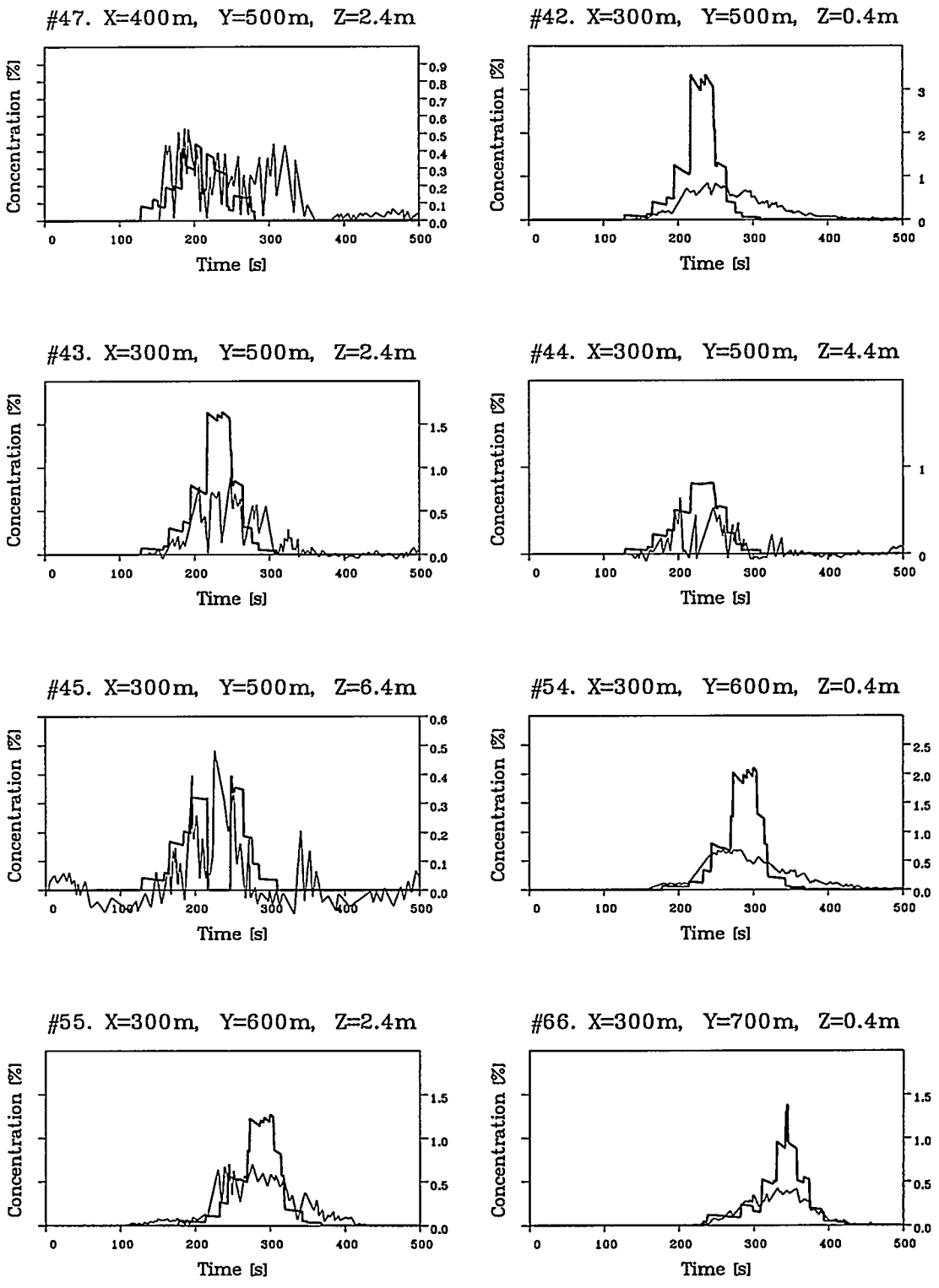

Figure 17. Thin lines: measured concentrations. Thick lines: SLAM results using fine grid.

5 Conclusions

Section 2 contains a discussion of the properties of the inviscid shallow water equations, focusing on existence and uniqueness of solutions and on the self-consistency of the whole concept. The assumptions needed to derive the equations are not always fulfilled in dense gas clouds, and unwanted features of the bare shallow water equations, have been pointed out. The symptoms are that solutions may not exist for certain initial conditions or may break down after a finite time, which was demonstrated analytically for some simple examples. It was concluded that (at least) two cures are needed:

1. Improvement of the hydrostatic approximation in order to make solutions with discontinuous h possible.
2. Addition of internal friction. This introduces dissipation at the right places and prevents spurious oscillations.

In Section 3 a set of layer integrated equations was derived starting from the Navier-Stokes equations. The equations describe budgets for mass, contaminant, momentum and turbulent kinetic energy. Turbulence, energy dissipation and entrainment were discussed, and attempts made to give precise definitions. The various steps in the derivation were accompanied by plausibility arguments. Although some of these may be characterized as 'hand-waving', they are the scientific basis of the model. Justifications for possible improvements must refer to flaws in the arguments. The main weak points in the derivation are:

- It is difficult to give a definition of the cloud height which justifies the manipulations made, and, at the same time, can be expressed in terms of observable quantities. Consequently h and w_e are difficult to measure unambiguously, and model validation becomes difficult.
- The closure assumption $\{\rho u\} \sim \{\rho\}\{u\}$ has the effect to prevent horizontal exchange of matter within the layer. This seems to be a severe restriction.
- In the layer integrated model the modeling of the entrainment rate is done as a separate matter. In a stably stratified layer turbulent diffusion may be well described be gradient transfer (K-theory), although perhaps best with non-locally determined diffusivities. Within such a framework it would be possible to calculate w_e and to find the effective velocity of the entrained air etc. However, we only have solid gradient transfer theory for a constant flux layer.
- The interactions at the cloud top are not accounted for in the framework of layer averaged equations, where they appear as boundary terms, which have to estimated in other ways. These estimates are not trivial to make, since the ambient flow is affected by the presence of the cloud. In particular a better understanding of why the velocity of the entrained air seems to be so low is required.

In Section 4 the principle of least action was introduced as a means of generating discrete equations for numerical models. In this framework discrete models automatically obey conservation laws and it is also relatively easy to improve the hydrostatic approximation. A numerical model called SLAM (Shallow LAyer Model) has been presented. The model uses a triangular grid (sectioning the cloud into triangular prisms). SLAM has some distinct features compared to other shallow layer models:

- Explicit modeling of the turbulent kinetic energy budget.

- The entrainment rate is estimated on the basis of the local turbulent kinetic energy.
- Non-hydrostatic pressure.
- A Lagrangian, moving grid.
- Numerical methods ensure that conservation laws are not violated even for coarse grids.

Thorney Island trial 8 was used as a reference case. This is an instantaneous isothermal release of a Freon/Nitrogen mixture. The entrainment constants were tuned by means of concentration data from sensors located at several heights in order to reproduce the doughnut shape of the cloud. The results are in reasonable agreement with observations, even when a small number of cells is used, and as a whole the model behaves well from a numerical point of view. However, the entrainment relation used is not consistent with relations obtained in the laboratory by means of continuous plumes. A much weaker dependence on the local Richardson number than observed in the various laboratory experiments had to be employed in order reproduce the field test data. A possible explanation is that vertical exchange of matter, which the model neglects, is important in the case of an instantaneous release such as Thorney Island trial 8. Further data comparison is needed to validate the model.

References

Benjamin, T. B. (1968). Gravity currents and related phenomena, *Journal of Fluid Mechanics*, **31**, 209–248.

Billeter, L. (1996). *Laborversuche zur instation ren Ausbreitung isothermer Schwergaswolken*, Ph.D. thesis, Eidgen ssischen technishen Hochschule, Z rich. Diss. ETH Nr. 11269.

Bo Pedersen, F. (1980). A Monograph on Turbulent Entrainment and Friction in Two–Layer Flow, *Series paper 25*, Technical Univesity of Denmark, Institute of Hydrodanamics and Hydraulic Engineering, Lyngby.

Brighton, P. W. M. (1987). A users critique of the Thorney Island dataset, *Journal of Hazardous Materials*, **16**, 457–500.

Britter, R. E. (1988). A review of some mixing experiments relevant to dense gas dispersion, *in* J. S. Puttock (ed.), *Stably Stratified flow and dense gas dispersion*, Clarendon Press, 1–38.

Britter, R. E. & Snyder, W. H. (1988). Fluid modeling of dense gas dispersion over a ramp, *Journal of Fluid Mechanics*, **18**, 37–67.

Eidsvik, K. (1980). A model for heavy gas dispersion in the atmosphere, *Atmospheric Environment*, **14**, 769–777.

Feynman, R. P., R. B. L. & Sands, M. (1964). *The Feynman Lectures on Physics*, Addison–Wesley.

Forest, E. & Ruth, R. (1990). Forth-order symplectic integration, *Physica D*, **43**, 105–117.

Goldstein, H. (1966). *Classical Mechanics*, Addison–Wesley.

Havens, J. A. & Spicer, T. O. (1985). Development of a heavier–than–air dispersion model for the US Coast guard hazard assessment computer system, *Technical Report CG-D-22-85*, U.S. Coast Guard.

Hunt, J. & Webber, D. (1979). A Lagrangian statistical analysis of vertical diffusion from a ground level source in a turbulent boundary layer, *Quart. J. Roy. Met. Soc.*, **105**, 423–443.

J.A. Businger, J.C. Wyngaard, Y. I. & Bradley, E. (1971). Flux-Profile Relationships in the Atmospheric Surface Layer, *Journal of the Atmospheric Sciences*, **28**, 181–189.

Kantha, L., Phillips, O. & R.S.Azad (1977). On turbulent entrainment at a stable density interface, *Journal of Fluid Mechanics*, **79**, 753–768.

Kantorovich, L. V. (1933). , *Bull. Acad. Sci. USSR*, **5**, 647.

McQuaid, J. (1976). Some experiments on the structure of stably-stratified flows., *Technical Report SMRE Technical Paper P21*, SMRE.

McQuaid, J. & Roebuck, B. (1983). Large scale field trials on dense vapour dispersion, *Technical report*, Health and Safety Executive.

McQuaid, J. & Roebuck, B. (1985). Large scale field trials on dense vapour dispersion., *Technical Report EUR 10029*, CEC.

Mercer, A. & Davies, J. K. W. (1987). An analysis of the turbulence records from the Thorney Island continuous release trials, *Journal of Hazardous Materials*, **16**, 21–42.

Mitchell, A. & Wait, R. (1977). *The Finite Element Method in Partial Differential Equations*, John Wiley & Sons.

Nielsen, M. (1997). *Dense gas dispersion in the atmosphere*, Ph.D. thesis, Technical University of Denmark.

Nielsen, M. & Ott, S. (1996). Fladis field experiments. Final report., *Technical Report Risoe-R-898(EN)*, Risø National Laboratory.

Osher, S. & Sweby, P. (1987). Recent developments in numerical solutions of nonlinear conservation laws., *in* A.Iserles & M. Powell (eds), *Proc. of the joint IMA/SIAM Conference on The state of the Art in Numerical Analysis, April 14-18 1996*, Clarendon Press.

Panofsky, H. A. & Dutton, J. A. (1984). *Atmospheric turbulence, models and methods for engineering applications*, Wiley–Interscience, John Wiley & Sons, New York.

Puttock, J. (1987). Analysis of meteorological data for the Thorney Island Phase I trials, *Journal of Hazardous Materials*, **16**, 43–74.

Salmon, R. (1982). Practical use of Hamilton's principle, *Journal of Fluid Mechanics*, **132**, 431–444.

Simpson, J. E. & Britter, R. E. (1979). The dynamics of a head of a gravity current advancing over a horizontal surface, *Journal of Fluid Mechanics*, 94, 447–495.

Simpson, J. E. & Britter, R. E. (1980). A laboratory model of an atmospheric mesofront, *Quart. J. R. Met. Soc*, **106**, 485–500.

Stretch, D. (1986). *The dispersion od slightly dense contaminants in a turbulent boundary layer*, University of Cambridge.

Tennekes, H. & Lumley, J. L. (1972). *A first cource in turbulence*, The Massachusetts Institute of Technology Press, MA.

van Ulden, A. (1986). The spreading and mixing of a dense gas cloud in still air., *in* J. Puttock (ed.), *Proc. I.M.A. Conference on Stably Stratified Flow and Dense Gas Dispersion, April 19, 1986*, Oxford University Press.

van Ulden, A. (1987). The heavy gas mixing process in still air at Thorney Island and in the laboratory, *Journal of Hazardous Materials*, **16**, 441–426.

Webber, D. M., Jones, S. J., Tickle, G. A. & Wren, T. (1992). A model of a dispersion dense gas cloud, and the computer implementation D*R*I*F*T*. II. Steady continuous releases, *Technical Report UKAEA-SRD/HSE-R587*, UK atomic energy authority, Safety and reliability directorate.

Webber, D. & Wheatley, C. (1987). The effect of initial potential energy on the dilution of a heavy gas cloud, *Journal of Hazardous Materials*, **16**, 357–380.

Wheatley, C. & Prince, A. (1987). Translational cloud speed in the Thorney Island trials: Mathematical modelling and data analysis., *Journal of Hazardous Materials*, **16**, 185–200.

Wheatley, C. & Webber, D. (1984). Aspects of the dispersion of denser-than-air vapours relevant to gas cloud explosions, *Technical Report XII/829/84-EN*, SRD,UKAEA.

Würtz, J. (1993). A Transient One-dimensional Shallow Layer Model for Dispersion of Denser-Than-Air Gases in Obstructed Terrain under Non-Isothermal Conditions, *Technical Report EUR 15343 EN*, Commision of the European Communities Joint Research Centre.

Yoshida, H. (1990). Construction of higher order symplectic integrators, *Physics Letters A*, **150**, 262–268.

Zalezak, S. (1981). Fully flux-corrected transport algorithms for fluids, *Journal of Computational Physics*, **40**, 497–508.

A Notation

The Cartesian coordinate system (x, y, z) is oriented with the x and y axes horizontal and the z axis vertical. If tensor notation is used, the coordinates are written as (x_1, x_2, x_3), and greek subscripts run only from 1 to 2.

u	$\equiv u_1$. Horizontal wind component along x-axis
w	$\equiv u_2$. Horizontal wind component along y-axis
w	$\equiv u_3$. Vertically wind component along z-axis
$\frac{\mathrm{d}}{\mathrm{dt}}$	$= \frac{\partial}{\partial t} + u\frac{\partial}{\partial x} + v\frac{\partial}{\partial y} + w\frac{\partial}{\partial z}$
u_*	$=\sqrt{-\overline{w'u'}}$ friction velocity
z_0	Surface roughness
b	Bottom code
h	Dense layer thickness
z_c	Height of centroid $= \beta h$
$[Q]$	Layer average of Q; $[Q] = 1/h \int_b^{h+b} Q\, dz$
$\hat{Q}$	$Q - [Q]$
$\overline{Q}$	Ensemble average
Q'	$= Q - \overline{Q}$
$\{Q\}$	Layer and ensemble average of Q; $\{Q\} = 1/h \int_b^{h+b} \overline{Q}\, dz$
$\tilde{Q}$	$= Q - \{Q\}$
ρ	Density of dense layer
ρ_a	Density of ambient air
$\Delta\rho$	$\equiv \rho - \rho_a$
ν	Kinematic viscosity
η	Dynamic viscosity
g	Acceleration of gravity
p	Pressure
Ri	Richardson number $= \frac{(\{\rho\}-\rho_a)gh}{\rho_a \tilde{u}^2}$
w_e	Entrainment rate
ϵ	Energy dissipation
$\mathcal{L}$	$=$ Lagrangian $= \mathcal{T}$-$\mathcal{V}$
$\mathcal{T}$	Kinetic energy
$\mathcal{V}$	Potential energy
$\mathcal{S}$	Action integral $= \int \mathcal{L}\, dt$
$\int \ldots ds$	Contour integral
X_P	Coordinates of corner point P (SLAM model)
U_P	Velocity of corner point P (SLAM model)
Ω_P	Domain surrounding point P (SLAM model)
H_Δ	Height of the triangular cell Δ (SLAM model)
M_Δ	Mass of the triangular cell Δ (SLAM model)
Ω_Δ	Base area of the triangular cell Δ (SLAM model)
K_Δ	Average diffusivity of the triangular cell Δ (SLAM model)
$W_{e\Delta}$	Top entrainment velocity of the triangular cell Δ (SLAM model)
$Ri_{e\Delta}$	Richardson number of the triangular cell Δ (SLAM model)
$\sum_{P \in \Delta}$	Summation over all corners P of the triangle Δ
$\sum_{\Delta \ni P}$	Summation over all triangles Δ that have P as one of the corners

Bibliographic Data Sheet **Risø–R–901(EN)**

Title and author(s)

Shallow layer modelling of dense gas clouds

Søren Ott – Morten Nielsen

ISBN	ISSN
87–550–2188–3	0106–2840
Dept. or group	Date
Systems Analysis	November 1996
Groups own reg. number(s)	Project/contract No.
MIR–02800–00	CEC D.G. XII EV5V–CT92–0069

Pages	Tables	Illustrations	References
71	0	16	38

Abstract (Max. 2000 char.)

Abstract

The motivation for making shallow layer models is that they can deal with the dynamics of gravity driven flow in complex terrain at a modest computational cost compared to 3d codes. The main disadvantage is that the air-cloud interactions still have to be added 'by hand', where 3d models inherit the correct dynamics from the fundamental equations.

The properties of the inviscid shallow water equations are discussed, focusing on existence and uniqueness of solutions. It is demonstrated that breaking waves and fronts pose severe problems, that can only be overcome if the hydrostatic approximation is given up and internal friction is added to the model.

A set of layer integrated equations is derived starting from the Navier-Stokes equations. The various steps in the derivation are accompanied by plausibility arguments. These form the scientific basis of the model.

The principle of least action is introduced as a means of generating consistent models, and as a tool for making discrete equations for numerical models, which automatically obey conservation laws. A numerical model called SLAM (Shallow LAyer Model) is presented. SLAM has some distinct features compared to other shallow layer models:

- A Lagrangian, moving grid.
- Explicit account for the turbulent kinetic energy budget.
- The entrainment rate is estimated on the basis of the local turbulent kinetic energy.
- Non-hydrostatic pressure.
- Numerical methods respect conservation laws even for coarse grids.

Thorney Island trial 8 is used as a reference case for model tuning. The model reproducesthe doughnut shape of the cloud and yield concentrations in reasonable agreement with observations, even when a small number of cells (e.g. 16) is used. It is concluded that lateral exchange of matter within the cloud caused by shear is important, and that the model should be improved on this point.

Descriptors INIS/EDB

CLOUDS; COMPLEX TERRAIN; DISPERSIONS; ENTRAINMENT; FLOW MODELS; GAS FLOW; INTERNAL FRICTION; LAYERS; MATHEMATICAL MODELS; NAVIER-STOKES EQUATIONS; S CODES; TWO-DIMENSIONAL CALCULATIONS; TURBULENCE

Available on request from:
Risø Library, Risø National Laboratory (Risø Bibliotek, Forskningscenter Risø)
P.O. Box 49, DK–4000 Roskilde, Denmark
Phone (+45) 46 77 46 77, ext. 4004/4005 · Telex 43 116 · Fax (+45) 46 75 56 27